FUNDAMENTALS & APPLICATIONS

CHEMELECTROCHEM

ANALYSIS & CATALYSIS, BIO & NANO, ENERGY & MORE

Accepted Article

Title: Synthesis, electronic structures and electrochemistry of 3-triarylphosphoraniminato-1,3,5-trithia-2,4,6,8-tetrazocines. Detection of trithiatetrazocinyl radical anions.

Authors: Xin Yu, Tracey L Roemmele, and René T. Boeré

To be cited as: *ChemElectroChem* 10.1002/celc.201701191

Link to VoR: http://dx.doi.org/10.1002/celc.201701191

A Journal of

ChemPubSoc Europe

WILEY-VCH

www.chemelectrochem.org

Submitted to ChemElectroChem **2017**, Alan Bond Festschrift issue

Article

Synthesis, electronic structures and electrochemistry of 3-triarylphosphoraniminato-1,3,5-trithia-2,4,6,8-tetrazocines. Detection of trithiatetrazocinyl radical anions.

Xin Yu,[a] **Tracey L. Roemmele**[a] **and René T. Boeré***[a,b]

Dedicated to Prof. Allen M. Bond for integration of electrochemistry with inorganic chemistry. His inspirational support is greatly appreciated by all who have been lucky enough to work with him.

Received: / Accepted: / Published:

Abstract: Reaction of the bicyclic sulfur-nitrogen heterocycles $RC_6H_4CN_5S_3$ (R = 4-CH_3O, 4-CH_3, 4-H, 4-Cl, 4-CF_3, 3-CF_3, with PR'_3 (R' =C_6H_5 or 4-$CH_3OC_6H_4$) produces 3-phosphoraniminato-7-aryl-1,3,5-trithia-2,4,6,8-tetrazocines $RC_6H_4CN_4S_3NPR'_3$. In all cases, only the *endo*-isomers were isolated and characterized by ^1H, ^{31}P, and ^{19}F NMR, UV spectroscopy, and X-ray crystallography. RB3LYP/6-311+G(d,p)// RB3LYP/6-31G(d,p) computations were undertaken to help explain the atom-exact syntheses *via* intermediates previously detected spectroscopically. Three reasonable intermediates have been computed as stationary points with energies consistent with the observed reaction path. Cyclic and square wave voltammetry studies of $RC_6H_4CN_4S_3NPR'_3$ using a glassy carbon working electrode in CH_2Cl_2 with 0.4 M [^{n}Bu$_4$N][PF_6] all displayed two IRR reduction processes at RT at approximately –1.9 V and –2.2 V, respectively, and one IRR oxidation process at approximately 1.0 V (versus $Fc^{+/0}$). $[RC_6H_4CN_4S_3NPR'_3]^{-\bullet}$ radical anions (R' = 4-$CH_3OC_6H_4$, R = 4-CH_3O, 4-H, 4-CF_3,) were detected at -50 °C in CH_2Cl_2 by *in-situ* electrolysis and simultaneous electron paramagnetic resonance spectroscopy: $[4\text{-}RC_6H_4CN_4S_3NP(4\text{-}CH_3OC_6H_4)_3]^{-\bullet}$, estimated $a(^{31}P)$ = 0.078 mT, $a(^{14}N_1)$ = 0.031 mT, $a(^{14}N_{2,3})$ = 0.256 mT, $a(^{14}N_{4,5})$ = 0.341 mT. The signals decay rapidly but after electrolysis is ended, a persistent EPR signal is always obtained with EPR parameters that match for known 4-aryl-1,2,3,5-dithiadiazolyls, e.g. a(N) = 0.51 mT and g = 2.0105, consistent with production of $[4\text{-}CF_3\text{-}C_6H_4CN_2S_2]^{\bullet}$.

Keywords: thiazyl; electrochemistry; redox-active; ring compounds; crystallography; electron paramagnetic resonance spectroscopy; reaction pathways; density functional theory

[a] Xin Yu and Dr. T. L. Roemmele
Dept. of Chemistry and Biochemistry, University of Lethbridge, Lethbridge, Alberta, Canada T1K 3M4

[b] Prof. Dr. R. T. Boeré
Dept. of Chemistry and Biochemistry and Canadian Centre for Advanced Fluorine Technologies, University of Lethbridge, Lethbridge, Alberta, Canada T1K 3M4
Fax: +1-403-329-2057
Email: boere@uleth.ca

Supporting Information for this article is available on the WWW under http:/dx.doi.org/xxxxxxxxxxxxxxxx

1. Introduction

Interest in unsaturated sulfur-nitrogen heterocycles continues apace due to their unique physical attributes and versatility in displaying interesting materials properties.[1] These include molecular (semi)conductors[2], ferromagnetism[3], bi-stability[4], novel ligands to transition metals[5] and the recent recognition of a role in biochemical signalling.[6] The large rings $[S_4N_4]^{2+}$, **A**,[7] trithiatetrazocines $[RCS_3N_4]^+$,[8] **B**, and the 1,5-dithia-2,4,6,8-tetrazocines, **C**,[9] all posses 10 π-electrons and have been predicted to be planar based on Banister's electron-counting rules for aromaticity (Chart 1).[10] While **A** – **C** retain nearly planar conformations with almost equal S–N distances, strong π-donor substituents (i.e. NR_2) at C (**D1**) or heteroatoms **D2,3** induce a strongly folded "butterfly" conformation in which a short transannular S···S contact develops. [11] Two such S···S contacts are found in the structure of the well-known parent cage compound S_4N_4 (from which **A** is derived via a two-electron chemical oxidation) but other binary sulfur nitrogen compounds such as the $[S_4N_5]^-$ anion **F** display a single S···S contact.[12] The electronic structures of these heteroaromatics are of intense current interest.[13]

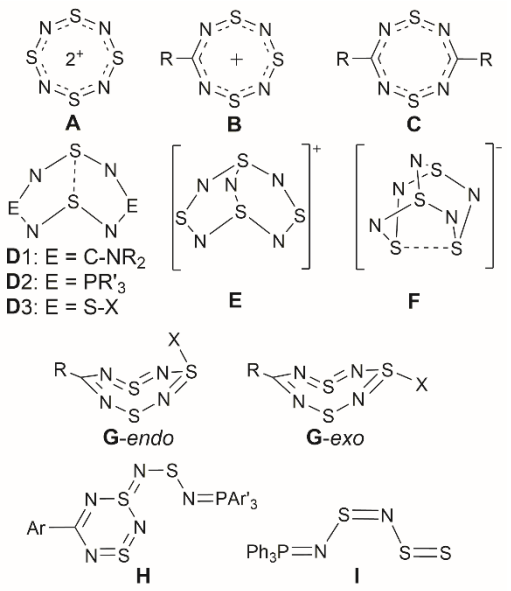

Chart 1

Our research group has been active in investigating the solution electrochemistry of binary sulfur-nitrogen compounds and of heterocycles that are rich in thiazyl linkages.[1h, 9a,b, 14] Thus we demonstrated that the electrochemical reduction of S_4N_4 induces a chemically-reversible conversion to $[S_3N_3]^-$,[14b] whilst the smaller S_2N_2 ring compound upon reduction first transforms to paramagnetic $[S_4N_4]^{-\bullet}$, which then rapidly converts to $[S_3N_3]^-$ also.[14c] The heterocyclic analogues **C** and **D**, by contrast, accept electrons to give EPR-active radical anions but thereafter rapidly decompose to unknown, EPR-silent, products.[9a,b] Our interest has now turned to the title compounds **G** which blend ring systems **A** and **C**.[8b, 15] These are neutral substituted analogues to the planar cations **B** which have Cl [15a,b] or $N=ER'_3$ (E = P, As) [15c-e] groups covalently bonded to the sulfur atom *trans* to the carbon atom in the eight-membered rings. The latter derivatives, $ArCN_2S_2N_2S–N=PAr'_3$, can be produced in high yields by nucleophilic attack of the bicyclic rings RCN_5S_3 **3** [16] (isoelectronic with $[S_4N_5]^+$, **E** in Chart 1) [17] by EPh_3, and exist solely in the folded conformation.

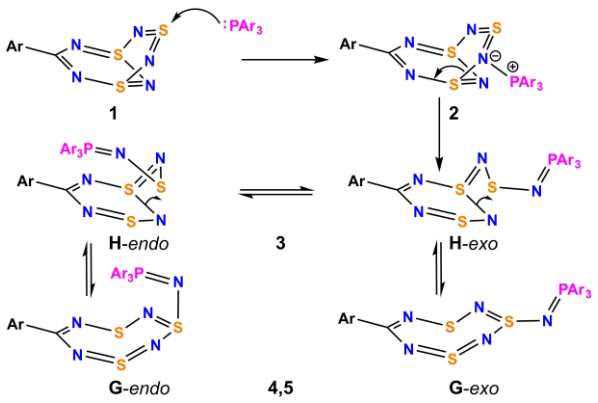

Scheme 1

Structural isomerism has been demonstrated in the case of E = As, with both the *endo* (thermodynamic isomer) and the *exo* (kinetic isomer) conformations characterized in the solid state (Chart 1).[15e] The known E = P derivatives also form both isomers, with the kinetic isomer converting over time to the final *endo* structure.[15c,d] Previous investigations of the conversion of specifically the Ar'$_3$P=N-substituted **G**-*exo* to **G**-*endo* using ^{13}P and ^{15}N NMR spectroscopy have provided structural and spectroscopic evidence that the rearrangement proceeds via a 1,3-nitrogen shift pathway, through rapidly formed 5-aryl-1$\lambda^4\delta^3$,3$\lambda^4\delta^2$,5-dithia-2,4,6-triazine intermediates, **H** (Scheme 1).[15c,d]

To date no electrochemical studies on either the cationic, **B**, or neutral trithiatetrazocines, **G**, have been reported in the literature. For diamagnetic and formally electron-rich thiazyl heterocycles of this type, voltammetry can assess (i) the redox stability window, also known as the "cell potential" E_{cell} between the most accessible oxidation and reduction processes [1h] and (ii) the degree of redox-tunability exerted by substituents on the R and ER'$_3$ groups. We have previously made use of a series of 3- and 4-substituted aryl R groups as a standard set of substituents for various thiazyl heterocycles to test relative redox-tunabilities.[1h, 14g,h] Here we report application of this concept to type **G** compounds by the synthesis and full chemical- and structural characterization of a double series of 3-triarylphosphoraniminato-7-aryl-1,3,5-trithia-2,4,6,8-tetrazocines **4** (with Ar' = Ph) and **5** (with Ar' = 4-$CH_3OC_6H_4$). The use of two phosphines was undertaken to also assess the influence of the Ar'$_3$P=N- moieties on the redox properties and in the hope that the more basic phosphine might allow for isolation and study of **G**-*exo* isomers since all the known Ph_3P=N- derivatives reported in the literature have thus far only been structurally characterized as **G**-*endo* isomers. Iminophosphoranes are known substituents for elements across the Periodic Table.[18]

2. Results and Discussion

2.1. Synthesis

The title compounds **4a-f** and **5a-f** (Scheme 2) were prepared by slight modifications of a published method [15c,d] by the reaction of triphenyl phosphine or *tris*(4-methoxyphenyl)phosphine, respectively, with six different 7-aryl-1λ^4,3$\lambda^4\delta^2$,5λ^4-trithia-2,4,6,8,9-pentaazabicylo[3.3.1]nona-1(9),2,3,5,7-pentaenes, **1a-f**,[16c] using anhydrous toluene as the reaction medium. The reaction mixtures typically turn a bright red color, previously identified by *in-situ* ^{31}P and ^{15}N NMR spectroscopies with the rapid formation of compounds of type **H**, but on longer standing turn a variety of colors between yellow and orange. Crystals of the purified products were obtained by slow-cooling of mixtures of CH_3CN/CH_2Cl_2 and were found to have a range of colors from almost colorless to deep orange.

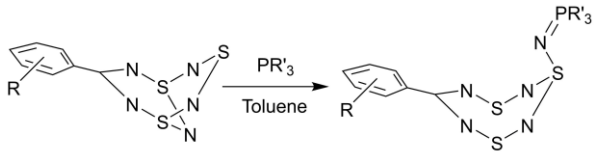

1 R =	PPh_3	$P(C_6H_4\text{-}4\text{-}OCH_3)_3$	4,5
4-CH_3O	**4a**	**5a**	
4-CH_3	**4b**	**5b**	
4-H	**4c**	**5c**	
4-Cl	**4d**	**5d**	
3-CF_3	**4e**	**5e**	
4-CF_3	**4f**	**5f**	

Scheme 2

2.2. Characterization

The previously reported **4c** was identified by MP and spectroscopy (see the full Experimental details in the SI) by comparison to the original report.[15c] The eleven new derivatives have been exhaustively characterized by solution NMR including ^{1}H, ^{13}C, ^{19}F and ^{31}P spectroscopy, with assignments verified by ^{1}H-^{1}H COSY, ^{1}H-^{13}C HMBC and ^{1}H-^{13}C HSQC methods. Key NMR results are listed in Tables 1 and S1,2. The molecular ions were confirmed by high resolution ESI-MS and fitting combustion analysis have been obtained.

Table 1. ^{31}P and selected ^{13}C NMR data for **4** and **5**.[a,b]

Substituent		P1	C1		P1	C1	$\Delta\delta^{1}$ [c]
4-CH_3O	**4a**	19.87	179.36	**5a**	19.59	179.25	0.28
4-CH_3	**4b**	20.05	179.88	**5b**	19.78	179.90	0.28
4-H	**4c**	20.21	179.63	**5c**	19.96	179.63	0.25
4-Cl	**4d**	20.31	178.52	**5d**	20.08	177.79	0.23
3-CF_3	**4e**	20.35	178.04	**5e**	20.16	177.78	0.19
4-CF_3	**4f**	20.50	178.03	**5f**	20.47	179.75	0.03
$\Delta\delta^{2}$		0.63			0.88		

[a] δ in ppm vs. external 85% H_3PO_4 measured on solutions in $CDCl_3$.
[b] The atom numbering is that used in Figure 1b,c. [c] $\Delta\delta^{1} = (\delta_{PPh3} - \delta_{P\{4\text{-}MeC6H4\}3})$. [b] $\Delta\delta^{2} = (\delta_{4\text{-}CF3} - \delta_{4\text{-}MeO})$.

The ^{31}P chemical shifts (Table 1) are characteristic of the *endo-anti* geometry demonstrated previously to be the most stable form for this class of compounds, specifically **4c** δ = 20.21 ppm (lit. 20.9 ppm)[15c] whereas the red-coloured intermediate **3c** (δ = 26.3 ppm) and *exo-anti* isomer of type **4c**-*exo* (δ = 27.0 ppm) have chemical shifts 6 - 7 ppm to higher frequency. There is a small but consistent trend towards higher frequency as the R substituents become more electron withdrawing, with the overall trend for the series $\Delta\delta^{2}$ = +0.63 ppm. There is a very small but consistent shift also to higher frequency when PPh_3 is replaced by the more basic $P(4\text{-}CH_3OC_6H_4)_3$, $\Delta\delta^{2}$. A single 4-CH_3O R group induces a shift difference $\Delta\delta^{2}$ of –0.34, while three such 4-CH_3O groups on the phosphine produce a shift difference $\Delta\delta^{1}$ of only –0.25 ppm. Thus the ground state nuclear magnetic properties of **4** and **5** are very weakly susceptible to substituent effects, which are consistent with greater shielding of the ^{31}P nucleus by stronger donors. The ^{13}C chemical shifts of the endocyclic carbons C1, closely similar at 178–179 ppm for all **4** and **5**, may be compared to the distinct values determined for dithiatetrazocines: for planar derivatives **C** with aryl substituents, δ(RC) is 137–138 ppm,[9c] for the *bis*-^{t}Bu derivative, δ(RC) = 144.8 ppm.[9d, 11g] However, for the folded derivatives **D1**, δ(RC) is 179–180 pm;[11] thus, the chemical shifts of C1 are characteristic of the folded geometry in solution for all these derivatives of **4** and **5**.

Initial attempts to measure mass spectra by conventional heated probe/EI methods were inconclusive. The dominant peak is usually that for $R_3P{=}NSNH^+$, which implies ring decomposition or at the very least significant re-arrangement. Thermolysis of bulk crystals to determine the MP indicated that **4** and **5** all darken to a cherry-red color well below the melting point, and that the melts retained this colour. Such deep red colouration is strongly indicative of the presence of R-$(NS)_n$- cumulene structures such as type **H** or **I** (Chart 1).[15d, 19] However, the crystals that were repeatedly isolated from thermolysis studies – despite a ruby-red appearance – were only those of $Ar'_3P{=}S$, compounds well-known to be colourless when pure. Eventually, by using electrospray ionization, high resolution mass spectra were obtained for all new compounds **4** and **5** which confirms their chemical compositions in conjunction with sample purity established by ^1H and ^{13}C NMR and EA.

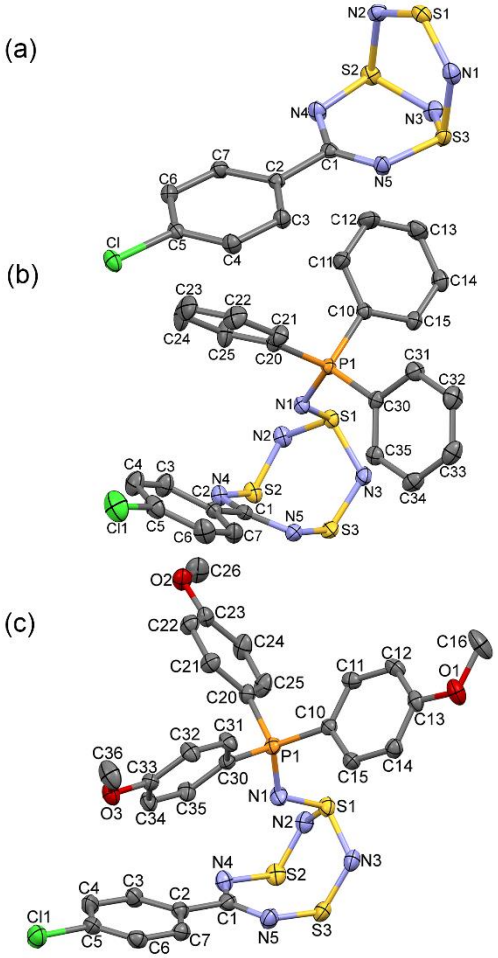

Figure 1. Displacement ellipsoids plots (40% probability) of the molecular structures of (a) **1d**, (b) **4d** and (c) **5d** as found in their crystals. The standardized atom numbering scheme for all structures is shown.

2.3. Crystal and molecular structures

Single crystal X-ray diffraction structures were determined for reactant **1d** and all the new **4** and **5**, twelve structures in all, in order to confirm their geometries and to correlate the considerable variation in colours of the crystalline solids with solid-state conformations. In fact, despite colors ranging from deep orange to colorless, all the crystallographically isolated exemplars have the *endo-anti* geometry first reported for **4c** in 1986,[15f] similar to the observations of Knapp *et al.*[15c] Here only three representative structures, **1d**, **4d** and **5d**, are illustrated (Figure 1) and described but the remainder are described in the Supporting Information.

2.3.1. Single-crystal diffraction structure of **1d**

The structure of **1d** (Fig. 1a) consists of a $1\lambda^4\delta^3,3\,\lambda^4\delta^2$,5-dithia-2,4,6-triazine ring which is planar for the five-atom fragment C1–N4–S2–S3–N5 to within 0.01 Å but with N3 tipped out of the plane by 0.585(2) Å (dihedral angle between the two planes is 139.4(1)°). A second five-member ring consisting of S2–N2–S1–N1–S3, itself planar to 0.03 Å, is hinged to the primary ring with a dihedral of 103.94(3)°. The molecule has a plane of symmetry; the equivalent bonds alternate in distinct sets with short C–N (1.319) and S–N (1.593) followed by slightly longer bonds to N3 (1.604), considerably longer S–N bonds (1.719) to the bridging NSN group and very short bonds (1.523 Å) consistent with a bridging N1=S1=N2 moiety.[16g] Bicyclic cages **1a-f** of this type are the synthetic precursors to all **4** and **5** reported here (see Experimental).

2.3.2. Representative single-crystal diffraction structure of **4d**

The picture of the geometry of **4d** (Fig. 1b) shows the common numbering scheme used for the series of molecules. Compared to its precursor **1d** (Fig. 1a) the loss of the bridging N3 atom results in *shorter* cross-ring distances, *d*(S···S) = 2.4330(6) in **4d** versus 2.657 Å in **1d**, and an enlarged folding angle (the dihedral in **4d** is 114.85(4)°, an increase of 11°). A comparison of bond lengths indicates that those in **4d** are more evenly distributed. The average C–N distance is *longer* at 1.334 Å, while the S–N distances for similar bonds are 1.633 (N4,5–S2,3), 1.602 (S2,3–N2,3), 1.654 (N2,3–S1) and 1.654 (S1–N1) Å, respectively. By comparison the average C–N and S–N distances in folded dithiatetrazocines **D1** are 1.348 and 1.605 Å, respectively.[11]

Table 2. Average distances and angles from twelve crystal structures assuming C_s symmetry. [a]

Distances (Å)	**P1–N1**	**S1-N1**	**S1-N2,3**	**S2,3-N2,3**	**S2,3-N4,5**	**N4,5-C1**	**C1-C2**	**S2···S3**
This work	1.604(5)	1.610(7)	1.653(4)	1.598(5)	1.632(3)	1.333(3)	1.482(4)	2.43(1)
4g[b]	1.599(8)	1.626(7)	1.654(8)	1.605(7)	1.615(6)	1.345(10)		2.452(3)
4h[c]	1.609(3)	1.602(3)	1.656(4)	1.582(4)	1.651(3)	1.318(6)	1.522(6)	2.454(2)
Cations **B** [d]			1.57(1)	1.56(1)	1.538(7)	1.33(1)		3.98(4)
Angles (°)	**P1-N1-S1**	**N1-S1-N2,3**	**N2,3-S2,3-N4,5**	**S2,3-N4,5-C1**	**dihedral 1**[e]	**dihedral 2**[f]		
	121(2)	107.1(3)	115.6(7)	117.8(3)	115(1)	144(1)		

[a] Obtained by averaging the corresponding values from single-crystal X-ray diffraction studies on **4a-f** and **5a-f**. Structure of **4c** reported in Ref. 15f. Note that the molecule located on the mirror plane in **4a** was excluded from this analysis. Errors are standard deviations of the values. The full data are provided in Table S6. For atoms numbers, see Figure 1.
[b] **4g**: directly bound Me_2N substituent at C1, from reference 15c.
[c] **4h**: directly bound CF_3 substituent at C1, from reference 15c.
[d] Data for approximately planar $RCN_4S_3^+$ ions from reference 8; see Chart 1.
[e] Dihedral angle between the C1N4N5S2S3 and the S2S3N2N3 planar ring fragments, expressed as the obtuse value.
[f] Dihedral angle between the S2S3N2N3 and the N2N3S1 planar ring fragments, expressed as the obtuse value.

2.3.3. Representative single-crystal diffraction structure of **5d**

The structure of **5d** as found in the crystal lattice is shown in Figure 1c, along with the slightly-modified numbering system required for the 4-methoxyphenyl groups on phosphorus. The bond distances and angles in the series **5** involving ArC and the thiazyl ring atoms are statistically indistinguishable from those in the series of structures of **4**. For example, the transannular S2···S3 contact in **5d** is 2.4369(8) Å, which cannot be differentiated from that found in **4d** at the 95% confidence level. Similar transannular contacts have been observed in mono- and dications of S_8 rings by crystallography as reported very recently.[20]

2.3.4. Summary of structural results

The full series of structures **4a-f** and **5a-f** now available is an excellent structurally characterized set of homologous thiazyl molecules. Differences between them are restricted to some conformational variation in the orientations of the Ar'$_3$P moieties about the PN–S bonds and within their lattice structures there are several different kinds of short contacts (reviewed in detail in the Supporting Information). That such intermolecular interactions are weak is convincingly demonstrated by the high similarity of the metric parameters of all the molecules investigated in this series (Table 2). Within the rings there are distinct variations among different symmetry-equivalent bonds. Thus, starting from S1, the bonds alternate in long [1.653(4)] - short [1.598(5)] - long [1.632(3)] fashion, though as mentioned above for **4d** this variation is much smaller than in the precursor cage compounds **1**. It would appear that the bonds in **4** and **5** are overall weaker than those in the corresponding **D1**, and significantly longer than those found for the planar aromatic structures **B** (the average S–N distances ranging from 2.9 to 6.4% longer – see Table 2). Indeed, we have calculated the *average* bond distance within the eight-member rings for the two classes of compounds: for **4** and **5** 1.554(4) and for **B** 1.50(1) Å, almost 4% longer in the folded covalent versus the planar cationic species. These results imply that the aromatic character detected in cations **B** has been weakened in **4** as a result of the second-order Jahn-Teller distortion that accompanies substitution at sulfur.[1l] All the observed structures of **4** and **5** have the *endo-anti* geometry with highly conserved dihedral angles of 115(1)° for the CN_2S_2–S_2N_2 and 144(1)° for the S_2N_2–N_2S pivots, respectively. Within this series, no obvious differences could be observed for these two values among the N=PPh$_3$ and N=P(C$_6$H$_4$OMe)$_3$ substituents nor, for that matter, with the RC ring substituents. Given the wide variety of crystal packing that occurs over this range of molecules, such a level of structural conservation implies that the geometries of this class of molecules are quite robust and resistant to distortion. On the other hand, if we consider the directly bound strong donor Me$_2$N (**4g**) or the strong acceptor CF$_3$ (**4h**) at the ring carbon, a distinct pattern in the bond lengths can be observed with, in each case, the aryl substituents intermediate between those of the other two types (Table 2).[15c]

*2.4. Computational insights into the mechanism for conversion of **1** into **4** and **5***

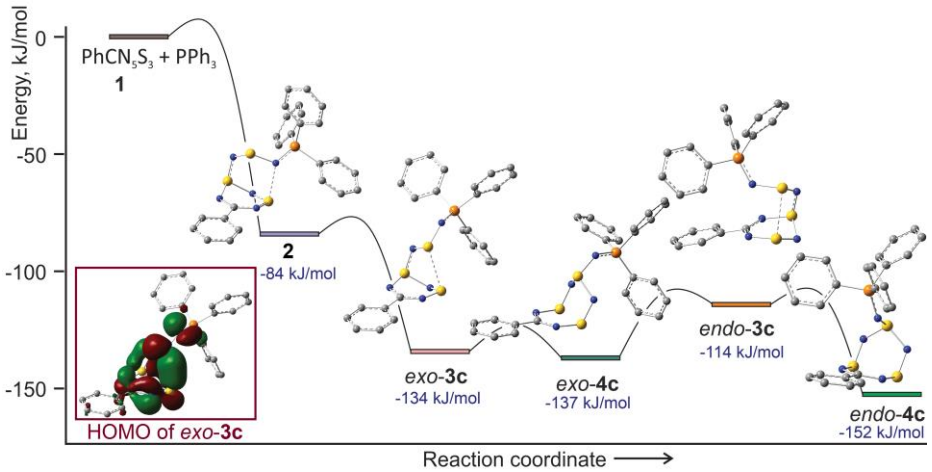

Figure 2. Reaction profile diagram showing the energies and structures (from RB3LYP/6-311+G(d,p)// RB3LYP/6-31G(d,p) calculations) for reaction of PPh$_3$ with **1**. The HOMO that stabilizes *exo*-**3c** is also shown.

The mechanism (Scheme 1) first proposed in 1987 for the *atom precise* transformation of **1** into **4** or **5** was based on strong evidence from *in-situ* ^{31}P and ^{15}N NMR [15d] and it has been substantiated thereafter by other researchers.[15c] Since equilibria in solutions involving **3** and **4** or **5** are relevant to the electrochemical study, we have undertaken a investigation of this mechanism using hybrid density functional theory (DFT) calculations at the RB3LYP/6-311+G(d,p)// RB3LYP/6-31G(d,p) level of theory (Figure 2). Ph$_3$P as nucleophile attacks the LUMO of **1**, a π* orbital centred on the bridging N1=S1=N2 moiety. While a stable computed structure with P attached

to S could not be found, a significantly stabilized structure **2** (-84 kJ/mol) was found with Ph_3P attached to N1 (Figure 2), which already has a greatly elongated N1–S3 bond (2.539 Å). Such a rapid migration from S to N has been demonstrated previously for the reaction of phosphines with sulfur diimides.[21] The reaction of Ph_3P with 1,3,2,4-benzodithiadiazines also results in the extrusion of a ring nitrogen atom to form an iminophosphorane substituent at sulfur in a smaller ring.[22] Complete severance of the N1–S3 bond leads to the chain intermediates **3** (all atom numbers refer to usage in Figure 1). Although stable intermediates can be found in both the *exo*-**3** and *endo*-**3** conformations, the former is 20 kJ/mol lower in energy. In both isomers, the folded conformations facilitate a through-space S···S contact (2.798 Å *exo*, 2.804 Å *endo*) in their HOMOs that strongly resemble the transannular bonds in the final products (inset to Figure 2). From these intermediates, a facile, symmetry-allowed 1,3-N shift, involving just a simple rotation about the S3–N3 bond, converts the N3–S2 linkage to an N3–S1 linkage, whereby the ArP=N– substituted trithiatetrazocines **4c**-*exo* or **4c**-*endo* isomers are produced. The isomeric preference in the final products are reversed from those in the computed intermediates, with the **4c**-*endo* isomer lower in energy than **4c**-*exo* by 16 kJ/mol. The small differences in energies amongst **4c**-*exo*, **4c**-*endo*, **3c**-*exo* and **3c**-*endo* fits well with the observed equilibria of these species in solution,[15c,d] though we note that there is spectroscopic evidence for only one isomer of **3**. These computed energies are estimates that do not take into account dispersion forces (which can be substantial in e.g. the folded geometries with many aryl groups) nor solvent influences. Nevertheless, these DFT-computed structures provide an appealing confirmation of the mechanism determined from NMR spectroscopy. There exist significant precedents for the Ph_3P=N–S–N– chain fragments in **3**; for example, Ph_3P=N–S–N=S=S, **I** (Chart 1), has been prepared in bulk and structurally characterized by single-crystal X-ray crystallography.[19]

2.5 Voltammetry

Cyclic and square wave voltammograms on solutions of the series of compounds **4** and **5** in CH_2Cl_2 at temperatures between 0 - 22 °C with 0.4 M [^{n}Bu$_4$N][PF_6] as the supporting electrolyte all gave rise to two closely spaced reduction processes and at least one oxidation process within the solvent/electrolyte window (–2.5 to +1.6 V). Representative voltammograms of compound **4c** in CH_2Cl_2 including the internal ferrocene reference are shown in Figure 3. All potential data are given with respect to $E^{0/}_{Fc^{+/0}}$, the formal potential for the $Fc^{+/0}$ redox couple, and are reported in Table 3 for a scan rate of 0.2 V s^{-1} (further details in the Supporting Information.) There is very good agreement between the potential data from SWV and CV experiments.

Table 3. Summary of cyclic voltammetric data for **4** and **5**. [a]

Compound	R =	conc (mM)	E_p^{c1}, V	E_p^{c2}, V	E_p^{a3}, V	E_{cell}^{a3-c1}, V
4a [b]	4-CH_3O	2.64	−1.99	−2.26	0.94	2.93
4b [b]	4-CH_3	4.55	−1.96	−2.23	1.00	2.96
4c [b]	4-H	2.53	−1.97	−2.26	1.03	3.00
4d [b]	4-Cl	2.91	−1.94	−2.27	1.06	3.00
4e [b]	3-CF_3	1.85	−1.86	−2.22	1.09	2.95
4f [b]	4-CF_3	1.66	−1.86	−2.23	1.09	2.95
5a [c]	4-CH_3O	2.15	−1.99	−2.34	0.94	2.93
5b [c]	4-CH_3	3.08	−1.98	−2.34	0.97	2.95
5c [c]	4-H	2.53	−1.95	−2.32	0.98	2.93
5d [c]	4-Cl	1.78	−1.94	−2.35	1.00	2.94
5e [c]	3-CF_3	1.35	−1.89	−2.31	1.06	2.95
5f [c]	4-CF_3	1.67	−1.89	−2.32	1.06	2.95

[a] Obtained at a GC electrode, area = 0.066 cm^2 at ν = 0.2 V s^{-1} and T = 21 ± 2 °C in CH_2Cl_2 solutions with 0.4 M [BuN_4][PF_6]. All potentials are vs. $E^{0/}_{Fc^{+/0}}$. [b] Ar_3P = PPh_3. [c] Ar_3P = P{C_6H_4-4-(OCH_3)}.

For all twelve compounds, the first cathodic process (E_p^{c1}) showed only a small return wave at scan rates of 50 V s^{-1} or greater and temperatures of 0 °C. There was also a small but noticeable shift in the peak potential E_p^{c1} towards more positive values as the substituent R on the heterocyclic aryl group varied from electron-donating to electron-withdrawing. The overall shift in potential was 0.13 V for **4a–f**, and 0.10 V for **5a–f**, with no noticeable effect which could be attributed to the nature of the iminophosphorane group. The oxidation process was also found to be irreversible at the temperatures and scan rates that were investigated. It displayed a similar trend in the peak potentials, with E_p^{a3} shifting to more positive values (0.15 V for **4a–f** and 0.12 V for **5a–f**) with the increased electron-withdrawing ability of R on the heterocyclic aryl ring. Again there is no influence on these potentials by the iminophosphorane group. By comparison to previous data on the related heterocycles **C** and **D1,2**, the E_p^{c1} and E_p^{a3} potentials indicate that **4** and **5** are more difficult to reduce and easier to oxidize by more than 0.5 V.[9a,c] Interestingly, the E_{cell} values (that is, the redox stability window for the neutral species) are extremely similar to that of **D1**:E = $CN(CH_3)_2$ (2.969 V).[9a,c]

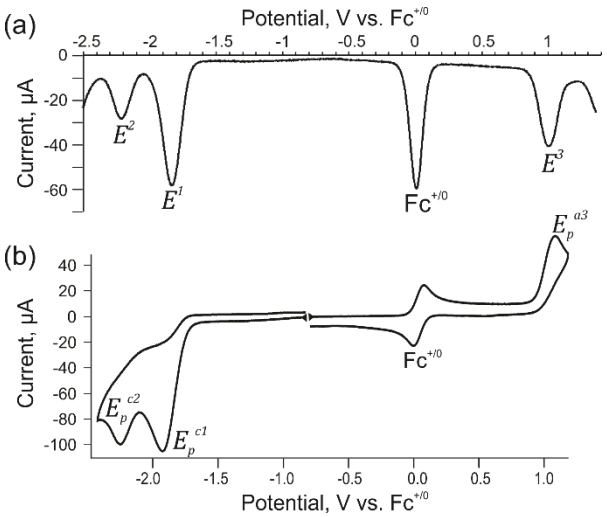

Figure 3. Square wave (a) and composite cyclic (b) voltammogram of a 2.9 mM soln. of **4d** in CH_2Cl_2 on a GC electrode at 22 °C, 0.4 M [^{n}Bu$_4$N][PF_6], v = 0.2 V s^{-1} along with 0.42 mM ferrocene, as an internal reference (initial scan directions from the open cell potential in CV are indicated).

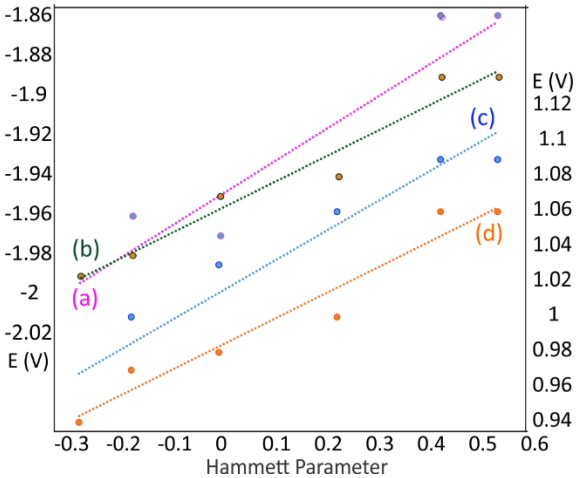

Figure 4. Correlations of peak potentials with Hammett σ_p and σ_m parameters for (a) E_p^{c1} of **4**; (b) E_p^{c1} of **5** (left hand vertical scale); (c) E_p^{a3} of **4** and (d) E_p^{a3} of **5** (right hand vertical scale).

The influence of the remote aryl substituents R on the redox potentials for all four series ($E_p^{c1}$and E_p^{a3} for **4** and **5**) correlate reasonably well with the Hammett parameters (Figure 4) of the substituents. The small slopes of the regression lines (0.13 to 0.16 V per Hammett index unit) compare well with those of other thiazyl

heterocycles. Thus, in 4-aryl-1,2-dithia-3,5-diazolyls **7**, neutral 7π heterocycles where the redox molecular orbital (RMO) is the same for oxidation and reduction and is nodal at the substituted C atom, slopes of 0.15 V per index were obtained.[14g,h] Similarly, the reduction of 1,2,3,5,7-dithiatetrazocines (**C**) for which the RMO is also nodal, the slope is 0.11 V per index. By contrast, for oxidation of these heterocycles, for which the RMO are conjugated to the aryl rings, the slope obtained was 0.51 V per index (see Supporting Information for the associated data).[9a,c] A consideration of the Kohn-Sham orbital surfaces for neutral **4c** is consistent with minimal aryl ring or iminophosphorane contributions to both RMO, in accordance with a purely inductive ring substituent influence. Both these RMO involve the transannular S···S bond, i.e. the filled, bonding, HOMO and the empty, anti-bonding, LUMO (Figure 5a,b). The similarity to the folded all-carbon analogue **D1**: E = $CN(CH_3)_2$ is again striking.[9a]

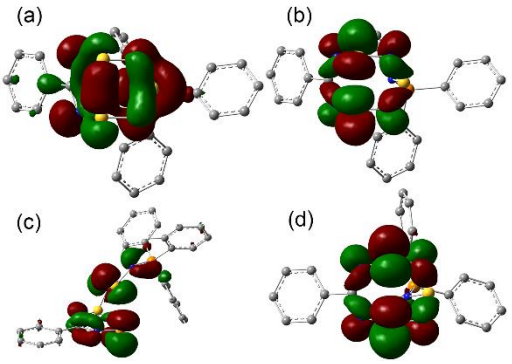

Figure 5. Redox Molecular Orbitals computed for **4c**: (a) Oxidation at the HOMO and (b) reduction at the LUMO. (c) RMO for reduction of **3c**-*exo*. (d) Computed SOMO of **4c**$^{-\bullet}$.

The peak potentials for the second cathodic process (E_p^{c2}) are, by contrast, essentially invariant with substituent type on the heterocyclic aryl ring, with average values of –2.25 ± 0.02 V for **4a–f** and –2.33 ± 0.02 V for **5a–f**. Significantly, these values do change between phosphine series (R' = Ph to 4-$CH_3OC_6H_4$) by approximately 0.1 V. A similar difference in potentials has been seen for the reduction of naphthalene versus mono-methoxynaphthalene,[23] suggesting that this potential shift is reasonably attributed to the greater electron-donating capacity of *tris*(4-methoxyphenyl)phosphine compared to triphenylphosphine. It may be inferred that this second process is localized on the Ar'$_3$P=N–S region of the molecule. First of all, with spectroscopic evidence for equilibria in solution, it needs to be considered whether E_p^{c2} could involve reduction of **3**-*exo* (Figure 5c). Against this notion is the known small concentration of **3a**-*exo* compared to the peak currents obtained for this process.[15d] On the other hand, in view of the results obtained from EPR studies (see below), the presence of phosphorane-centred decomposition products formed even at greatly reduced temperatures subsequent to the one electron reduction process E_p^{c1} is also strongly indicated. Attempts to outrun such (a) chemical step(s) by fast scanning (>1 V s^{-1}) are hindered by significant broadening of the peaks and an overall shift of the E_p^{c2} values towards more negative values which are outside of the solvent/electrolyte window. As a result, the identification of this second reduction process remains unconfirmed. Nevertheless, a proposed mechanism for the decomposition of **4**$^{-\bullet}$ or **5**$^{-\bullet}$ induced by E_p^{c1} produces neutral Ar'$_3$P=N-S≡N; perhaps E_p^{c2} involves a *first* reduction of this iminophosphorane (see below).

2.6. In situ electrochemical-EPR spectroscopy experiments

The irreversible nature of the CV processes for reduction suggested that the observation of any radicals from this system would be challenging. However, given our recent success with the $C_2N_4S_2$ and $P_2N_4S_2$ rings [9a] coupled with the development of the *in situ* electrochemical cell which could be used for low temperature studies,[14a] the detection of such transient radicals seemed worth attempting. *In situ* electrochemical EPR reduction

experiments were conducted in CH_2Cl_2 at temperatures between –90 and 0 °C for compounds **5a**, **5c**, and **5e** utilizing the low-temperature SEEPR cell and a modified version of the gold-micromesh working electrode first described by Neudeck and Kress.[24] For these three compounds**,** reductive electrolysis at –2.0 V vs $E^{0/}_{Fc^{+/0}}$ at –50 °C gave rise to strong EPR signals from single 82 s scans.

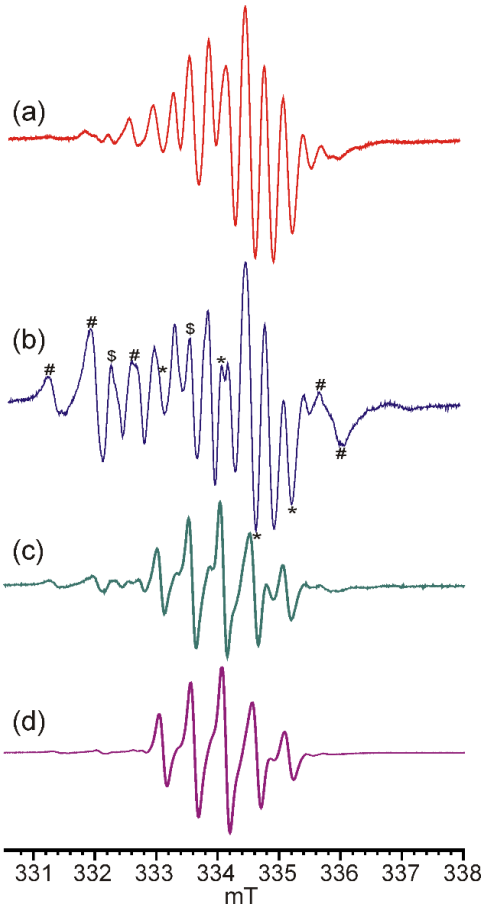

Figure 6. (a) *In situ* first derivative EPR spectrum obtained during reductive electrolyses (82 s single scan) of a 3.14 mM solution of **5a** in CH_2Cl_2 at a gold mesh electrode at –50 °C; (b) – (d) EPR spectra observed from further 82 s scans collected subsequent to reductive electrolysis, with a 6-minute wait before (d).

Representative spectra from the reductive electrolysis of **5a** are shown in Figure 6. The spectra for these three derivatives show a remarkably uniform *first* signal and similar subsequent evolution of the signals after electrolysis is halted. The spectra were notably difficult to measure as merely raising the temperature a further 10 °C rendered the primary radicals unobservable. At a temperature of –50 °C the spectrum for the radical anion **5a**$^{-\bullet}$ could be observed, but other peaks stemming from decomposition products were already evident on the first scan (Figure 6a). Subsequent scans of **5a** show the radical anion spectrum decaying rapidly with the growth of peaks stemming from other species (Figure 6b,c). After two or more sequential 82 s scans without additional electrolysis at –50°C, the signals became dominated by a five-line pattern with hyperfine splitting (HFS) of 0.51 mT (Figure 6c). After just a few minutes, only the signal for this final, persistent, decomposition product remained (Figure 6d). The five-line pattern with a 1:2:3:2:1 intensity ratio and a(N) = 0.51 mT and g = 2.0105, indicates that the decomposition product is almost certainly the stable neutral radical 4-methoxyphenyl-1,2,3,5-dithiadiazolyl **8a**,[14h] albeit distorted by a line-width variation caused by slow molecular tumbling at –50 °C of this known radical.

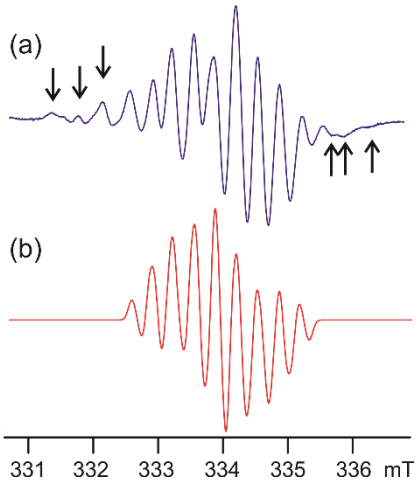

Figure 7. (a) *In situ* first derivative EPR spectrum obtained during reductive electrolyses (82 s single scan) of a 3.14 mM solution **5e** at a gold mesh electrode at –50°C in CH_2Cl_2 (0.4 M [^{n}Bu$_4$N][PF_6]) and modulation frequency 100 kHz, modulation amplitude = 0.2 mT, and (b) simulation obtained using WinSim v.0.98 [25] using the parameters in Table 4. For spectra of **5a**$^{-\bullet}$ and **5c**$^{-\bullet}$, see Supporting Information.

After careful comparison of all spectra, it became possible to distinguish the primary radical signal from those of the various decomposition species (signal locations indicated by arrows in Figure 7a). There is *remarkable similarity* in these signals from e.g. **5a**$^{-\bullet}$, **5c**$^{-\bullet}$ and **5e**$^{-\bullet}$, such that within the experimental error they have identical splitting and intensities. A very good simulation of these signals could be obtained by using single ^{31}P and ^{14}N nuclei and two sets of two ^{14}N (experimental and simulation shown for a spectrum of **5e**$^{-\bullet}$ in Figure 7), with Gaussian line shapes indicative of further unresolved splitting (to various ^{1}H nuclei). These simulations are in excellent agreement to the computed HFS values at the UB3LYP/6-311G+(d,p)//UB3LYP/6-31G(d,p) level of theory on geometry optimized *endo*-**4c**$^{-\bullet}$ (Table 4, Figure 8). The proportionately poorer fit of the ^{31}P HFS is a known limitation of this DFT method for phosphorus and indeed for other 3rd-period non-metals.[26] The line-fitting procedure we used is affected by the presence of the minor impurity signals, so that simulations taken on different spectra lead to slightly different results. The similarity of spectra from different species is consistent with the computed σ* SOMO of *endo*-**4c**$^{-\bullet}$ (Figure 5d), which is almost identical to that of the LUMO of neutral *endo*-**4c** except for the increase in S···S to 3.036 Å due to population with the single electron. That is to say, the spin density is heavily concentrated on the heterocyclic CN_4S_3 core of the radical anions and the substituent effects are weak. With the quality of EPR spectra available in this work further optimization of fits to reliably detect subtle differences in HFS amongst different **4**$^{-\bullet}$ and **5**$^{-\bullet}$ species is not feasible.

Table 4. Experimental and DFT calculated EPR data for free radical **5e**$^{-\bullet}$.[a]

line width mT	nucleus	expt HFS (mT)	calcd HFS (mT)[b]
0.05	^{31}P	0.078	–0.053
	$^{14}N_1$	0.031	–0.042
	$^{14}N_{2,3}$	0.256[c]	0.295
	$^{14}N_{4,5}$	0.341[c]	0.336

[a] The *g*-value is 2.0098. [b] Gas-phase values from UB3LYP/6-311G+(d,p) calculations of **4c**$^{-\bullet}$. [c] The assignment of these two nitrogen HFS values depends entirely on the fit to the calculated values.

2.7. Possible Mechanism for the Decomposition of the Radical Anions

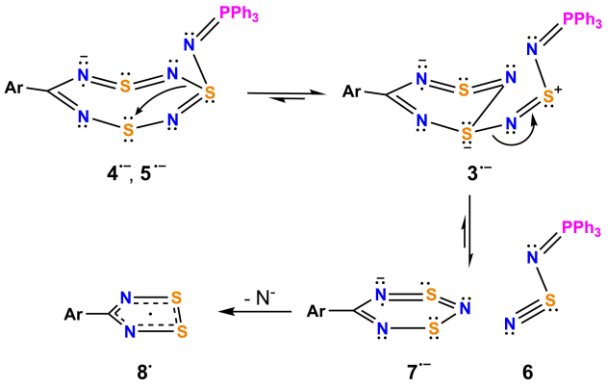

Scheme 3. Proposed mechanism for the decay of **4**$^{-\bullet}$ and **5**$^{-\bullet}$

These interesting EPR data, in conjunction with the electrochemical evidence, suggest that the radical anions **4** $^{-\bullet}$ and **5** $^{-\bullet}$ can decompose (Scheme 3) in such a way that the unpaired electron is retained in the carbon-containing portion of the initial larger ring (which starts off with the higher spin density). It is suggested that the well-attested 1,3-nitrogen shift reaction would produce the radical anion **3**$^{-\bullet}$, for which the neutral analogue has been shown to be an intermediate in the formation of **4** from **5** (see above).[15d] Elimination of the neutral $R_3P{=}N{-}S{\equiv}N$ compound **6** from **3**$^{-\bullet}$ may produce **7**$^{-\bullet}$, the unstable radical anion of a dithiatriazine. This will decompose rapidly to neutral **8**$^{\bullet}$. DFT calculations at the UB3LYP/6-311+G(d,p)//UB3LYP/6-31G(d,p) level of theory indicate that hyperfine splitting in **7**$^{-\bullet}$ (Figure 8) should be dominated by one very large ^{14}N term (~1.1 mT); signals marked by $ in Figure 6b are consistent with this prediction, and in some experiments these peaks predominate shortly after decay of the radical anions **4** $^{-\bullet}$ and **5** $^{-\bullet}$. The behavior of trithiatetrazocine radical anions is thus fundamentally different from that of the symmetrical radical anions $[RCN_2S_2N_2CR]^{-\bullet}$, **C** and **D1**,**2**, whose first-order decomposition does not produce any persistent radicals.[9a] DFT computation at the same level of theory on **3**$^{-\bullet}$ predicts a much larger ^{31}P HFS value and predicts spectra that are overall *wider* than those of **4c** $^{-\bullet}$ and **5**$^{-\bullet}$. Thus, the signals observed immediately subsequent to electrolysis, marked as # in Figure 6b, could be due to this radical anion. However, we cannot exclude the possibility that the decomposition of the initially produced radicals **4**$^{-\bullet}$ and **5**$^{-\bullet}$ can proceed by several divergent paths, and that therefore the species responsible for the signals marked # or $ are due to spin-bearing moieties centred on the iminophosphorane fragments, such as **9**$^{-\bullet}$ (Figure 8). In this connection, we recall the evidence from voltammetry that process E_p^{c2} occurs at an RMO that is iminophosphorane-centred. That *may* be the intermediate **3**$^{-\bullet}$ (Figure 8); alternatively it could be due to reduction of a dissociated iminophosphorane species such as **6** (see above), producing yet other radicals.[19]

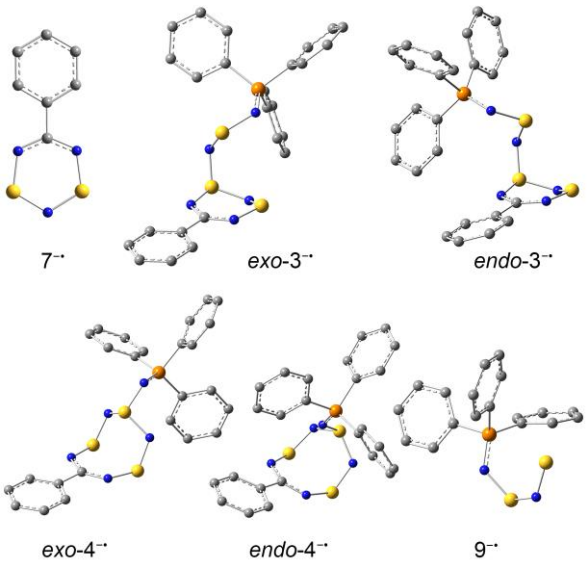

Figure 8. UB3LYP/6-31G(d,p) computed geometries for several radical anions.

3. Experimental Section

The full experimental details for synthesis, spectroscopic and analytical characterizations are provided in the Supporting Information.

3.3. Crystallography

Details of the crystallographic experiments for **1d**, **4a,b,d-f** and **5a-f** are provided in the Supporting Information. Tables of crystal and refinement parameters are found in Table S4. Full archival data has been deposited with the Cambridge Structure Database under deposition numbers CCDC 1581293-1581304.

3.4. Electrochemical Procedures

Voltammetry, SEEPR, bulk electrolysis, and *ex situ* EPR experiments were conducted as in our previous studies using the same apparatus, electrodes and so forth except as noted below.[9a, 14] The potentials for **4** and **5** are reported versus the operative formal potential, $E^{0/}_{Fc^{+/0}}$, for the ferrocene/ferrocenium redox couple designated as $Fc^{+/0}$, which was used as an internal standard. In situ EPR experiments (Bruker EMX Plus spectrometer, 9.8 GHz) were conducted on solutions of compounds **5a**, **5c**, and **5e** in CH_2Cl_2/[^{n}Bu$_4$N][PF_6] at temperatures between –90 and 0 °C using the miniature solution cell described previously.[9a] Simulations of EPR spectra were performed with Bruker Simfonia (version 1.25) and WinSim (version 0.98, 2002) softwares.[25] Spectral parameters: conversion times = 81.92 s, sweep width = 10.0 mT, modulation amplitude = 0.2 mT.

3.5. Computation

Computational studies were performed with Gaussian 03W version 6.1 at the B3LYP/6-311G+(d,p)//B3LYP/6-31G(d,p) level of theory for the diamagnetic species and UB3LYP/6-311G+(d,p)//UB3LYP/6-31G(d,p) for the radical anions.[27] That the reported structures are at least local minima was confirmed by frequency calculations showing no imaginary frequencies. GaussView 5.0 was used for visualization of structures and molecular surfaces.

4. Conclusions

By the combined use of electrochemistry, EPR spectroscopy and hybrid DFT calculations, we have been able to identify the radical anions of phosphoraniminato-trithiatetrazocines $\mathbf{4}^{-\bullet}$ and $\mathbf{5}^{-\bullet}$ for the first time. The spectra are extremely difficult to obtain, requiring painstaking work within a very narrow accessible temperature window. Compared to our previous study of the related dithiatetrazocines, $\mathbf{4}^{-\bullet}$ and $\mathbf{5}^{-\bullet}$ decompose to several EPR-active species in an apparent cascade process, with the final signal intensity eventually residing in known stable radical $\mathbf{8}^{\bullet}$, which is a very logical breakdown product of $\mathbf{4}^{-\bullet}$ or $\mathbf{5}^{-\bullet}$. The assignment of the signals from $\mathbf{4}^{-\bullet}$ and $\mathbf{5}^{-\bullet}$ is strongly dependent upon the predictive power that the DFT calculations provide and we were unable to obtain an ideal EPR spectrum for any example of this radical anion. It is particularly interesting that $\mathbf{4}^{-\bullet}$ and $\mathbf{5}^{-\bullet}$ break down to $\mathbf{8}^{\bullet}$ while neither $\mathbf{C}^{-\bullet}$ nor $\mathbf{D1}^{-\bullet}$ produce any persistent radicals upon *in-situ* electrolysis. For these latter systems, decomposition of the primary radical leads exclusively to diamagnetic products. Conceivably, it is the asymmetry in spin distribution of the trithiatetracocinyl that biases towards the generation of $\mathbf{8}^{\bullet}$. We note that *thermal* and *photochemical* degradation of thiazyl compounds has been demonstrated to produce very similar types of free radicals.[28] Further work on thiazyl-rich compounds is underway in our laboratory. An investigation of the aromatic heterocycles **B** presents a particularly interesting target.

Acknowledgments

The authors gratefully acknowledge financial support from the Natural Sciences and Engineering Research Council (Canada), the Alberta Ingenuity Fund (T.L.R.) and the University of Lethbridge. The Canadian Foundation for Innovation and the Government of Alberta funded the EPR Spectrometer. The University of Lethbridge and NSERC funded the X-ray Diffractometer. Support from Prof. T. Chivers, University of Calgary, during early phases of this project is gratefully acknowledged, as is the Department of Chemistry for hosting our visits.

Conflicts of Interest

The authors declare no conflict of interest.

References and Notes

1. For important reviews see: (a) T. Chivers, *A Guide to Chalcogen-Nitrogen Chemistry* **2005**, Singapore: World Scientific Publishing Co. (b) T. Chivers, R. S. Laitinen, *Chem Soc. Rev.* **2017**, *46*, 5182-5192. (c) R. T. Boeré, T. L. Roemmele, *Chalcogen–Nitrogen Radicals*. In: Jan Reedijk and Kenneth Poeppelmeier, editors. *Comprehensive Inorganic Chemistry II*, Vol 1. **2013**, Oxford: Elsevier, 375-411. (d) A. V. Lonchakov, O. A. Rakitin, N. P. Gritsan, A. V. Zibarev, *Molecules* **2013**, *18*, 9850-9900. (e) R. G. Hicks, in Stable Radicals Fundamentals and Applied Aspects of Odd-Electron Compounds, ed. R. G. Hicks, 2010, Wiltshire: John Wiley & Sons, Ltd., p. 317. (f) F. Blockhuys, N. P. Gritsan, A. Y. Makarov, K. Tersago, A. V. Zibarev, *Eur. J. Inorg. Chem.* **2008**, 655-672. (g) J. M. Rawson, F. Palacio, *Struct. Bonding (Berlin)* **2001**, *100*, 93–128. (h) R. T. Boeré, T. L. Roemmele, *Coord. Chem. Rev.* **2000**, *210*, 369-445. (i) J. M. Rawson, *Coord. Chem. Rev.* **1999**, *189*, 135–168. (j) T. Torroba, *J. Prakt. Chem.* **1999**, *341*, 99-113. (k) J. M. Rawson, A. J. Banister, I. Lavender, *Adv. Heterocycl. Chem.* **1995**, *62*, 137-247. (l) R. T. Oakley, *Prog. Inorg. Chem.* **1988**, *36*, 299-391. (m) T. Chivers, in *The Chemistry of Inorganic Homo- and Heterocycles*; I. Haiduc, D. B. Sowerby, Eds., **1987** London, U.K.: Academic, Vol. 2, pp 793-870.
2. (a) A. Mailman, A. A. Leitch, W. Yong, E. Steven, S. M. Winter, R. C. M. Claridge, A. Assoud, J. S. Tse, S. Desgreniers, R. A. Secco, R. T. Oakley, *J. Am. Chem. Soc*. **2017**, *139*, 2180-2183. (b) A. Mailman, J. W. L. Wong, S. M. Winter, R. C. M. Claridge, C. M. Robertson, A. Assoud, W. Yong, E. Steven, P. A. Dube, J. S. Tse, S. Desgreniers, R. A. Secco, R. T. Oakley, *J. Am. Chem. Soc*. **2017**, *139*, 1625-1635. (c) J. M. Rawson, A. Alberola, A. Whalley, *J. Mater. Chem.* **2006**, *16*, 2560–2575. (d) A. W. Cordes, R. C. Haddon, R. T. Oakley,

Adv. Mater. **1994**, *6*, 798–802. (e) A. J. Banister, I. Lavendar, J. M. Rawson, *Adv. Heterocycl. Chem.* **1995**, *62*, 137-247.

3. (a) K. Lekin, K. Ogata, A. Maclean, A.Mailman, S. M. Winter, A. Assoud, M. Mito, J. S. Tse, S. Desgreniers, N. Hirao, P. A. Dube, R. T. Oakley, *Chem. Commun*. **2016**, 52, 13877-13880. (b) S. M. Winter, S. Hill, R. T. Oakley, *J. Am. Chem. Soc.* **2015**, *137*, 3720-3730. (c) Y. Beldjoudi, A. Arauzo, F. Palacio, M. Pilkington, J. M. Rawson, *J. Am. Chem. Soc.* **2016**, *138*, 16779-16786. (d) J. M. Rawson, J. Luzon, F. Palacio, *Coord. Chem. Rev.* **2005**, *249*, 2631–2641. (e) A. Alberola, R. J. Less, C. M. Pask, J. M. Rawson, F. Palacio, P. Oliete, C. Paulsen, A. Yamaguchi, D. M. Murphy, R. D. Farley, *Angew. Chem., Int. Ed. Engl*. **2003**, *42*, 4782–4785.

4. (a) S. Vela, F. Mota, F, M. Deumal, R. Suizu, Y. Shuku, A. Mizuno, K. Awaga, M. Shiga, J. J. Novoa, J. Ribas-Arino, *Nature Communications* **2014**, *5*, 4411:1-9. (b) A. J. Banister, N. Bricklebank, W. Clegg, M. R. J. Elsegood, C. I. Gregory, I. Lavender, J. M. Rawson, B. K. Tanner, *J. Chem. Soc., Chem. Commun.* **1995**, 679-680. (c) A. J. Banister, N. Bricklebank, I. Lavender, J. M. Rawson, C. I. Gregory, B. K. Tanner, W. Clegg, M. R. J. Elsegood, F. Palacio, *Angew. Chem. Int. Ed. Engl.* **1996**, *35*, 2533-2535.

5. (a) S. V. Klementyeva, N. P. Gritsan, M. M. Khusniyarov, A. Witt, A. A. Dmitriev, E. A. Suturina, N. D. D. Hill, T. L. Roemmele, M. T. Gamer, R. T. Boeré, P. W. Roesky, A. V. Zibarev, S. N. Konchenko, *Chem. Eur. J.* **2017**, *23*, 1278-1290. (b) D. A. Haynes, L. J. van Laeren, O. Q. Munro, *J. Am. Chem. Soc.* **2017**, *139,* 14620-14637. (c) C. Y. Ang, S. L. Kuan, G. K. Tan, L. Y. Goh, T. L. Roemmele, X. Yu, R. T. Boeré, *Can. J. Chem.* **2015**, *93*, 181-195. (d) K. E. Preuss, *Coord. Chem. Rev.* **2015**, *289-290*, 49-61. (e) K. E. Preuss, *Dalton Trans.* **2007**, 2357–2369. (f) N. G. R. Hearns, R. Clerac, M. Jennings, K. E. Preuss, *Dalton Trans.* **2009**, 3193–3203. (g) N. G. R. Hearns, E. M. Fatila, R. Clerac, M. Jennings, K. E. Preuss, *Inorg. Chem.* **2008**, *47*, 10330–10341.

6. M. M. Cortese-Krott, A. R. Butler, J. D. Woollins, M. Feelisch, *Dalton Trans*. **2016**, *45*, 5908-5919.

7. (a) R. J. Gillespie, J. P. Kent, J. F. Sawyer, Dr. R. Slim, J. D. Taylor, *Inorg. Chem.* **1981**, *20*, 3799-3812. (b) M. Trsic, W. G. Laidlaw, R. T. Oakley, *Can J. Chem.* **1982**, *60*, 2281-2285.

8. (a) C. Knapp, P. G. Watson, E. Lork, D. H. Friese, R. Mews, A. Decken, *Inorg. Chem.* **2008**, *47*, 10618–10625. (b) H. U. Höfs, G. Hartmann, R. Mews, G. M. Sheldrick, *Angew. Chem., Int. Ed. Engl.* **1984**, *23*, 988-989.

9. (a) R. T. Boeré, A. M. Bond, T. Chivers, S. W. Feldberg, T. L. Roemmele, *Inorg. Chem.* **2007**, *46*, 5596–5607. (b) K. H. Moock, K. M. Wong, R. T. Boeré, *Dalton Trans.* **2011**, *40*, 11599-11604. (c) R. T. Boeré, K. H. Moock, S. Derrick, W. Hoogerdijk, K. E. Preuss, J. Yip, M. Parvez, *Can. J. Chem.* **1993**, *71*, 473–486. (d) M. Parvez, R. T. Boeré, S. Derrick, K. H. Moock, *Acta Crystallogr., Sect. C* **1995**, *51*, 2116–2118. (e) François Magnan, I. Korobkov, J. Brusso, *New. J. Chem.* **2015**, *39*, 7272-7280. (f) S. S. Afjeh, A. A. Leitch, I. Korobkov, J. L. Brusso, *RSC Adv.*, **2013**, *3*, 23438-23444. (g) A. D. Bond, D. A. Haynes, J. M. Rawson, *Can. J. Chem.* **2002**, *80*, 1507–1517. (h) U. Scholz, H. W. Roesky, J. Schimkowiak, M. Noltemeyer, *Chem. Ber.* **1989**, *122*, 1067-1070.

10. A. J. Banister, *Nature Physical Science*, **1972**, *237*, 92-93.

11. (a) S. Dell, D. M. Ho, R. A. Pascal, Jr., *Inorg. Chem.* **1996**, *35*, 2866-2871. (b) R. A. Pascal, Jr., R. P. L'Esperance, *J. Am. Chem. Soc.* **1994**, *116*, 5167-5171. (c) M. Amin, C. W. Rees, *J. Chem. Soc., Perkin Trans. I* **1989**, 2495–2501. (d) M. Amin, C. W. Rees, *J. Chem. Soc., Chem. Commun.* **1989**, 1137-1138. (e) R. T. Boeré, A. W. Cordes, S. L. Craig, R. T. Oakley, R. W. Reed, *J. Am. Chem. Soc.* **1987**, *109*, 868-874. (f) R. T. Boeré, A. W. Cordes, R. T. Oakley, R. W. Reed, *J. Chem. Soc., Chem. Commun.* **1985**, 655-656. (g) I. Ernest, W. Holick, G. Rihs, D. Schomburg, G. Shoham, D. Wenkert, R. B. Woodward, *J. Am. Chem. Soc.* **1981**, *103*, 1540-1544.

12. (a) R. T. Boeré, T. L. Roemmele, M. K. Krall, *Molecules*, **2014**, *19*, 1956-1975. (b) T. Chivers, R. T. Oakley, *Top. Curr. Chem*. **1982**, *102*, 117-147 (c) T. Chivers, L. Fielding, W. G. Laidlaw, M. Trsic, *Inorg. Chem.* **1979**, 18, 3379-3388. (d) H. P. Fritz, R. Bruchhaus, *Electrochim. Acta* **1984**, *29*, 947-950.

13. (a) R. Gleiter, G. Haberhauer, *Coord Chem. Rev*. **2017**, *344*, 263-298. (b) A. G. Papadopoulos, N. D. Charistos, A. Muñoz-Castro, *New. J. Chem.* **2016**, *40*, 5090-5098. (c) R. Gleiter, G. Haberhauer, S.

Woitschetzki, *Chem. Euro. J*. **2014**, *20*, 13801-13810. (d) K. E. Preuss, *Polyhedron* **2014**, *79*, 1-15. (e) Z-H Cui, H. Lischka, H. Z. Beneberu, M. Kertesz, *J. Am. Chem. Soc.* **2014**, *136*, 12958-12965. (e) J. Moilanen, A. J. Karttunen, H. M. Tuononen, T. Chivers, *J. Chem. Theory Comput*. **2012**, *8*, 4249−4258.

14. (a) R. T. Boeré, T. L. Roemmele, X. Yu, *Inorg. Chem.* **2011**, *50*, 5123-5136. (b) R. T. Boeré, T. Chivers, T. L.Roemmele, H. M. Tuononen, *Inorg. Chem.* **2009**, *48*, 7294-7306. (c) T. L. Roemmele, J. Konu, R. T. Boeré, T. Chivers, *Inorg. Chem.* **2009**, *48*, 9454-9462. (d) H. F. Lau, V. W. L. Ng, L. L. Koh, G. K. Tan, L. Y. Goh, T. L. Roemmele, S. D. Seagrave, R. T. Boeré, *Angew. Chem. Int. Ed. Engl.* **2006**, *45*, 4498-4501. (e) R. T. Boeré, L. Y. Goh, C. Y. Ang, S. L. Kuan, H. F. Lau, V. W. L. Ng, T. L. Roemmele, S. D. Seagrave, *J. Organomet. Chem.* **2007**, *692*, 2697-2704. (f) H. F. Lau, P. C. Y. Ang, V. W. L. Ng, S. L. Kuan, L. Y. Goh, A. S. Borisov, P. Hazendonk, T. L. Roemmele, R. T. Boeré, R. D. Webster, *Inorg. Chem.* **2008**, *47*, 632-644. (g) R. T. Boeré, K. H. Moock, *J. Am. Chem. Soc.* **1995**, *117*, 4755-4760. (h) R. T. Boeré, K. H. Moock, M. Parvez, *Z. Anorg. Allg. Chem.* **1994**, *620*, 1589-1598.

15. (a) R. T. Boeré, R. T. Oakley, A. W. Cordes, *Acta Cryst.* **1985**, *C41*, 1686–1687. (b) T. Chivers, J. F. Richardson, N. R. M. Smith, *Inorg. Chem.* **1986**, *25*, 272–275. (c) C. Knapp, E. Lork, R. Maggiulli, P. G. Watson, R. Mews, T. Borrmann, W. D. Stohrer, U. Behrens, *Z. Anorg. Allg. Chem.* **2004**, *630*, 1235-1244. (d) R. T. Boeré, A. W. Cordes, R. T. Oakley, *J. Am. Chem. Soc.* **1987**, *109*, 7781–7785. (e) R. T. Boeré, A. W. Cordes, S. L. Craig, J. B. Graham, R. T. Oakley, J. A. J. Privett, *J. Chem. Soc., Chem. Comm.* **1986**, 807-808. (f) R. T. Boeré, G. Ferguson, R. T. Oakley, *Acta Cryst.* **1986**, *C42*, 900-902. (f) The closely analogous $Ph_2PN_2S_2N_2S$–N=PPh_3 has been reported: A. W. Cordes, S. W. Liblong, S. G. Phillips, R. T. Oakley, *Inorg. Chem.* **1989**, *28*, 4147-4150.

16. (a) C. Knapp, E. Lork, R. Mews, A. V. Zibarev, *Eur. J. Inorg. Chem.* **2004**, 2446-2451. (b) C. Knapp, E. Lork, T. Borrmann, W.-D. Stohrer, R. Mews, *Eur. J. Inorg. Chem.* **2003**, 3211-3220. (c) R. T. Boeré, J. Fait, K. Larsen, J. Yip, *Inorg. Chem.* **1992**, *31*, 1417-1423. (d) K. T. Bestari, R. T. Boeré, R. T. Oakley, *J. Am. Chem. Soc.* **1989**, *111*, 1579-1584. (e) R. T. Boeré, R. T. Oakley, M. Shevalier, *Chem Comm.* **1987**, 110-112. (f) R. T. Boeré, A. W. Cordes, R. T. Oakley, *J. Chem. Soc., Chem. Commun*. **1985**, 929–930. (g) R. T. Boeré, C. L. French, R. T. Oakley, A. W. Cordes, J. A. J. Privett, S. L. Craig, J. B. Graham, *J. Am. Chem. Soc.* **1985**, *107*, 7710-7717. (h) Cordes, A. W.; Oakley, R.T.; Boeré, R.T. *Acta Crystallogr., Sect. C: Cryst. Struct. Commun.* **1985**, *41*, 1833-1834.

17. (a) C. Knapp, E. Lork, T. Borrmann, W-D. Stohrer, R. Mews, *Z. Anorg. Allg. Chem.* **2005**, *631*, 1885-1892. (b) W. Isenberg, R. Mews, *Z. Naturforsch.* **1982**, *37b*, 1388-1392. (c) T. Chivers, L. Fielding, *Chem. Comm.* **1978**, 212-213.

18. K. Dehnicke, F. Weller, *Coord. Chem. Rev.* **1997**, *158*, 103-169.

19. (a) T. Chivers, R. T. Oakley, A. W. Cordes, P. Swepston, *Chem. Commun.* **1980**, 35-36. (b) T. Chivers, R. T. Oakley, A. W. Cordes, P. Swepston, *Inorg. Chem.* **1981**, 2376-2380.

20. J. Derendorf, C. Jenne, M. Keßler, *Angew. Chem. Int. Ed*. **2017**, *56*, 8281-8284; J. Derendorf, C. Jenne, M. Keßler, *Angew. Chem.* **2017**, *129*, 8395-8398.

21. G. Kresze, in *Organic Sulphur Chemistry*. C. J. M. Stirling, Ed., **1975**, London: Butterworths, p. 65-93.

22. T. D. Grayfer, A. Yu. Makarov, I. Yu. Bagryanskaya, I. G. Irtegova, Y. V. Gatilov, A. V. Zibarev, *Heteroatom Chem.* **2015**, *26*, 42-50.

23. (a) A. Zweig, A. K. Hoffmann, *J. Org. Chem.* **1965**, *30*, 3997–4001. (b) A. Zweig, A. H. Maurer, B. G. Roberts, *J. Org. Chem.* **1967**, *32*, 1322–1329.

24. A. Neudeck, L. Kress, *J. Electroanal. Chem.* **1997**, *437*, 141–156.

25. D. R. Duling, *J. Magn. Reson., Ser. B* **1994**, *104*, 105–110.

26. (a) L. Hermosilla, P. Calle, J.M. García de la Vega, C. Siero, *J. Phys. Chem.* **2005**, *A109*, 1114-1124. (b) L. Hermosilla, P. Calle, J.M. García de la Vega, C. Siero, *J. Phys. Chem.* **2005**, *A109*, 7626-7635. (c) R. T. Boeré, H. M. Tuononen, T. Chivers, T. L. Roemmele, *J. Organomet. Chem.* **2007**, *692*, 2683–2696. (d) H. M.

Tuononen, T. Chivers, A. Armstrong, C. Fedorchuk, R. T. Boeré, *J. Organomet. Chem.* **2007**, *692*, 2705-2715.

27. Gaussian 03, Revision C.02, M. J. Frisch, G. W. Trucks, H. B. Schlegel, G. E. Scuseria, M. A. Robb, J. R. Cheeseman, J. A. Montgomery, Jr., T. Vreven, K. N. Kudin, J. C. Burant, J. M. Millam, S. S. Iyengar, J. Tomasi, V. Barone, B. Mennucci, M. Cossi, G. Scalmani, N. Rega, G. A. Petersson, H. Nakatsuji, M. Hada, M. Ehara, K. Toyota, R. Fukuda, J. Hasegawa, M. Ishida, T. Nakajima, Y. Honda, O. Kitao, H. Nakai, M. Klene, X. Li, J. E. Knox, H. P. Hratchian, J. B. Cross, V. Bakken, C. Adamo, J. Jaramillo, R. Gomperts, R. E. Stratmann, O. Yazyev, A. J. Austin, R. Cammi, C. Pomelli, J. W. Ochterski, P. Y. Ayala, K. Morokuma, G. A. Voth, P. Salvador, J. J. Dannenberg, V. G. Zakrzewski, S. Dapprich, A. D. Daniels, M. C. Strain, O. Farkas, D. K. Malick, A. D. Rabuck, K. Raghavachari, J. B. Foresman, J. V. Ortiz, Q. Cui, A. G. Baboul, S. Clifford, J. Cioslowski, B. B. Stefanov, G. Liu, A. Liashenko, P. Piskorz, I. Komaromi, R. L. Martin, D. J. Fox, T. Keith, M. A. Al-Laham, C. Y. Peng, A. Nanayakkara, M. Challacombe, P. M. W. Gill, B. Johnson, W. Chen, M. W. Wong, C. Gonzalez, and J. A. Pople, **2004**, Gaussian, Inc.: Wallingford CT.

28. (a) N. P. Gritsan, K. V. Shuvaev, S. N. Kim, C. Knapp, R. Mews, V. A. Bagryanskya, A. V. Zibarev, *Mendeleev Commun.* **2007**, *17*, 204-206. (b) K. V. Shuvaev, V. A. Bagryansky, N. P. Gritsan, A. Yu. Makarov, Y. N. Molinb, A. V. Zibarev, *Mendeleev Commun.* **2003**, *13*, 178-179.

TOC entry (text and graphics)

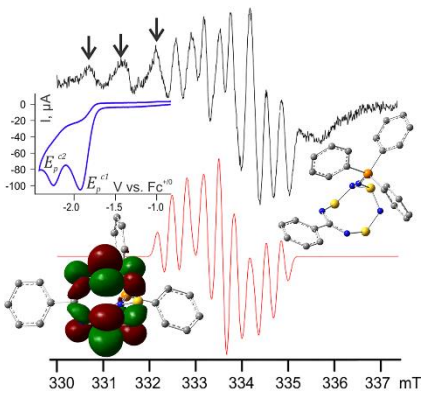

Reduction of the title compounds at -2.0 V vs. $Cp_2Fe^{0/+}$ forms anion radicals $[ArCN_2S_2N_2SN{=}PAr'_3]^{-\bullet}$, identified for the first time through *in-situ* EPR spectroelectrochemistry supported by UB3LYP/6-311+G(d,p)//UB3LYP/6-31G(d,p) hybrid DFT calculations. Even at 223 K in $CH_2Cl_2/[^nBu_4N][PF_6]$ solutions, the initially formed radicals rapidly decompose to secondary radical products amongst which well-known and stable 1,2,3,5-dithiadiazolyls $ArCN_2S_2^{\bullet}$ could be identified.

Supporting Information

Index **Page**

Section S1. Chemical Synthesis

S1.1. Reagents and General Procedures

Chlorotrimethylsilane, various organic nitriles, sulfuryl chloride, triphenylphosphine and tris(4-methyloxyphenyl)-phosphine were all obtained commercially (Aldrich). Solvents for synthetic work (CH_3CN, CH_2Cl_2) were purified using an M.Braun SPS immediately before use. S_4N_4[1], $S_3N_3Cl_3$[2], and the cage compounds **1a–f** [3] were synthesized following literature procedures and characterized by MP and IR spectroscopy. For electrochemical experiments, CH_2Cl_2 (BDH, reagent grade) was purified by distillation from CaH_2 under a nitrogen atmosphere and was purged with dry nitrogen prior to use. Electrochemical grade tetrabutylammonium hexafluorophosphate [^{n}Bu$_4$N][PF_6] (Fluka) was used as the supporting electrolyte and was kept in a desiccator prior to use. Ferrocene (Fc) was sublimed prior to use.

NMR spectra were recorded in $CDCl_3$ solutions (^{1}H and ^{13}C) on a 300 MHz Bruker Avance II spectrometer and are referenced to the solvent residuals, relative to TMS at 0 ppm. Infrared data were collected at RT on a Bruker Alpha FTIR spectrometer (diamond ATR attachment). Elemental analyses were obtained on an Elementar vario MICRO-Cube analyzer. Electronic absorption spectra were obtained on a Cary 5000 UV-Vis-NIR spectrophotometer in 1 cm quartz cuvettes. ESI Mass spectra were determined at the Mass Spectrometry Facility of the Department of Chemistry, University of Alberta in positive ion mode as CH_2Cl_2 solutions.

S1.2. Synthesis

S1.2.1. Synthesis of $PhC_6H_4CN_4S_3$-N=PPh_3 (**4c**)

At room temperature, 1.67 g (6.54 mmol) of **1c** was mixed with 1.875 g (7.148 mmol) of PPh_3 in 50 mL of dry toluene. The mixture was stirred for a few hours and, as the time passed, the color of the solution turned from reddish orange to light orange color. After stirring over night, the solvent was removed by rotary evaporator. The yellow solids were recrystallized in 50/50 mixture of CH_3CN and CH_2Cl_2, yielded 2.40 g (70.9% yield) light yellow, plate shaped crystals. M.P. (dec.): 172.6-175.3°C. IR (4000-400 region): 1456 (m), 14738 (s), 13678 (s), 1339 (s), 1291 (w), 1170(m), 1115 (s), 1082 (s), 1025 (w), 998 (w), 637 (w), 603 (w), 534 (s), 525 (s), 483 (m), 436 (w) in agreement with the literature.[4]

S1.2.2. Synthesis of $PhC_6H_4CN_4S_3$-N=PPh_3 (**4a**)

4a was prepared by the same method as **4c** by using 0.515 g (1.96 mmol) of **1a** and 0.527 g (1.85 mmol) of PPh_3 in 50 mL of distilled toluene. Recrystallization afforded 1.030 g (99.0% yield) of light yellow, needle shaped crystals. M.P. (dec.) 174.2-175.5°C. IR (4000-400 region): 1615 (s), 1516 (w), 1490 (w), 1439 (s), 1360 (vs), 1307 (m) ,1254 (s), 1172 (s), 1115 (vs), 1087 (s), 1029 (s), 998 (w), 919 (vs), 889 (s), 843 (w), 792 (s), 721 (s), 693 (s), 596 (m), 525 (s), 501 (m), 446 (s). Mass spec. m/Z (high res. ESI): 548.07905 (548.07969 cal.). Anal calc. for $C_{26}H_{22}N_5OPS_3 \cdot 0.60CH_2Cl_2$: C 53.37, H 3.91, N 11.70%, found: C 53.55, H 3.72, N 11.95% (X-ray crystallography confirms the nominal 1:1 ratio of **4a**:CH_2Cl_2 and confirms partial solvent depletion.

S1.2.3. Synthesis of *p*-$CH_3C_6H_4CN_4S_3$-N=PPh_3 (**4b**)

4b was prepared by the same method as **4c** by using 1.0185 g (3.781 mmol) of **1b** and 0.778 g (2.97 mmol) of PPh_3 in 50 mL of distilled toluene. Recrystallization afforded 1.022 g (64.8% yield) of light yellow plate shaped crystals. M.P. (dec.) 170.4-172.4°C. IR (4000-400 region): 1678 (w), 1463 (w), 1483 (m), 1437 (s), 1359 (s), 1342 (s), 1216 (m), 1178 (s), 1148 (s), 1116 (s), 1087 (s), 1026 (m), 988 (w), 918 (vs), 888 (s), 832 (m), 791 (s), 782 (s), 773 (s), 693 (s), 676 (m), 605 (m), 536 (s), 520 (s), 488 (m), 463 (s). Mass spec. m/Z (high res. ESI): 532.08482 (532.08478 cal.). Anal calc. for $C_{26}H_{22}N_5S_3P$: C 58.74, H 4.17, N 13.17%, found: C 58.82, H 4.30, N 12.90%.

3.2.4. Synthesis of *p*-$ClC_6H_4CN_4S_3$-N=PPh_3 (**4d**)

4d was prepared by the same method as **4c** by using 0.409 g (1.41 mmol) of **1d** and 0.377 g (1.44 mmol) of PPh_3 in 50 mL of distilled toluene. Recrystallization afforded 0.73 g (80.7% yield) of light yellow, plate shaped crystals. M.P. (dec.): 167.4-169.2°C. IR (4000-400 region): 1592 (m), 1574 (w), 1483 (s), 1437 (s), 1409 (s), 1350 (s), 1290 (w), 1170 (m), 1150 (vs), 1116 (vs), 1026 (w), 1016 (m), 996 (w), 917 (vs), 885 (s), 840(s), 818 (w), 786 (vs), 7636 (s), 752 (s), 719 (s), 695 (s), 658 (s), 631 (m), 616 (m), 604 (s), 537 (s), 523 (s), 498 (s), 482 (m), 449 (s). Mass spec. m/Z (high res. ESI): 552.03047 (552.03015 cal.). Anal calc. for $C_{25}H_{19}N_5S_3PCl$: C 54.39, H 3.47, N 12.69%, found: C 54.12, H 3.70, N 12.43%.

S1.2.5. Synthesis of *m*-$CH_3C_6H_4CN_4S_3$-N=PPh_3 (**4e**)

4e was prepared by the same method as **4c** by using 0.4089 g (1.255 mmol) of **1e** and 0.3983 g (1.518 mmol) of PPh_3 in 50 mL of distilled toluene. Recrystallization afforded 0.5254 g (70.9% yield) of yellow or orange, block shaped crystals. M.P. (dec.): 152.1-155.4°C. IR (4000-400 region): 1439 (m), 1366 (s), 1349 (m), 1315 (s), 1273 (s), 1169 (s), 1115 (vs), 1090 (s), 1069 (s), 1027 (w), 998 (w), 931 (s), 913 (s), 788 (s), 766 (w), 754 (m), 723 (s), 691 (s), 708 (m), 691 (s), 679 (m), 627 (w), 624 (w), 608 (w), 536 (m), 523 (s), 498 (w), 470 (m). Mass spec. m/Z (high res. ESI): 586.05771 (586.05651 cal.). Anal calc. for $C_{26}H_{19}N_5S_3PF_3$: C 53.32, H 3.27, N 11.96%, found: C 52.89, H 3.43, N 12.06%.

S1.2.6. Synthesis of *p*-$CF_3C_6H_4CN_4S_3$-N=PPh_3 (**4f**)

4f was prepared by the same method as **4c** by using 0.199 g (0.613 mmol) of **1f** and 0.162 g (0.618 mmol) of PPh_3 in 50 mL of distilled toluene. Recrystallization affording 0.250 g (69.6% yield) of orange, plate shaped crystals. M.P. (dec.) 157.4-159.4°C. IR (4000-400 region): 1439 (w), 1419 (m), 1366 (w), 1319 (vs), 1171 (m), 1114 (vs), 1065 (s), 1016 (w), 929 (s), 887 (w), 855 (w), 783 (m), 751 (w), 723 (m), 694 (m), 686 (m), 603 (w), 534 (w), 524 (m), 524 (m), 494 (w), 471 (w). Mass spec. m/Z (high res. ESI): 586.05650 (586.05651 cal.). Anal calc. for $C_{26}H_{19}N_5S_3PF_3$: C 53.32, H 3.27, N 11.96%, found: C 53.12, H 3.65, N 11.86%.

S1.2.7. Synthesis of *p*-$OCH_3C_6H_4CN_4S_3$-N=P(*p*-$OCH_3C_6H_4$)$_3$ (**5a**)

5a was prepared by the same method as **4c** by using 0.198 g (0.622 mmol) of **1a** and 0.210 g (0.596 mmol) of P(*p*-$OCH_3C_6H_4$)$_3$ in 25 mL of distilled toluene. Recrystallization afforded 0.270 g (71.3% yield) of light yellow, plate shaped crystals. M.P. (dec.): 162.7-166.7°C. IR (4000-400 region): 1595 (s), 1568 (m), 1502 (s), 1452 (m), 1406 (m), 1359 (s), 1303 (s), 1291 (s), 1261 (s), 1178 (s), 1115 (vs), 1058 (s), 1027 (s), 921 (vs), 889 (m), 836 (s), 804 (s), 782 (s), 664 (m), 621 (m), 586 (m), 541 (s), 446 (s). Mass spec. m/Z (high res. ESI): 638.11109 (638.11139 cal.). Anal calc. for $C_{29}H_{28}N_5S_3PO_4$: C 54.62, H 4.43, N 10.98%, found: C 54.75, H 4.22, N 11.05 %.

S1.2.8. Synthesis of *p*-$CH_3C_6H_4CN_4S_3$-N=P(*p*-$OCH_3C_6H_4$)$_3$ (**5b**)

5b was prepared by the same method as **4c** by using 0.508 g (1.88 mmol) of **1b** and 0.684 g (1.94 mmol) of P(*p*-$OCH_3C_6H_4$)$_3$ in 25 mL of distilled toluene. Recrystallization afforded 1.145 g (98.0% yield) of yellow, plate shaped crystals. M.P. (dec.): 171.6-172.8°C. IR (4000-400 region): 1595 (s), 1569 (s), 1502 (s), 1457 (m), 1439 (m), 1409 (m), 1357 (s), 1308 (s), 1260 (s), 1178 (s), 1115 (vs), 1081 (s), 1023 (s), 918 (vs), 887 (s), 826 (s), 803 (s), 780 (s), 726 (m), 668 (m), 620 (m), 637 (s), 450 (s). Mass spec. m/Z (high res. ESI): 622.11657 (622.11647 cal.). Anal calc. for $C_{29}H_{28}N_5S_3PO_3$: C 56.02, H 4.54, N 11.26%, found: C 55.76, H 4.48, N 11.39%.

S1.2.9. Synthesis of $PhC_6H_4CN_4S_3$-N=P(*p*-$OCH_3C_6H_4$)$_3$ (**5c**)

5c was prepared by the same method as **4c** by using 0.161 g (0.628 mmol) of **1c** and 0.216 g (0.613 mmol) of P(*p*-$OCH_3C_6H_4$)$_3$ in 50 mL of distilled toluene. Recrystallization afforded 0.280 g (75.1% yield) of orange, plate shaped crystals. M.P. (dec.): 165.8-168.7°C. IR (4000-400 region): 1595 (s), 1570 (w), 1502 (s), 1453 (w), 1409 (w), 1355 (m), 1345 (m), 1260 (s), 1179 (m), 1115 (vs), 1088 (m), 1023 (m), 882 (s), 829 (m), 804 (m), 780 (m),

699 (w), 674 (w), 624 (w), 590 (w), 541 (w), 483 (w), 441 (w). Mass spec. m/Z (high res. ESI):608.10067 (608.10082 cal.). Anal calc. for $C_{28}H_{26}N_5S_3PO_3$: C 55.34, H 4.31, N 11.52%, found: C 55.60, H 4.20, N 11.43%.

S1.2.10. Synthesis of *p*-$ClC_6H_4CN_4S_3$-N=P(*p*-$OCH_3C_6H_4)_3$ (**5d**)

5d was prepared by the same method as **4c** by using 0.160 g (0.550 mmol) of **1d** and 0.206 g (0.585 mmol) of P(*p*-$OCH_3C_6H_4)_3$ in 50 mL of distilled toluene. Recrystallization afforded 0.240 g (67.9% yield) of light orange, plate shape crystals. M.P. (dec.): 151.4-152.3°C. IR (4000-400 region): 1591 (v)s, 1565 (m), 1512 (s), 1409 (m), 1353 (s), 1308 (m), 1260 (s), 1180 (m), 1115 (vs), 1089 (s), 1024 (m), 924 (vs), 887 (w), 828 (s), 804 (s), 781 (s), 700 (m), 666 (m), 623 (w), 538 (s), 448 (s). Mass spec. m/Z (high res. ESI): 642.06170 (642.06185 cal.). Anal calcd for $C_{28}H_{25}N_5S_3PO_3Cl$: C 52.37, H 3.92, N 10.91%, found: C 52.17, H 3.96, N 11.04%.

S1.2.11. Synthesis of *m*-$CF_3C_6H_4CN_4S_3$-N=P(*p*-$OCH_3C_6H_4)_3$ (**5e**)

5e was prepared by the same method as **4c** by using 0.486 g (1.50 mmol) of **1e** and 0.558 g (1.58 mmol) of P(*p*-$OCH_3C_6H_4)_3$ in 25 mL of distilled toluene. Recrystallization afforded 0.917 g (90.3% yield) of pale yellow, needle shape crystals. M.P. (dec.): 175.3-176.1°C. IR (4000-400 region): 1595 (s), 1586 (w), 1503 (s), 1452 (w), 1365 (s), 1317 (s), 1259 (s), 1174 (m), 1117 (vs), 1025 (m),932 (m), 913 (m), 834 (w), 804 (s), 785 (m), 695 (w), 625 (w), 541 (m), 470 (w). Mass spec. m/Z (high res. ESI): 676.08822 (676.08821 cal.). Anal calc. for $C_{29}H_{25}N_5S_3PO_3F_3$: C 51.54, H 3.73, N 10.37%, found: C 51.38, H 3.81, N 10.27%.

S1.2.12. Synthesis of *p*-$CF_3C_6H_4CN_4S_3$-N=P(*p*-$OCH_3C_6H_4)_3$ (**5f**)

5f was prepared by the same method as **4c** by using 0.198 g (0.612 mmol) of **1f** and 0.214 g (0.607 mmol) of (*p*-$OCH_3C_6H_4)_3$ in 30 mL of distilled toluene. Recrystallization afforded 0.410 g (99.8% yield) of orange, block shaped crystals. M.P. (dec.): 160.6-162.8°C. IR (4000-400 region): 1596 (s), 1568 (m), 1502 (s), 1452 (w), 1419 (m), 1396 (w), 1322 (s), 1298 (s), 1259 (s), 1180 (s), 1120 (vs), 1066 (m), 1067 (m), 1049 (s), 925 (vs), 885 (w), 833 (m), 804 (m), 781 (s), 668 (w), 623 (w), 535 (m), 472 (w). Mass spec. m/Z (high res. ESI): 676.08817 (676.08821 cal.). Anal calc. for $C_{29}H_{25}N_5S_3PO_3F_3$: C 51.54, H 3.73, N 10.37%, found: C 51.72, H 3.94, N 10.30%.

Section S2. ^{1}H NMR Characterization

The ^{1}H NMR chemical shifts (Table S1) are those that are expected for the substitution patterns that are present. Thus, the *ortho* and *meta* H atoms of the 4-$CH_3OC_6H_4$ rings show the expected ^{3}J(P,H) and ^{4}J(P,H) values of 12 Hz and 2 Hz reflecting the greater distance to the phosphorus for *meta* H nuclei. These phosphine ring shifts are invariant for **4** and **5**. The chemical shifts of the RC_6H_4C groups are typical for a combination of the substituents *R* and the effect of the thiazyl heterocycle. The latter acts as a strongly electron-withdrawing substituent on the di-substituted benzene ring. Thus, the chemical shifts of H_3 and H_5 are found at high frequency (7.92–8.28 ppm), values similar to those seen for other neutral thiazyl heterocycles [5] and with no evident effect by a change in the phosphine. Similar shifts have been reported previously by Knapp [6] for $CF_3CN_4S_3NPPh_3$ (δ = 7.47–7.69 (m, C_6H_5)), $Me_2NCN_4S_3NPPh_3$ (δ = 2.85 (s, 6H, CH_3), 7.34–7.69 (m, 15H, C_6H_5)), and $CF_3CN_4S_3NAsPh_3$ (δ = 7.50–7.70 (m, C_6H_5)). Other comparative parameters are for CF_3/PPh_3: ^{31}P δ = 23.8 (s, PPh_3); ^{19}F δ = −71.4. For $CF_3/AsPh_3$: ^{19}F δ = −70.9 (s, *exo*-form), −71.3 (s, *endo*-form), -75.3 (s,). For Me_2N/PPh_3: ^{31}P δ = 19.8 (s, PPh_3).

Table S1. ^{1}H and ^{19}F NMR data for **4** and **5**. [a]

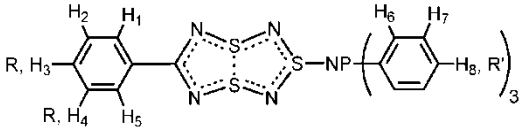

	H_1		H_2			H_6			H_7	
		J_H	δ	J_H	R	δ	J_H	J_P	δ	J_P
4a	7.98	8.7	6.73	8.7	3.77		7.36–7.58 *m* [b]			
4b	7.91	8.1	7.03	8.1	2.29		7.38–7.58 *m* [b]			
4c	8.00	7.5	7.25	7.5	7.43		7.22–7.45 *m* [b]			
4d	7.92	6.9	7.17	6.9	—		7.18–7.57 *m* [b]			
4e [c]	8.15	7.6	7.31 *t*	7.6	−61.65 [d]		7.35–7.60 *m* [b]			
4f	8.06	8.1	7.44	8.1	−61.99 [d]		7.38–7.63 *m* [b]			
5a	7.89	8.4	6.74	8.4	3.77	7.32	8.4	12	6.85	1.8
5b	7.91	8.1	7.05	8.1	2.30	7.32	8.7	12	6.84	2.1
5c	8.00	7.5	7.25	7.5	7.41	7.32	8.7	12	6.84	2.1
5d	7.93	8.7	7.21	8.7	—	7.32	8.7	12.4	6.85	2.4
5e [e]	8.15	7.8	7.32 *t*	7.9	−61.51 [d]	7.31	8.7	12	6.86	2.4
5f	8.08	8.1	7.48	8.1	−61.52 [d]	7.30	8.7	12.4	6.84	2.1

[a] Versus TMS, δ in ppm and *J* in Hz. R' (**4g-l**) = 3.84 ± 0.01. [b] Phosphine phenyl ring protons are not resolvable for the PPh_3 group in **4a**–**f**. [c] H_3 = 7.52, *d* J_H = 7.6; H_5 = 8.28 *s*. [d] For CF_3 groups, δ(^{19}F) relative to external $CFCl_3$. [e] H_3 = 7.54, *d* J_H = 7.9; H_5 = 8.31 *s*.

Section S3. ^{13}C NMR Characterization

Table S2. ^{13}C NMR data for **4** and **5** δ (ppm) vs. TMS and *J*(Hz) for coupling to ^{31}P or ^{19}F.[a]

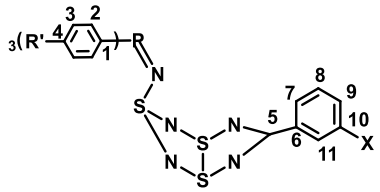

	C1	C2	C3	C4	C5	C6	C7	C8	C9	C10	C11	X	R'
	δ / J_P	δ / J_P	δ / J_P	δ / J_P	δ	δ	δ	δ	δ / J_F	δ / J_F	δ / J_F	δ / J_F	δ
4a	127.24	132.91	129.05	133.00	179.36	127.28	132.30	113.49	162.23	—	—	55.52	—
	101.3	*10.5*	*13.5*	*2.3*									
4b	127.18	132.89	129.03	132.99	179.88	141.98	130.47	128.95	131.87	—	—	21.67	—
	100.5	*11.3*	*12.8*	*3*									
4c	127.16	132.00	129.09	133.04	179.63	134.53	130.43	128.20	131.58	—	—	—	—
	100.5	*10.5*	*12.8*	*3*									
4d	127.06	132.00	129.09	133.15	178.52	137.56	131.62	128.38	133.07	—	—	—	—
	101.3	*10.5*	*12.8*	*2.25*									
4e	126.91	132.80	129.09	133.20	178.04	135.32	133.4	128.64	127.91	130.62	127.13	123.98	—
	101.3	*10.5*	*12.8*	*3*						*32.5*	*32.3*	*273.3*[b]	
4f	126.98	132.83	129.09	132.21	178.03	133.37	130.5	125.03	132.77	—	—	124.00	—
	101.3	*10.5*	*12.8*	*3*				*3.8*	*31.5*			*271.5*[b]	
5a	118.84	134.72	114.53	163.09	179.25	127.47	132.27	113.45	162.27	—	—	55.39	55.59
	108.8	*12.0*	*13.5*	*2.3*									
5b	118.83	134.72	114.52	163.12	179.90	132.09	130.47	128.90	141.75	—	—	21.66	55.59
	108.75	*12.0*	*12.8*	*3*									
5c	118.44	134.72	114.55	163.13	179.63	135.16	130.43	131.37	128.17	—	—	—	55.63
	108.8	*12.0*	*14.3*	*3*									
5d	118.65	134.70	114.57	163.24	177.79	137.36	128.36	131.68	133.34	—	—	—	55.65
	108.8	*108.8*	*12.8*	*3*									
5e	118.40	134.60	114.56	163.25	177.78	135.50	133.45	128.66	127.7	130.50	127.10	124.10	55.62
	108.8	*12.0*	*14.25*	*3*					*38*	*32.3*	*3.8*	*270.8*[b]	
5f	118.01	134.68	114.60	163.28	179.75	135.60	130.56	124.99	128.31	—	—	124.25	55.61
	134.7	*12.0*	*13.5*	*3*				*3.8*	*33.8*			*271.0*	

[a] Atom numbering scheme for the table is given in the diagram above. [b] Coupling to ^{19}F.

The ^{13}C NMR parameters (Table S2) are extremely consistent for this series of molecules, and are fully in agreement with data previously reported by Knapp *et al.* for $CF_3CN_4S_3NPPh_3$ and $Me_2NCN_4S_3NPPh_3$.[6] Noteworthy is the systematic pattern of coupling constants to both ^{31}P and ^{19}F as a function of the distance of the nucleus from the heteroatom. Also of significance is the chemical shift of the endocylic RC carbon which is 178–179 ppm for all these derivatives and may be compared to the distinct values determined for dithiatetrazocines in different conformers: for planar derivatives of the latter with aryl substituents, δ(RC) is 137–138 ppm, for the *bis*-^{t}Bu derivative, δ(RC) = 144.8 ppm, but for the bent Me_2N and ^{t}BuMeN derivatives δ(RC) is 179–180 pm. Thus, the chemical shift of this carbon is characteristic of the bent structural form in all derivatives of **4**, and confirms that the conformation found in the solid state (*vide infra*) is also retained in solution for this series of compounds.

Section S4. Solution speciation and Electrospray Mass Spectroscopy

Only in the case of **5d** was evidence obtained for the existence of **3d** in solution by ^{31}P NMR (δ = 26 ppm). However, the presence of a small amount of the latter species could be ascertained for most of these compounds by making use of UV-vis absorption spectroscopy.

UV-vis Electronic Absorption Spectroscopy

Whereas in the spectra of **4** and **5**, the pale yellow-orange colours are due to a strong UV band that tails into the blue region of the visible spectrum, distinct peaks are observed for a minor component (very week absorbance) in CH_2Cl_2 solutions.

Table S3. Electronic absorption spectroscopic data in solutions of **4** and **5**

Compound	λ_{max}, nm
4a	—
4b	481.4
4c	480.0
4d	—
4e	481
4f	481
5a	—
5b	480
5c	—
5d	480
5e	480
5f	479.1

These results are all very similar and speak to a chromophore that is well-removed from substituent effects. Based on earlier reports on **4c**, these absorptions, which are the direct complement to red, are caused by the presence of a very small amount of **3** in equilibrium with the *endo* isomers of **4** and **5** in solution. The much higher sensitivity of electronic absorption spectroscopy can detect these components even when they are not easily observable by NMR spectroscopy.

Electrospray Mass Spectroscopy

When conventional mass spec on a heated probe failed, recourse was made to using Electrospray Ionization from dichloromethane solutions. The results (Table S3) uniquely identify all the parent ions and identify fragments under these conditions to be of the type $R_3PN_2SH^+$ and $R_3PNH_2^+$.

Table S4. Electrospray mass spectral results

PR_3	C_6H_4X	Conditions	Parent species	Found	Calc	Error (ppm)	Frag 1 mass	Frag 1 identity	Frag 2 mass	Frag 2 identity
PPh_3	CH_3	DCM soln; EtOH carrier	MH+	532.08482	532.08478	0.1	323.1	Ph_3PN_2SH+	278.1	Ph_3NH_2+
PPh_3	Cl	DCM soln; $MeNO_2$ carrier	MH+	552.03047	552.03015	0.6	323.1	Ph_3PN_2SH+	278.1	Ph_3NH_2+
PPh_3	OCH_3	DCM soln; EtOH carrier	MH+	548.07905	548.07969	-1.2	323.1	Ph_3PN_2SH+	278.1	Ph_3NH_2+
PPh_3	*p*-CF_3	DCM soln; EtOH carrier	MH+	586.05650	586.05651	0	323.1	Ph_3PN_2SH+	278.1	Ph_3NH_2+
PPh_3	*m*-CF_3	DCM soln; $MeNO_2$ carrier	MH+	586.05771	586.05651	2	323.1	Ph_3PN_2SH+	278.1	Ph_3NH_2+
$P(C_6H_4OMe)_3$	H	DCM soln; EtOH carrier	MH+	608.10067	608.10082	-0.2	413.1	R_3PN_2SH+	368.1	Ph_3NH_2+
$P(C_6H_4OMe)_3$	CH_3	DCM soln; $MeNO_2$ carrier	MH+	622.11657	622.11647	0.2	413.1	R_3PN_2SH+	368.1	R_3NH_2+
$P(C_6H_4OMe)_3$	Cl	DCM soln; $MeNO_2$ carrier	MH+	642.06170	642.06185	-0.2	413.1	R_3PN_2SH+	368.1	R_3NH_2+
$P(C_6H_4OMe)_3$	OCH_3	DCM soln; $MeNO_2$ carrier	MH+	638.11109	638.11139	-0.5	413.1	R_3PN_2SH+	368.1	R_3NH_2+
$P(C_6H_4OMe)_3$	*p*-CF_3	DCM soln; $MeNO_2$ carrier	MH+	676.08817	676.08821	-0.1	413.1	R_3PN_2SH+	368.1	R_3NH_2+
$P(C_6H_4OMe)_3$	*m*-CF_3	DCM soln; $MeNO_2$ carrier	MH+	676.08822	676.08821	0	413.1	R_3PN_2SH+	368.1	R_3NH_2+

Section S4. Single-Crystal X-ray Diffraction Studies

S4.1 Experimental

Crystals were selected and mounted in Paratone™ on the ends of thin glass fibers and cooled on the goniometer head to –100°C with the Bruker low-temperature accessory attached to the Bruker APPEX-II diffractometer. Mo Kα radiation (λ = 0.71073 Å) was used throughout. Multi-scan absorption corrections were applied to all the data sets, and refinement was conducted with full-matrix least-squares on F^2 using SHELXTL 6.14. During refinement of the structure model for **4a** there was strong evidence for the presence of a disordered solvent molecule – apparently CH_2Cl_2 – within the lattice. The solvent void volume of 286 $Å^3$ detected by Platon in the final model is consistent with this (see also Figure S2b). After failing to find a reasonable model, the electron density due to the solvent was removed using the PLATON "Squeeze" function; thereafter refinement of a disorder model succeeded for 8 of the 24 molecules that are located on a mirror plane perpendicular to the *a* axis. The methoxy methyl group and one phenyl ring (C10A-C15D) lack the mirror symmetry of the site and are thus half-occupied; moreover, the twisted phenyl rings mesh with the methoxy methyl groups which leads to false apparent short contacts between these entities. In the final cycle of least squares refinement, the largest peak with almost 1.0 $e^-/Å^3$ reflects a small amount of the residual solvent electron density that was not fully removed by "Squeeze". For the rest, this is a very successful disorder refinement.

The structure of **4e** has two independent but chemically identical molecules per equivalent position. Both display evidence of CF_3 rotational disorder. The major components are well behaved and are present in refined occupancies of 67 and 74%, respectively. Further details are provided in electronic supplementary materials. The structure of **4f** also has two independent molecules per equivalent position, which also show evidence for CF_3 rotational disorder. Here too the main components refine anisotropically as well-defined groups with occupancies of 90 and 82%, respectively. The minor rotational components were refined isotropically.

The structure of **5e** displayed a less-common type of disorder in which the 3-$CF_3C_6H_4$ ring is twisted about the exocyclic C2–C1 bond with two fairly well defined limiting positions with about 15° dihedral between mean aryl planes and refined occupancies of 53 and 47%. The major component has very reasonable geometry and thermal displacement parameters (all refined anisotropically); the second component has noticeably higher thermal displacement indicative of a higher degree of "twisting" motion for this component. RIGU and SIMU restraints as well as selected use of EADP was required to restrain this model, but then refinement went to convergence. The full disorder model is shown in Figure S12. By contrast, the CF_3 group in **5f** is rotationally disordered in typical fashion. A simple two-part restrained model with refined occupancies of 71 and 29% and offset between rotamers of only 28° provided a very satisfactory resolution.

Table S5a. Crystal, Data Collection and Structure Refinement

Compound [1]	**4a** [2]	**4b**	**4d**	**4e**	**4f**	**5a**
empirical formula	$C_{26}H_{21}N_5OPS_3$	$C_{26}H_{22}N_5PS_3$	$C_{25}H_{19}ClN_5PS_3$	$C_{26}H_{19}F_3N_5PS_3$	$C_{26}H_{19}F_3N_5PS_3$	$C_{29}H_{28}N_5O_4PS_3$
FW	546.63	531.64	552.05	585.61	585.61	637.71
cryst. size (mm)	0.25×0.12× 0.10	0.19×0.11× 0.09	0.19×0.12×0.06	0.23×0.20×0.18	0.20×0.16×0.02	0.15×0.13 ×0.05
crystal color	Yellow	Yellow	Yellow	Yellow	Orange	Orange
temperature (K)	173(2)	173(2)	173(2)	173(2)	173(2)	173(2)
space group	C*mce*	$P\bar{1}$	$P\bar{1}$	$P2_1/c$	$P\bar{1}$	$P\bar{1}$
a (Å)	37.0224(18)	9.4077(5)	9.3884(5)	19.8664(19)	9.6633(9)	9.9094(6)
b (Å)	18.9806(9)	10.8007(6)	10.7922(6)	14.3630(13)	13.6006(12)	10.2435(6)
c (Å)	24.6031(12)	13.1819(7)	13.1399(7)	19.1773(18)	21.1803(19)	15.3755(9)
α (°)		82.7850(10)	83.0240(10)		101.2900(10)	88.4930(10)
β (°)		74.1550(10)	73.9700(10)	107.4530(10)	96.9340(10)	82.7640(10)
γ (°)		85.6540(10)	85.5820(10)		105.4070(10)	77.9830(10)
volume (Å^3)	17288.8(14)	1277.11(12)	1268.79(12)	5220.2(8)	2587.4(4)	1514.36(16)
Z	24	2	2	8	4	2
Z'	1.5	1	1	2	2	1
D_{calc} (g/cm^3)	1.260	1.383	1.445	1.490	1.503	1.399
μ (mm$^{-1)}$	0.340	0.378	0.486	0.394	0.397	0.341
$2\vartheta_{max}$ (°)	28.80	28.76	28.77	27.10	28.23	28.75
refl. collected	99820	15102	15006	56192	30948	17895
indep. refl.	11048	6077	6029	11536	12263	7185
R_{int}	0.0355	0.0155	0.0149	0.0238	0.0409	0.0153
completeness (%)	99.8	99.3	99.8	100	99.7	99.5
restraints	0	0	0	756	720	342
parameters	531	317	145	747	733	383
*R*1, *wR*2	0.0406, 0.1180	0.0320, 0.0840	0.0299, 0.0812	0.0306, 0.0863	0.0462, 0.1124	0.0307, 0.0841
GOF	1.011	1.028	1.046	1.025	1.022	1.046

[1] Semi-empirical Absorption corrections from equivalents applied to all data sets.

[2] 24 CH_2Cl_2 solvent molecules of which 8 disordered at *m* have been removed from the model and data using Platon 'squeeze'.

Table S5b. Crystal, Data Collection and Structure Refinement

Compound [1]	**5b**	**5c**	**5d**	**5e**	**5f**	**1d**
empirical formula	$C_{29}H_{28}N_5O_3PS_3$	$C_{28}H_{26}N_5O_3PS_3$	$C_{28}H_{25}ClN_5O_3PS_3$	$C_{29}H_{25}F_3N_5O_3PS_3$	$C_{29}H_{25}F_3N_5O_3PS_3$	$C_7H_4ClN_5S_3$
FW	621.71	607.69	642.13	675.69	675.69	289.78
cryst. size (mm)	0.15×0.10×0.10	0.20×0.10×0.09	0.25×0.24×0.23	0.23×0.06×0.04	0.20×0.17×0.13	0.24×0.08×0.06
crystal color	Yellow	Pink	Orange	Colorless	Colorless	Yellow
temperature (K)	173(2)	173(2)	173(2)	173(2)	173(2)	173(2)
space group	$P2_1/n$	$P2_1/n$	$P2_1/n$	$Pbca$	$P\bar{1}$	$P\bar{1}$
a (Å)	14.781(3)	9.5261(5)	9.4541(5)	9.4711(6)	9.6116(14)	4.6767(7)
b (Å)	13.157(3)	13.5974(8)	14.1671(8)	23.6565(15)	10.8670(15)	10.2525(14)
c (Å)	16.036(3)	21.4462(12)	21.6329(13)	27.4470(17)	14.743(2)	11.4772(16)
α (°)					91.513(2)	64.9990(10)
β (°)	112.919(2)	91.0700(10)	90.7260(10)		90.885(2)	86.7620(10)
γ (°)					105.349(2)	81.7800(10)
vol. (Å^3)	2872.3(10)	2777.4(3)	2897.2(3)	6149.6(7)	1484.1(4)	493.62(12)
Z	4	4	4	8	2	2
Z'	1	1	1	1	1	1
D_{calc} (g/cm^3)	1.438	1.453	1.472	1.460	1.512	1.950
μ (mm$^{-1)}$	0.355	0.366	0.444	0.352	0.365	0.995
$2\vartheta_{max}$ (°)	2.07 to 27.86	1.77 to 28.78	1.72 to 28.89	1.72 to 26.52	1.94 to 28.70	1.96 to 29.08
refl. collected	31719	32037	33470	62598	17172	6011
indep. refl.	6746	6672	7108	6368	6993	2431
R_{int}	0.0632	0.0256	0.0157	0.0636	0.0243	0.0259
completeness (%)	100	99.5	99.7	99.8	99.4	99.8
restraints	0	0	0	734	531	0
parameters	374	364	373	470	437	145
$R1$, $wR2$	0.0597, 0.1980	0.03304, 0.0907	0.0330, 0.0949	0.0395, 0.0984	0.0357, 0.0946	0.0236, 0.0711
GOF	1.047	1.029	1.023	1.017	1.000	1.086

[1] Semi-empirical Absorption corrections from equivalents applied to all data sets.

S4.2 Full descriptions of crystal and molecular structures

S4.2.1 Crystal and molecular structure of **1d**

The crystal structure of **1d** in common with many such RCN_5S_3 bicyclic cage molecules shows strong intermolecular contacts. By virtue of the $P\bar{1}$ crystal symmetry (with Z = 2) the structure of **1d** is highly regular. There are short S(δ^+)···N(δ^-) contacts forming a trapezoid of ring N5 — S3 (1.524 Å) and cross-ring N5 — S3' (3.237 Å) contacts that align the S_3N_2 planes of neighboring atoms into infinite co-planar sheets. There are also short contacts between the apical N3 with both S3' (2.918 Å) and C1' (3.104 Å) on neighbors that lead to a "nesting" stack of bent CN_4S_3 units along a lattice vector. This packing motif (Figure S1) is identical to that found for the isostructural 4-cyanophenyl derivative [7] and highly similar to that observed for the directly-bound 7-CF_3 derivative,[8]although this latter structure adopts a different space group.

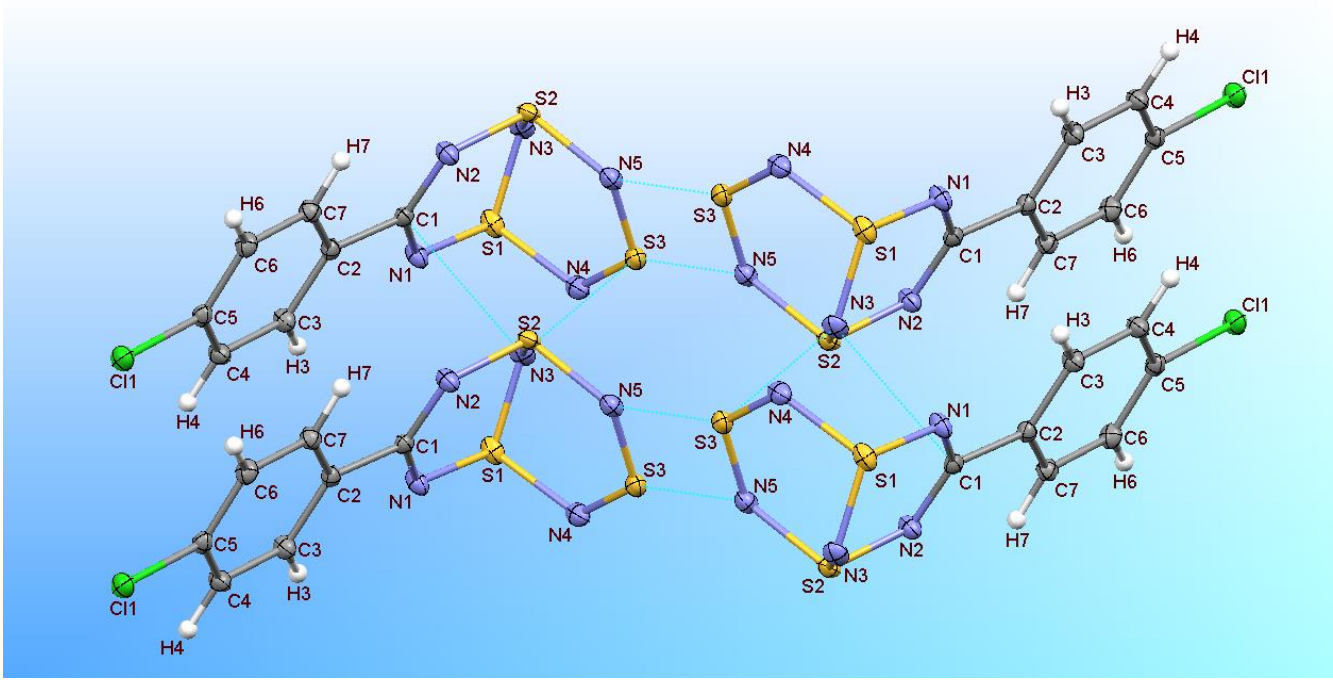

Figure S1. Crystal packing interactions within the solid-state structure of **1d**.

S4.2.3. Crystal and molecular structures of **4a**

While the molecular geometries of **4** are highly similar across the series, there is considerably variation in the crystal packing and in particular with regard to intermolecular contacts involving thiazyl rings. In addition to the 9 TTTA derivatives reported here there are ten others in the literature. Across these 19 structures, 9 show general short contacts (*I*) with no apparent pattern. Four of them form centrosymmetric *trans*-cofacial arrangements (*II*) of the $ArCN_2S_2$ ring components. Two have short δ^-(N)···δ^+(S) contacts with a *trans*-cofacial arrangements (*III*) of the S_3N_2 component of the rings, while four contain short S··· S contacts *via* single sulfur atoms on two molecules (*IV*).

Several data sets were collected on crystals of **4a** grown from the usual mixture of CH_2Cl_2 and CH_3CN, but all crystals investigated seemed to contain the same disordered molecules in the orthorhombic space group *Cmce* (with Z = 24, 16 ordered and 8 disordered about the mirror plane perpendicular to the *a* axis, Figure S2, with semi-occupancy of the methoxy methyl groups and one of the phosphine phenyl rings). The disorder model is well behaved and has been fully refined; it does not cast any doubt upon the conformation adopted by the substituent and both independent molecules are clearly *endo-anti*. This structure is also quite interesting in that *neither* molecule displays any significant short contacts involving the thiazyl linkages. A close analysis of both geometry and thermal displacement parameters shows that the molecule on the mirror plane shows possible distortions resulting from the disorder, especially for the phosphine phenyl rings; hence all geometric comparisons of **4a** will be limited to the ordered molecule. For a view of the disordered atoms see Figure S2. The atom numbering scheme for the non-hydrogen atoms is provided on the Figure. The packing arrangement is of type *I* (general).

Disordered CH_2Cl_2 of crystallization were removed from the e.d. map using the PLATON "squeeze" utility before refinement could be completed. Apparent contacts shorter than the sum of the v.d.Waals radii that involve interactions between the disordered phosphine phenyl ring atom C12A and aryl methoxy carbon C8A on adjacent molecules are an artifact of the disorder across the mirror. Figure S2b depicts a packing diagram of the

unit cell with the void spaces occupied by the solvent molecules. Amongst the eleven TTTA iminophosphorane adducts reported in this work, only **4a** crystallizes with solvent molecules in the lattice.

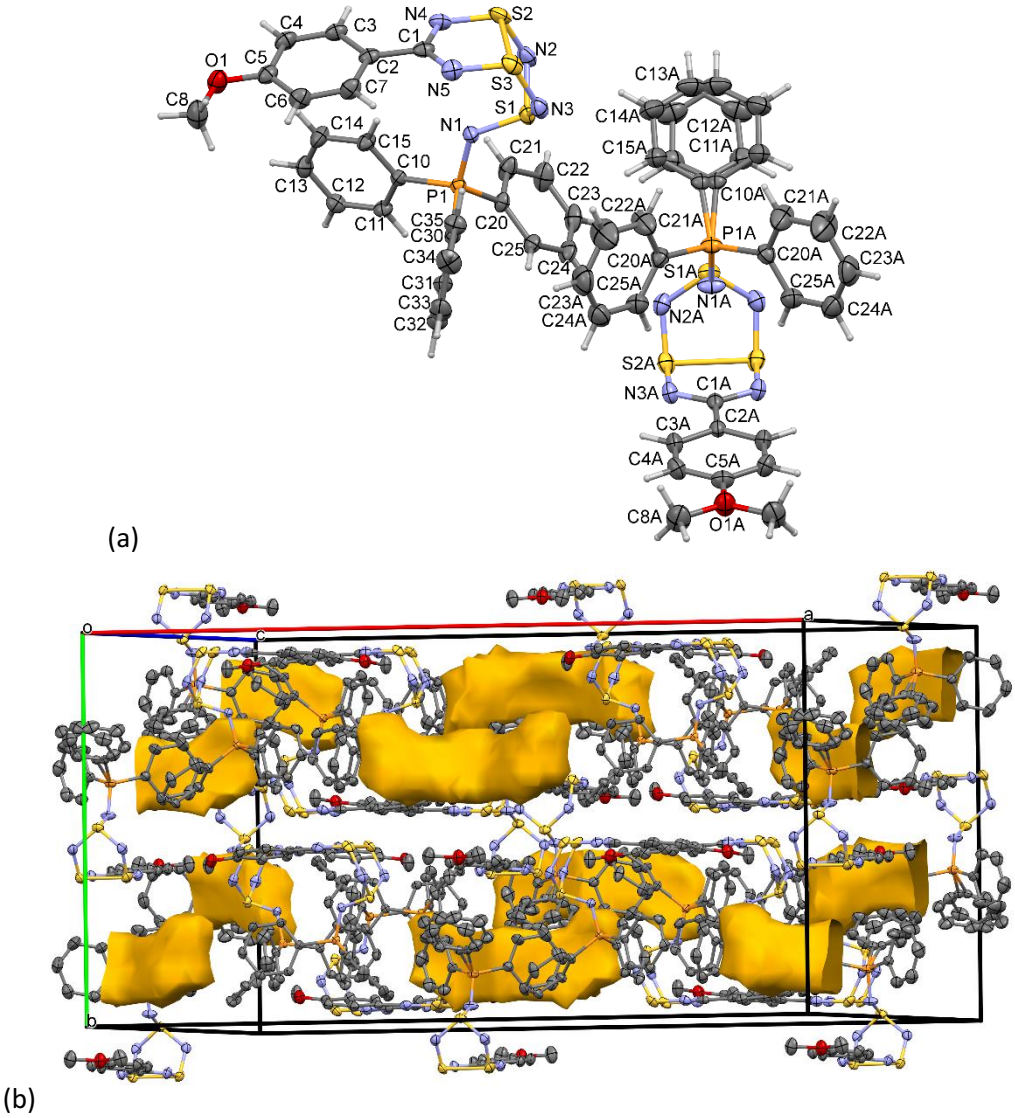

Figure S2. (a) A thermal ellipsoids plot (Mercury 2.0, 50% probability) of the structure of **4a** in the crystal viewed such that the basal *bc* plane bisects the r.h.s molecule through O1A, C1A, N1A and P1A. There are 1.5 molecules per equivalent position. The transannular S···S contact for the ordered molecule shown at left (S2···S3) = 2.431 Å, while that of the one disordered about the crystallographic mirror plane shown at right (S2A···S2A') = 2.421 Å. (b) Packing diagram showing the voids occupied by 24 CH_2Cl_2 molecules in the unit cell.

S4.2.3. Crystal and molecular structures of isostructural **4b** and **4d**

The structures of **4b** and the isostructural **4d** contain short contacts of type *II*, forming centrosymmetric dimers *via* the CN_2S_2 segment of the TTTA rings (Figure S3). For these two cases it is the endocyclic C atoms C1 that form the shortest contacts with sulfur atoms S3 at 3.365 Å so that it is the CN_2S_2 half of the heterocycle that is involved in this lattice interaction. These interactions are likely to be electrostatic in nature between δ^- N–C–N and δ^+ S atoms. A weaker secondary contact connects S2 to phosphine ring carbon C33 on an adjacent molecule at 3.455 Å. The heterocycle conformation here is indisputably *endo-anti*. In the molecular structure of **4b**, the

transannular S···S contact = 2.4325(6) Å, while the short intermolecular C···S contact = 3.365 Å. In isostructural **4d**, with Cl atoms in the place of the 4-CH_3 groups of **4b** (same atom numbering sequence is used for both), the S···S contact = 2.433(6) Å, while the short C···S contact = 3.344 Å.

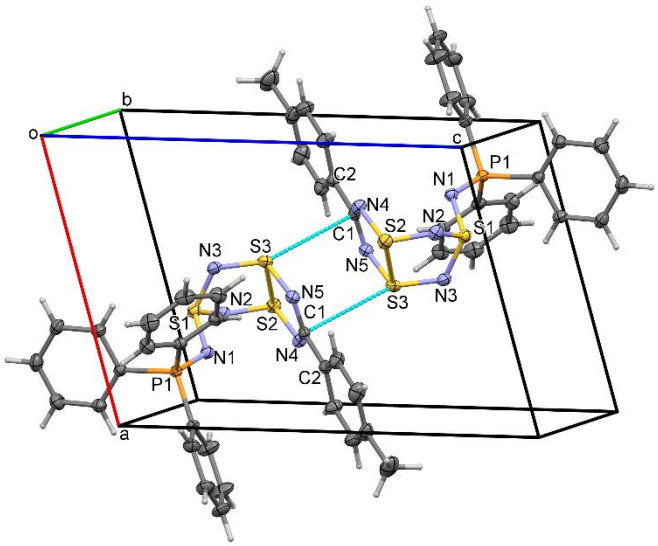

Figure S3. Displacement ellipsoids plot (Mercury, 40% probability) of the structure of **4b** in the crystal, depicting the *trans*-cofacial arrangement of two CN_2S_2 ring portions. Isostructural **4d** is not depicted (but see the main article)

S4.2.4. Crystal and molecular structures of **4e**

The *Z*' = 2 structure of **4e** shows minor rotational disorders in the CF_3 groups (see experimental) and shows no short-contacts involving the thiazyl rings, but there are short links between F4A of one of the two independent molecules per equivalent position and phenyl ring carbon C4 (3.124 Å) on the other (Figure S4). These contacts are best explained as being due to packing effects that in this structure seem to allow the molecular shapes to pack together as closely as possible. The two transannular S···S contacts are 2.434 and 2.439 Å; the average transannular S···S distance is 2.437(1) Å.

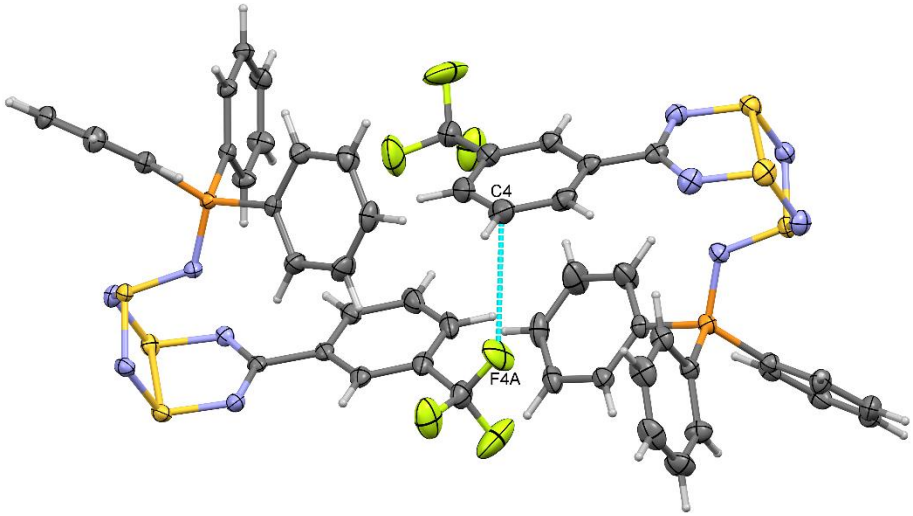

Figure S4. A thermal ellipsoids plot (Mercury 2.0, 50% probability) of the structure of **4e** in the crystal. There are two independent molecules in the unit cell, weakly linked by the indicated short C4···F4A contacts at 3.124 Å. Only the main rotamers of the disordered CF_3 groups are shown (67% occupancy for F1A-F3A, 74% for F4-F6A).

S4.2.5. Crystal and molecular structures of **4f**

The structure of **4f** in the crystal (Figure S5) also involves two atoms per equivalent position but the space group is different than in the case of **4e**. The "B" molecule (S4-S6 etc; transannular S···S contact = 2.415(1) Å) is involved in a centrosymmetric dimer relationship *via* short contacts between S6, N10, and C41, atoms that are part of the CN_2S_2 component of the heterocycle: C···S, 3.353; N···S, 3.332 Å (Figure S5, left). This is very similar to that seen for **4b,d** except for the additional involvement of a nitrogen atom in the interaction. For the "A" molecules (i.e. those with the lower-digit atom labels; intra-ring S···S = 2.418(1) Å) there are short S3···C33 contacts of 3.401 Å forming an infinite chain and centrosymmetric N3···C24 (phosphine ring) contacts of 3.125 Å that doubles the chain to a ribbon.

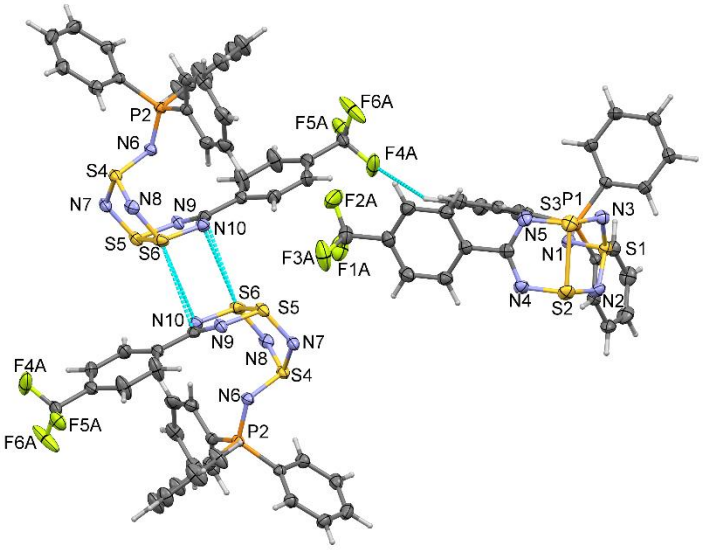

Figure S5. A displacement ellipsoids plot (Mercury, 40% probability) of the structure of **4f** in the crystal. The "B" molecules are centrosymmetrically paired via the CN_2S_2 rings through both S···C = 3.353 and S···N = 3.332 Å contacts. The "A" molecules have general short contact in the lattice. Only the major rotamers for the disordered CF_3 groups are shown in the diagram.

S4.2.6. Orientation of the Ar_3PN units w.r.t. the TTA rings

Three major orientations of the Ar_3PN groups w.r.t. the TTTA rings can be detected. In the solid structures of **4b,d,e**, one ArP ring is oriented (Figure S6) above the $ArCN_2S_2$... ring in an approximate π-stacking orientation. The second and most common orientation (Figure S7) has one of the ArP rings approximately perpendicular to the $ArCN_2S_2$... portion to induce an intramolecular aryl-ring "T" interaction. It is found for **4a** (ordered), **4f**, **5a**, **5b**, **5c**, **5d** and **5f**. A third orientation in the molecule in **4a** that is located at a mirror plane and **5e** have two ArP rings perpendicularly held out in a welcome gesture (Figure S8) or embrace. No specific interaction with the thiazyl rings can be noted for this third motif. In **4a** the two rings "embrace" if anything the solvent molecules (CH_2Cl_2). In **5e**, the "embrace" is directed to the unsubstituted edge of the mCF3-phenyl ring of a neighbouring molecule in the unit cell. These intramolecular interactions are difficult to distinguish from others with neighbouring molecules. At RT in the solution phase NMR, there is no evidence of any persistent preferred orientations and the Ar_3P groups display rotationally equivalent signals.

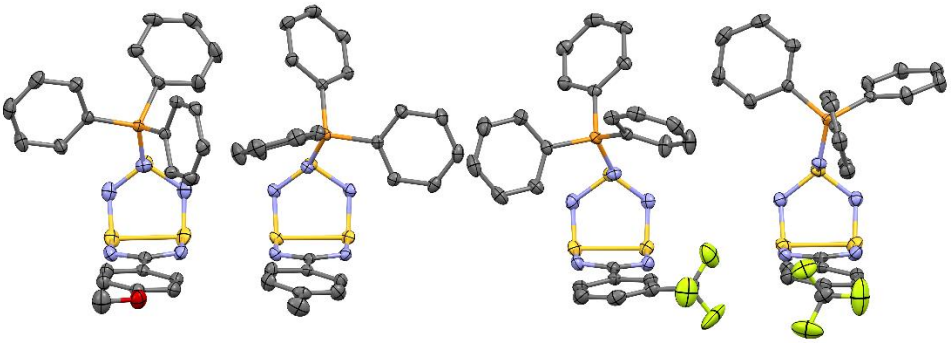

Figure S6. Conformations of the $Ph_3P{=}N$ groups w.r.t. the $ArCN_5S_3$ rings in **4a** – **4f**

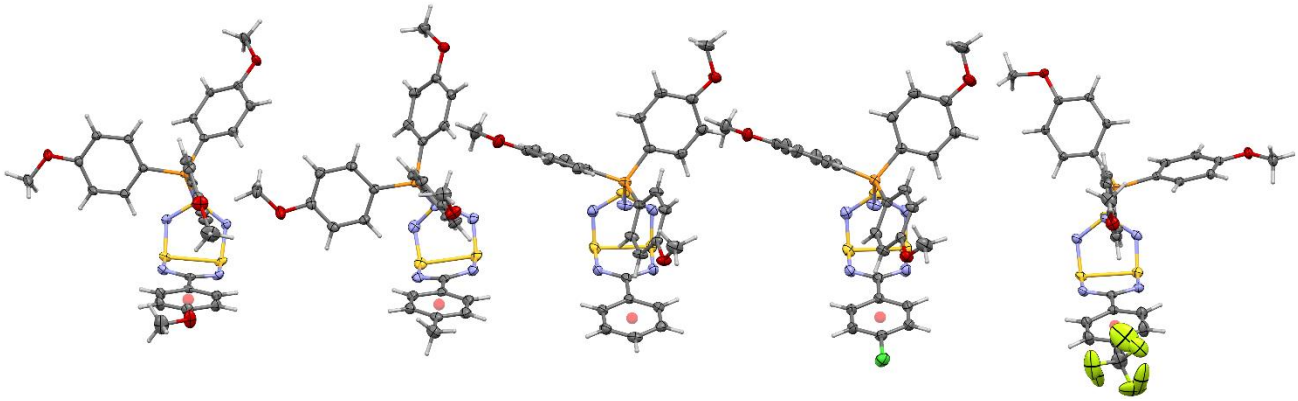

Figure S7. Conformations of the $Ph_3P{=}N$ groups w.r.t. the $ArCN_5S_3$ rings in **4a** – **4f** & **5e**

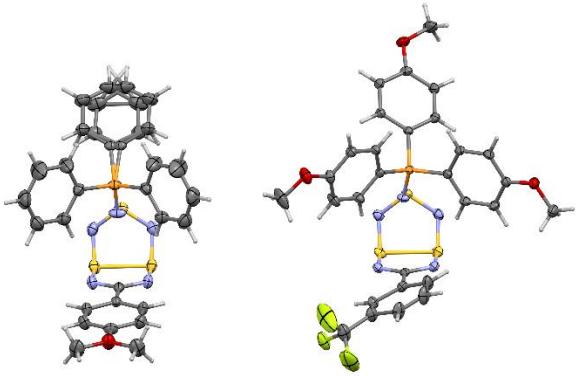

Figure S8. Conformations of the $Ph_3P{=}N$ groups w.r.t. the $ArCN_5S_3$ rings in **4a** & **5e**

S4.2.7 Crystal and molecular structures of **5a**

The structure of **5a** in the lattice (Figure S9) is the first in this series to show a centrosymmetric dimer through four co-facial sulfur and nitrogen atoms of the S_3N_2 half of the heterocyclic ring. The short S2···N3' and S3···N2' contacts are 3.292 and 3.310 Å and the transannular S···S distance within the molecule is short at 2.4066(5) Å. This mode of dimerization is very similar to that found in crystals of **4c**, the first structure of this kind to have been reported back in 1985.[9] This latter structure has *longer* S···N distances at 3.338 and 3.412 Å but a smaller offset between the ring centroids (centroid spacing 3.374 vs. 3.300 Å in **5a**, albeit this latter was measured some 125°C lower in temperature). There are additional short contacts between C13 and O3 of 3.115 and C14 to S3 of 3.357 Å as well as numerous interactions involving CH atoms.

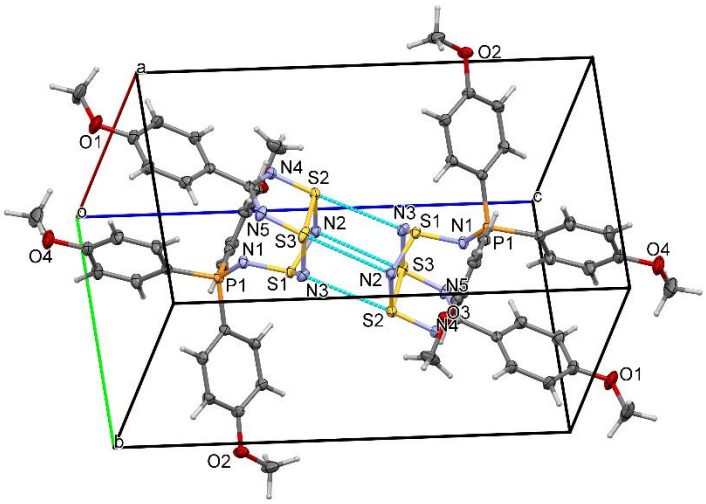

Figure S9. A displacement ellipsoids plot (Mercury, 40% probability) of the centrosymmetric dimer of **5a** in the crystal lattice connected through short S···N contacts of 3.292 and 3.310 Å.

S4.2.8 Crystal and molecular structures of **5b**

The centrosymmetric intermolecular interaction of **5b** in the crystal has shortest contacts between C1 and S3 from the CN_2S_2 planes as found for **4b,d** with d(S3···C1') = 3.314 Å (Figure S10). However, there are several other short contacts such as C5 with C25 at 3.334 Å and the especially short interaction between phosphine methoxy groups of 2.952 Å between O1 and C26 (this is over 8% less than the sums of the v.d.Waals radii.) The transannular S2···S3 distance within the thiazyl heterocycle is 2.428(1) Å.

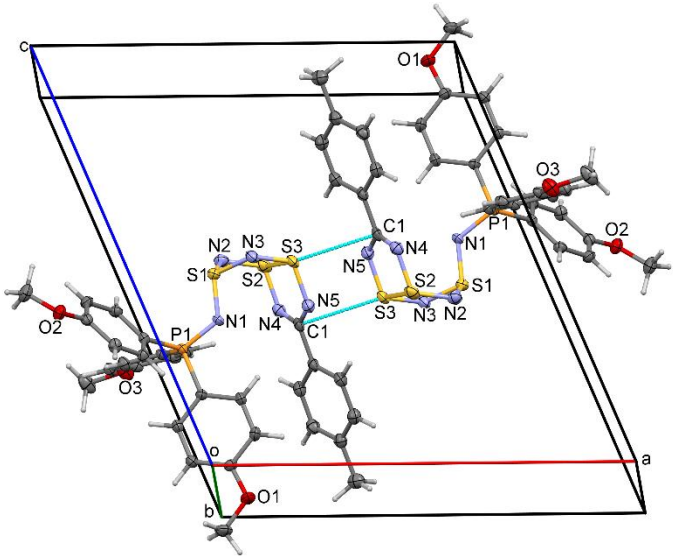

Figure S10. thermal ellipsoids plot (Mercury 2.0, 50% probability) of the centrosymmetric dimer of **5b** in the crystal showing dimerization through the CN_2S_2 ring atoms with an S3···C1' distance of 3.314 Å. There are also strong contacts between phosphine O and CH_3 groups O1 and C26 of 2.952 Å.

S4.2.9 Crystal and molecular structures of isostructural **5c** and **5d**

The structure of **5c** in the lattice, by contrast, shows few interactions other than those involving H atoms and has a transannular S···S distance of 2.4264(6) Å (Figure S11). The diagram shows clearly how the folded heterocycle is dominated by the expanse of the tri-substituted iminophosphorane group. There is a non-classical hydrogen bond that weakly dimerizes CH_3O groups on neighbouring molecules but the interactions involving O2

and C26 are much longer than that noted for **5b** above (3.365 Å). In the crystal lattice **5d** is essentially isostructural with **5c** except that the dominant centrosymmetric organizing principle is between one of the CH_3O groups and the aryl ring Cl atoms, contacts at 3.234 and 3.237 Å that are marginally less than the sum of the v.d.Waals radii and the methoxy groups are slightly further apart as a consequence. The inter-annular S2···S3 distance in **5d** is also larger at 2.4398(6) Å.

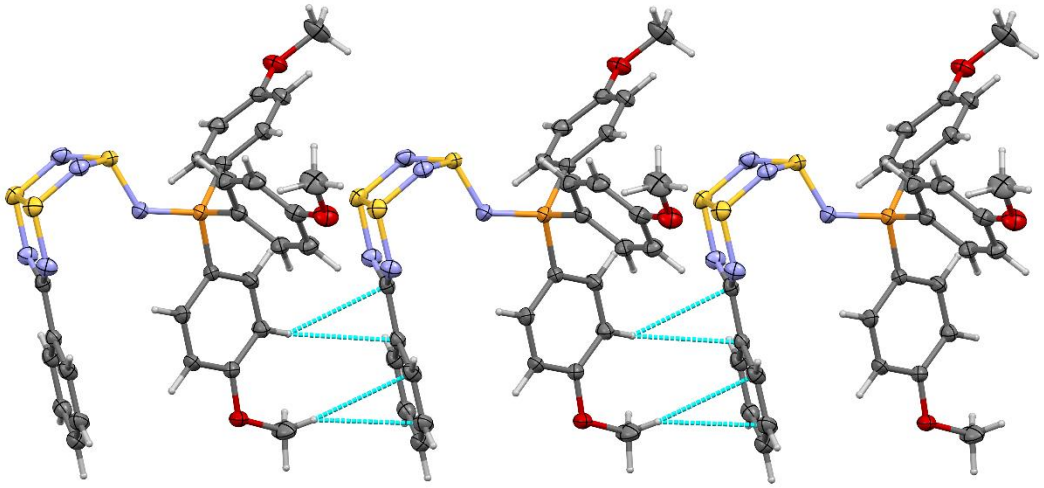

Figure S11. Displacement ellipsoids plot of chains of **5c** in the crystal lattice showing the *endo-anti* conformation of the heterocyclic ring; d(S2···S3) for this structure is 2.4264(6) Å. The isostructural **5d** is not shown; it has d(S2···S3) = 2.4398(6) Å

S4.2.10. Crystal and molecular structures of **5e**

The structure of **5e** in the lattice (Fig. S12), like that of **5c,d** is also essentially isolated with only general contacts other than to H atoms between O1 and F3A at 2.912, F2 and C22 at 3.122 and S2 to C12 at 3.492 Å, respectively. Of interest in this structure, and distinct from what is observed for **4e**, disorder of the trifluoromethyl group is not simply due to rotation about the CF_3–C bond, but is rather a waging motion of the complete $CF_3C_6H_4$ ring about the bond that attaches to the heterocycle. Such motion sweeps out a considerable volume of space and perhaps not surprisingly this is the lowest density crystal containing a CF_3 group of the four examples studied here (**4e**, **4f**, **5e** and **5f**). The short contacts involving fluorine may be artifacts of this disorder. The transannular S2···S3 contact within the thiazyl heterocycle is 2.4369(8) Å.

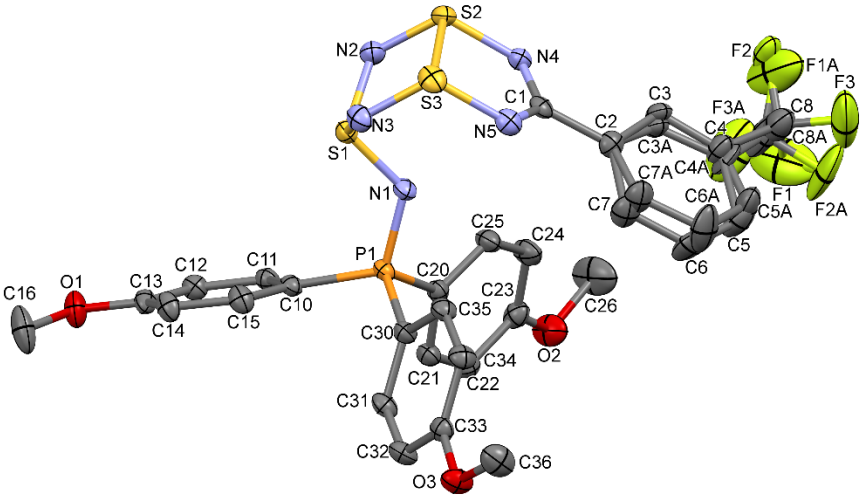

Figure S12. The structure of **5e** as found in the crystal lattice. Notice the disorder involving the whole 3-$CF_3C_6H_4$ ring in place of the more common rotational disorder of just the CF_3 group. Hydrogen atoms are omitted.

The structure of **5f** in the lattice is the only structure among these nine trithiatetrazocine structures which displays centrosymmetric dimerization through the S1 atom of the heterocycle, i.e. the sulfur atom that bears the exocyclic iminophosphorane substituent (Fig. S13). This contact at 3.297 Å is at 9% significantly shorter than the sum of the v.d.Waals radii for two sulfur atoms (3.60 Å). The origin of such a short contact in bonding is not obvious. The transannular S2···S3 distance in this molecule is 2.4101(7) Å.

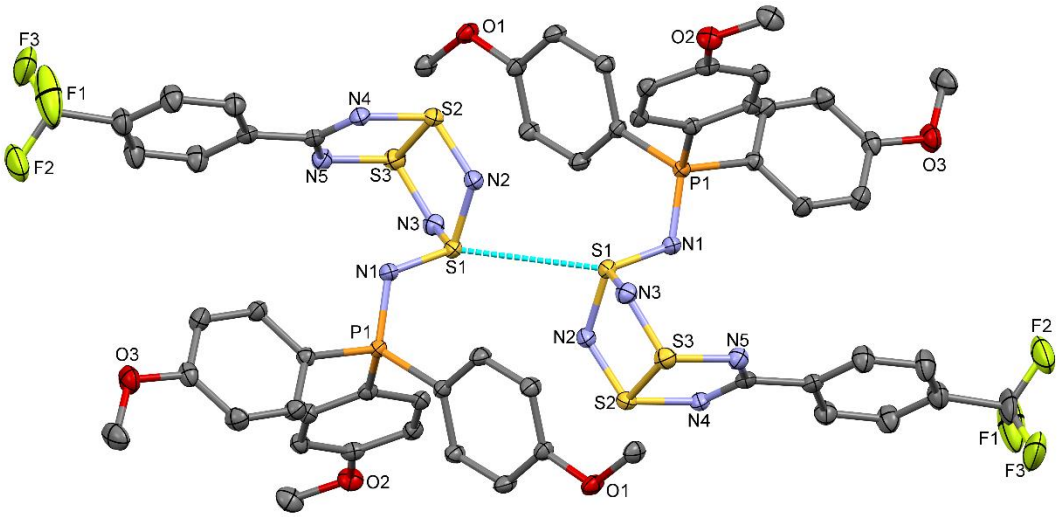

Figure S13. Centrosymmetric dimers of **5f** linked *via* S1···S1' contacts of 3.279 Å which are 9% less than the sum of their v.d.Waals radii. Typical rotational disorder is observed for the terminal CF_3 group; only the major rotamer (75% occupancy) is shown.

Table S6. Compiled Intermolecular Distances and Angles for the ten crystal structures of aryl phosphoraniminato-trithiatetrazocines

		Compound:		4a	4b	4c	4d	4e	4e	4f	4f	5a	5b	5c	5d	5e	5f		
Substitue	**Average**	**StdDev**	**Report**	MeO	Me	Ph	Cl	mCF3	2nd molec	pCF3	2nd molec	MeO	Me	Ph	Cl	mCF3	pCF3		
Code				7033	7030	DOTVUT	7034	7026	7026	7024	7024	7035	7032	7038	7036	7039	7041		
P1-N1	1.603636	0.004608	1.604(5)	1.6006	1.6000	1.601	1.6018	1.6065	1.6031	1.601	1.596	1.6117	1.603	1.6006	1.6091	1.6049	1.6116		
S1-N1	1.609629	0.007305	1.610(7)	1.6065	1.6155	1.612	1.6133	1.6156	1.6077	1.613	1.608	1.6199	1.612	1.6016	1.6029	1.5916	1.6152		
S1-N2	1.653229	0.004297		1.6536	1.652	1.647	1.6514	1.658	1.6558	1.646	1.652	1.6564	1.66	1.6472	1.6565	1.6529	1.6564		
S1-N3	1.652593	0.005557		1.658	1.655	1.638	1.6556	1.6533	1.657	1.648	1.653	1.6492	1.652	1.6472	1.6557	1.6595	1.6548		
av(N2,3-S	1.652911	0.00432	1.653(4)	1.6558	1.6535	1.6425	1.6535	1.65565	1.6564	1.647	1.6525	1.6528	1.656	1.6472	1.6561	1.6562	1.6556		
S2-N2	1.598143	0.005726		1.598	1.6079	1.591	1.6053	1.596	1.6017	1.593	1.6	1.5999	1.606	1.5934	1.5989	1.59	1.5929		
S3-N3	1.596943	0.005249		1.599	1.5985	1.589	1.5986	1.6	1.6001	1.586	1.599	1.6045	1.6	1.5967	1.6012	1.595	1.5896		
av(S2,3-N	1.597543	0.004948	1.598(5)	1.5985	1.6032	1.59	1.60195	1.598	1.6009	1.5895	1.5995	1.6022	1.603	1.59505	1.60005	1.5925	1.59125		
S2···S3	2.426086	0.010997	2.43(1)	2.4325	2.4325	2.415	2.433	2.4374	2.4341	2.4184	2.4149	2.4066	2.4276	2.4264	2.4398	2.4369	2.4101		
S2-N4	1.632193	0.004019		1.634	1.6257	1.63	1.6266	1.629	1.6328	1.63	1.629	1.6381	1.633	1.6318	1.6367	1.6376	1.6364		
S3-N5	1.632707	0.005391		1.632	1.6352	1.629	1.6376	1.63	1.635	1.631	1.632	1.6258	1.637	1.6233	1.6301	1.645	1.6349		
av(S2,3-N	1.63245	0.003417	1.632(3)	1.633	1.63045	1.6295	1.6321	1.6295	1.6339	1.6305	1.6305	1.63195	1.635	1.62755	1.6334	1.6413	1.63565		
N4-C1	1.332714	0.00403		1.329	1.336	1.334	1.3306	1.338	1.333	1.334	1.323	1.3364	1.334	1.327	1.335	1.334	1.334		
N5-C1	1.334121	0.005551		1.345	1.339	1.323	1.3371	1.333	1.333	1.332	1.334	1.3336	1.341	1.334	1.332	1.335	1.326		
av(N4,5-C	1.333418	0.003079	1.333(3)	1.337	1.3375	1.3285	1.33385	1.3355	1.333	1.333	1.3285	1.335	1.3375	1.3305	1.3335	1.3345	1.33		
C1-C2	1.482136	0.003764	1.482(4)	1.473	1.479	1.481	1.482	1.482	1.485	1.479	1.487	1.4799	1.482	1.484	1.486	1.483	1.487		
P1-N1-S1	121.4629	2.048341	121(2)	121.16	121.77	121	121.99	121.39	122.56	119.45	123.96	117.54	122.88	123.45	122.92	123.01	117.4		
N1-S1-N2	107.1029	1.539647		106.1	105.39	106.6	105.32	109.28	109.37	106.37	108.68	108.69	109.07	106.63	105.79	105.86	106.29		
N1-S1-N3	107.0214	1.396935		107.47	108.43	107.1	108.25	105.69	105.37	106.96	105.13	106.32	104.64	107.48	108.3	107.98	109.18		
av(N-S-N2	107.0621	0.327001	107.1(3)	106.785	106.91	106.85	106.785	107.485	107.37	106.665	106.905	107.505	106.855	107.055	107.045	106.92	107.735		
N2-S2-N4	115.4643	0.849812		116.14	114.62	115	114.49	115.33	114.76	115.88	114.11	115.05	115.68	116.71	116.81	116.44	115.48		
N3-S3-N5	115.7321	0.614431		115.86	115.63	114.6	115.6	115.8	115.17	116.32	114.89	115.19	115.75	116.55	116.54	116.49	115.86		
av(N-S-N)	115.5982	0.702267	115.6(7)	116	115.125	114.8	115.045	115.565	114.965	116.1	114.5	115.12	115.715	116.63	116.675	116.465	115.67		
S2-N4-C1	117.785	0.387591		118.41	118.16	117.5	118.12	118.17	117.46	117.96	117.56	117.25	117.8	117.85	117.57	118.08	117.1		
S3-N5-C1	117.7993	0.345442		117.77	118.06	118.2	117.78	117.77	118.14	117.53	117.13	118.01	117.5	118.27	118.11	117.49	117.43		
av(N-S-C)	117.7921	0.255755	117.8(3)	118.09	118.11	117.85	117.95	117.97	117.8	117.745	117.345	117.63	117.65	118.06	117.84	117.785	117.265	PPh3	POMe3
CN2S2-S2I	115.3564	1.035082	115(1)	115.42	113.99	114.5	113.85	114.8	114.28	117.13	116.34	114.67	115.41	116.35	116.52	116.13	115.6	115.04	115.78
S2N2-N3S	143.9593	1.193157	144(1)	143.62	143.89	145	143.46	145.13	142.71	146.74	143.51	143.05	142.9	143.66	143.17	143.01	145.58	144.26	143.56
Notes				Disorder structure not used		ActaC42 1986 900-902													
AveBondError				0.0021	0.0015	0.0029	0.0014	0.0021	0.0020	0.0023	0.0022	0.0013	0.0029	0.0015	0.0015	0.0021	0.0016		
AveAnglError				0.10	0.08	0.13	0.07	0.11	0.10	0.14	0.12	0.07	0.14	0.08	0.08	0.11	0.09		

Data for **4c** is taken from: Boeré, R. T.; Ferguson, G.; Oakley, R. T. *Acta Cryst.* **1986**, *C42*, 900–902.

Section S7. Voltammetry and bulk electrolysis

TableS7. Full Electrochemical Data for the Trithiatetrazocines in CH_2Cl_2 on a GC electrode at v = 0.2 V s^{-1}.

R'	**Ph**						
R		**OCH_3**	**CH_3**	**H**	**Cl**	**mCF_3**	**pCF_3**
Conc (mM)		2.64	4.55	2.53	2.91	1.85	1.66
0/+1							
CV	E_p^{a3}, V	0.94	1.00	1.03	1.06	1.09	1.09
	I_p^{a3}, µA	47	86	48	53	29	24
SWV	E^3, V	0.88	0.96	0.98	1.00	1.06	1.06
	$w_{½}$, mV	120	157	147	154	148	142
	I_p^3, µA	37	54	33	34	21	16
-1/0							
CV	E_p^{c1}, V	-1.99	-1.96	-1.97	-1.94	-1.86	-1.86
	I_p^{c1}, µA	78	166	81	100	66	56
SWV	E^1, V	-1.88	-1.88	-1.87	-1.83	-1.80	-1.80
	$w_{½}$, mV	166	200	180	160	131	125
	I_p^1, µA	49	73	43	28	46	41
-2/-1							
CV	E_p^{c2}, V	-2.26	-2.23	-2.26	-2.27	-2.22	-2.23
	I_p^{c2}, µA	84	139	89	94	56	48
SWV	E^2, V	-2.19	-2.22	-2.20	-2.20	-2.18	-2.18
	$w_{½}$, mV	146	189	179	172	151	153
	I_p^2, µA	19	37	25	59	17	18

TableS7., Continued.

R'	**$pOCH_3C_6H_4$**						
R		**OCH_3**	**CH_3**	**H**	**Cl**	**mCF_3**	**pCF_3**
Conc (mM)		2.15	3.08	2.53	1.78	1.35	1.67
0/+1							
CV	E_p^{a3}, V	0.94	0.97	0.98	1.00	1.06	1.06
	I_p^{a3}, μA	40	59	55	29	18	17
SWV	E^3, V	0.85	0.93	0.92	0.95	1.03	1.01
	$w_{½}$, mV	114	130	136	134	143	136
	I_p^3, μA	34	35	36	20	15	11
-1/0							
CV	E_p^{c1}, V	-1.99	-1.98	-1.95	-1.94	-1.89	-1.89
	I_p^{c1}, μA	72	86	94	44	36	34
SWV	E^1, V	-1.90	-1.89	-1.87	-1.86	-1.81	-1.83
	$w_{½}$, mV	161	172	156	163	144	145
	I_p^1, μA	45	52	53	30	25	20
-2/-1							
CV	E_p^{c2}, V	-2.34	-2.34	-2.32	-2.35	-2.31	-2.32
	I_p^{c2}, μA	81	96	104	53	40	38
SWV	E^2, V	-2.28	-2.28	-2.26	-2.28	-2.25	-2.28
	$w_{½}$, mV	194	194	175	186	104	144
	I_p^2, μA	27	31	34	19	15	14

Table S8. Data for correlation of peak potentials with Hammett Parameters for aryl substituents

Data for the Hammett plots for **4** and **5**

R	phosphine	E_p^{c1} (V)	E_p^{a3} (V)	Hammett σ_m or σ_p[10]
[]MeO	PPh_3	-1.99	0.94	-0.27
Me	PPh_3	-1.96	1	-0.17
H	PPh_3	-1.97	1.03	0.00
Cl	PPh_3	-1.94	1.06	0.23
m-CF3	PPh_3	-1.86	1.09	0.43
p-CF3	PPh_3	-1.86	1.09	0.54
MeO	$P\{C_6H_4(CH_3O)\}_3$	-1.99	0.94	-0.27
Me	$P\{C_6H_4(CH_3O)\}_3$	-1.98	0.97	-0.17
H	$P\{C_6H_4(CH_3O)\}_3$	-1.95	0.98	0.00
Cl	$P\{C_6H_4(CH_3O)\}_3$	-1.94	1	0.23
m-CF3	$P\{C_6H_4(CH_3O)\}_3$	-1.89	1.06	0.43
p-CF3	$P\{C_6H_4(CH_3O)\}_3$	-1.89	1.06	0.54

Data for the Hammett plots for 4-aryl-1,2,3,5-dithiadiazolyls and diaryl derivatives of **C**

R	heterocycle type	E_p^{c1} (V)	E_p^{a3} (V)	Hammett σ_m or σ_p[10]
MeO	dtda	-0.85	0.73	-0.27
Me	dtda	-0.83	0.77	-0.17
H	dtda	-0.82	0.78	0.00
Cl	dtda	-0.78	0.82	0.23
m-CF3	dtda	—	—	—
p-CF3	dtda	-0.73	0.86	0.54
MeO	dtta	-1.366	1.123	-0.27
Me	dtta	-1.37	1.31	-0.17
H	dtta	-1.355	1.457	0.00
Cl	dtta	-1.309	1.491	0.23
m-CF3	dtta	-1.288	1.567	0.43
p-CF3	dtta	-1.299	1.603	0.54

So the TTTA are comparably tunable to dtda (but this one is a 7π neutral, so only *one* RMO.

Also like the DTTA -1/0 process, which is nodal, but unlike the 0/+1 process, which is not, and has by far the greatest substituent tunability, sloe of 0.551 V per Hammett unit.

The Linear Regression plots of the above data is presented in the following (unnumbered) graph figures.

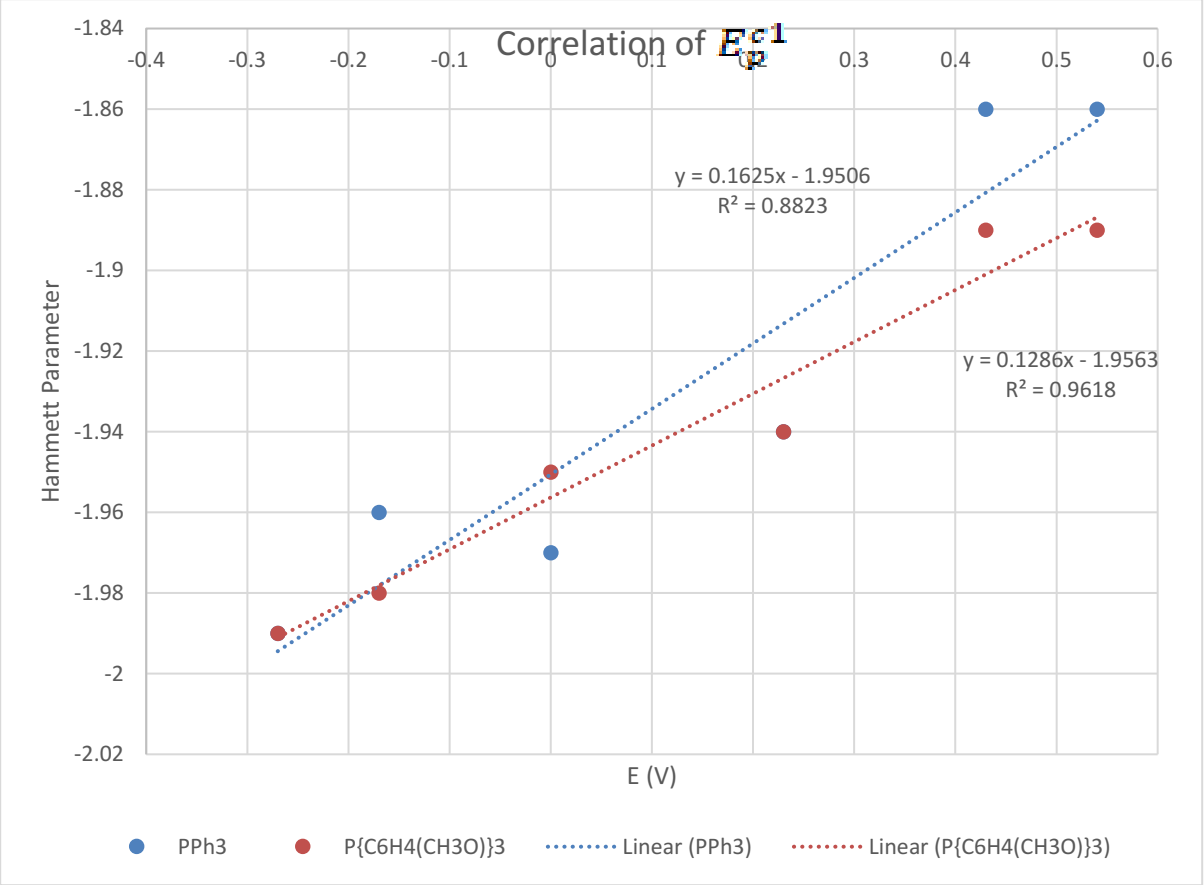
Correlation of E_p^{c1}
y = 0.1625x - 1.9506
R² = 0.8823
y = 0.1286x - 1.9563
R² = 0.9618
Hammett Parameter
E (V)
PPh3
P{C6H4(CH3O)}3
Linear (PPh3)
Linear (P{C6H4(CH3O)}3)

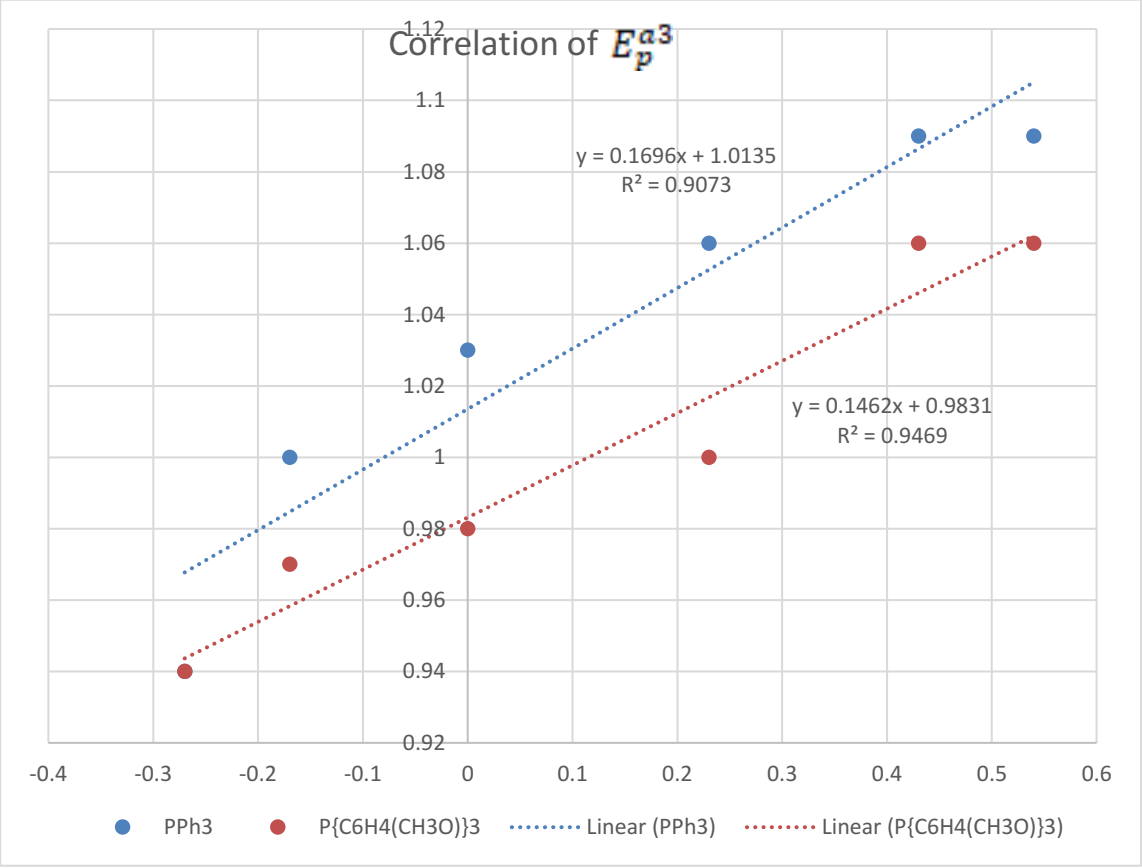
Correlation of E_p^{a3}
y = 0.1696x + 1.0135
R² = 0.9073
y = 0.1462x + 0.9831
R² = 0.9469
PPh3
P{C6H4(CH3O)}3
Linear (PPh3)
Linear (P{C6H4(CH3O)}3)

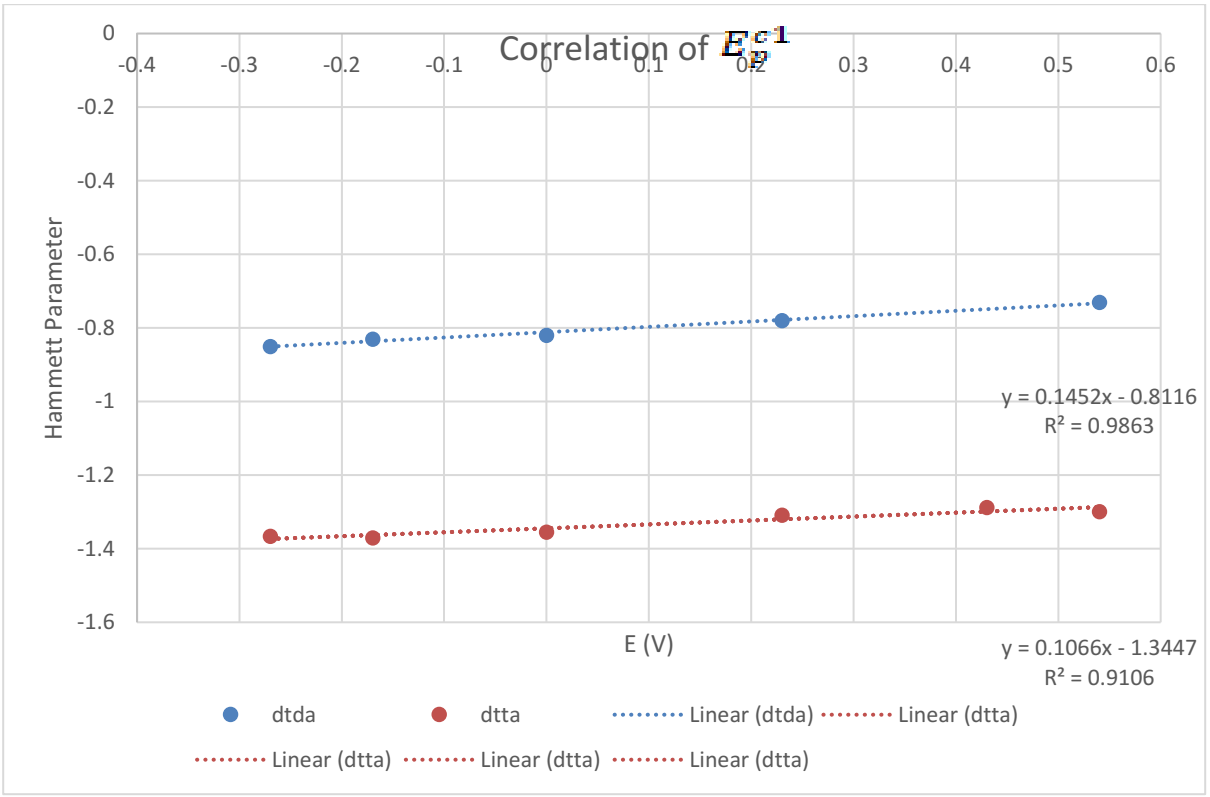
Correlation of E_p^{c1}
Hammett Parameter
E (V)
y = 0.1452x - 0.8116
R² = 0.9863
y = 0.1066x - 1.3447
R² = 0.9106
dtda
dtta
Linear (dtda)
Linear (dtta)
Linear (dtta)
Linear (dtta)
Linear (dtta)

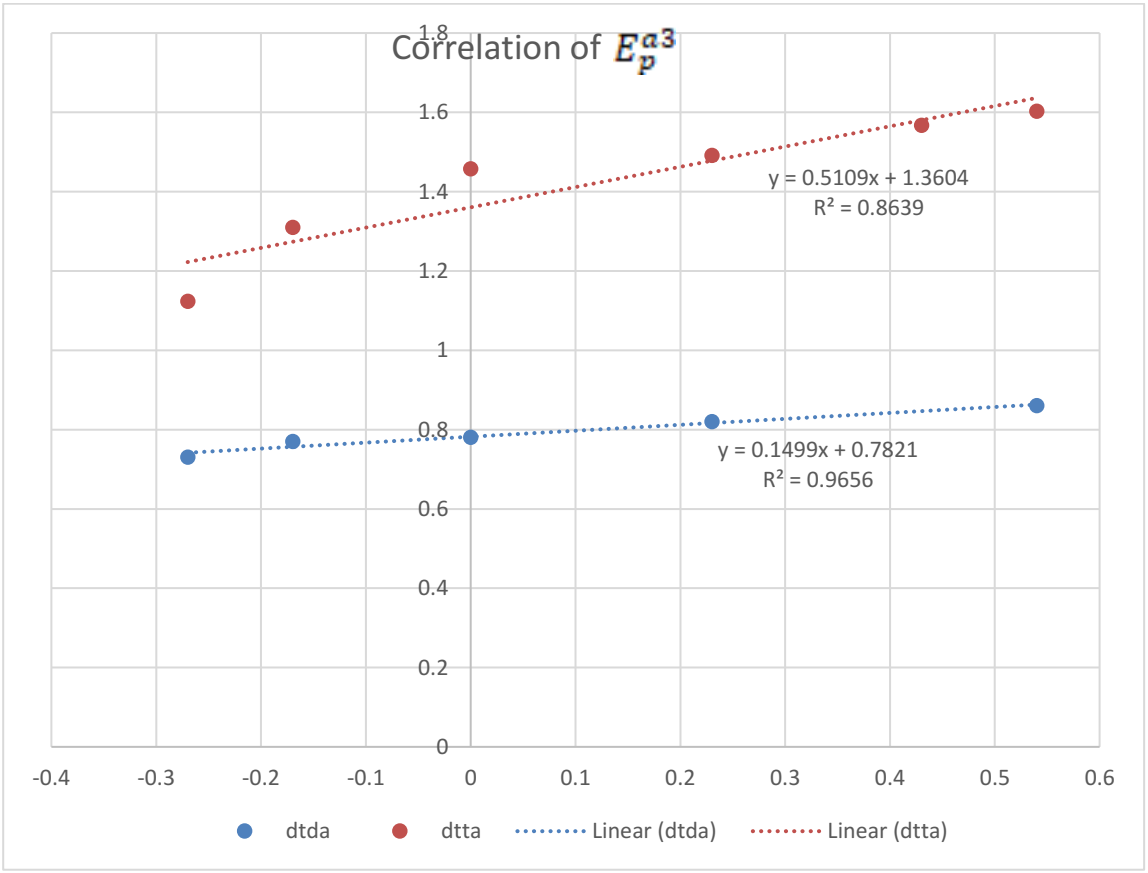
Correlation of E_p^{a3}
y = 0.5109x + 1.3604
R² = 0.8639
y = 0.1499x + 0.7821
R² = 0.9656
dtda
dtta
Linear (dtda)
Linear (dtta)

Section S6. EPR spectroscopy

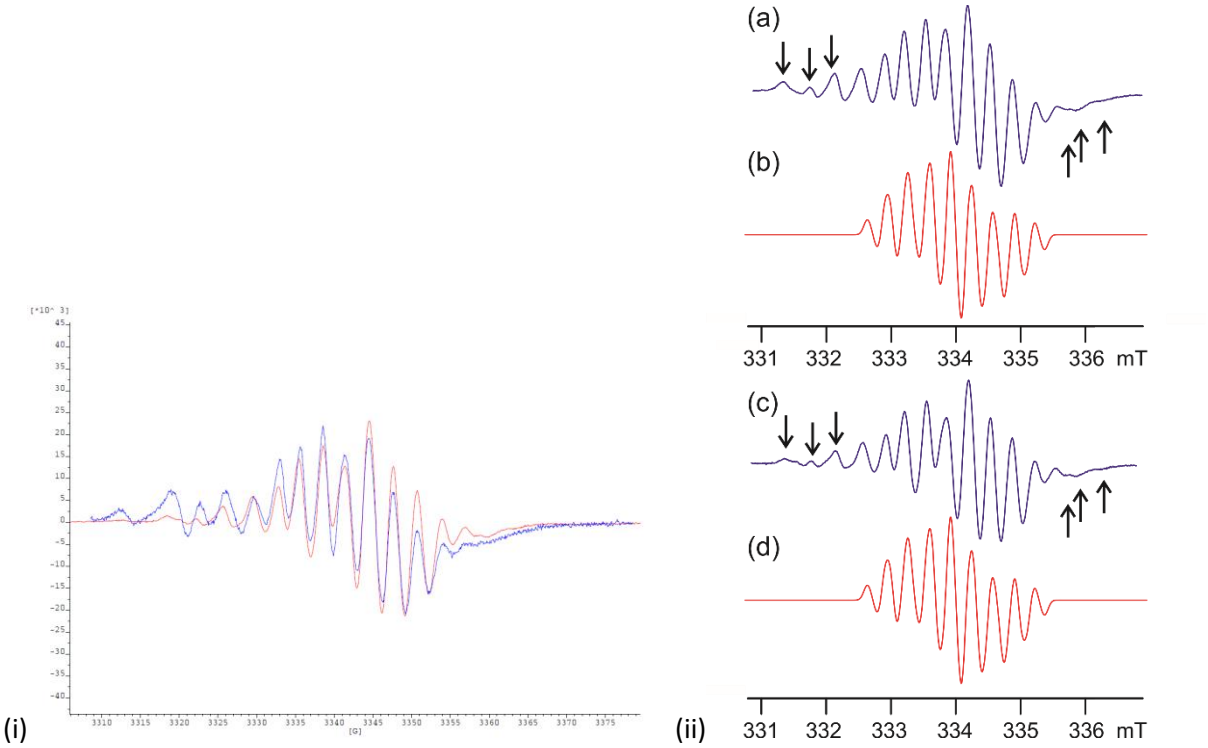

Figure S20. Two views that emphasize the similarity of the initially formed EPR signals from reduction of the title compounds. (i) Overlay of EPR scans taken during electrolysis of solutions of (red) **5a**$^{-\bullet}$ and (blue) **5e**$^{-\bullet}$ showing the similarity of their signals when decomposition signals are ignored. (ii) Best-fit simulations, traces (b) and (d), using the parameters in Table 5 with (a) **5a**$^{-\bullet}$ and (c) **5e**$^{-\bullet}$.

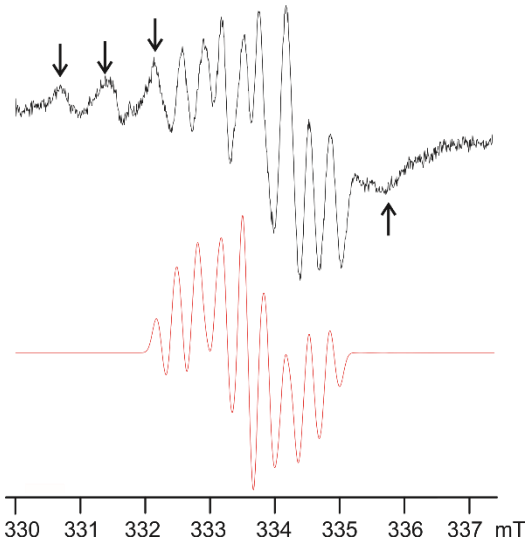

Figure S21. Best-fit simulation, using the parameters in Table 5, bottom (red) with early-sequence spectrum of **5c**$^{-\bullet}$ above (black). As in other views, the black arrows designate some of the peaks occasioned by the decomposition products which here are already quite intense.

Section S7. Computational Studies

The electronic structures of the neutral examples and anion radicals of **4** and **5** were investigated with DFT methods at the B3LYP-6-311G+(d,p)/B3LYP-6-31G(d,p) and UB3LYP-6-311G+(d,p)/UB3LYP-6-31G(d,p) levels of theory, respectively. The general suitability of this method for the purpose of calculating EPR hyperfine coupling constants has been verified through an extensive study by Sieiro *et al.*[11] However, the failure of this level of theory to accurately gauge ^{31}P hfs is well known from their work as well as from our own experience.[12] In view of the large size of the phosphoraniminato adducts, our calculations were restricted to two necessary levels of approximation. First of all, a very thorough study of geometry and reactivity was undertaken using the simplified model system **2'** (HC and PH_3 substituents). Then a model of **4c** (PhC and PPh_3 substituents) was built up for both neutral and anion radical by sequential growth of substituents using only the conformations corresponding to the lowest energies. Our computational resources did not permit for investigations of the influence of aryl ring substituents, nor were they deemed necessary for this study. There were several goals for this project. First, we wished to ascertain the nature of the geometric preference for the four possible conformations (Chart S1) and the possible substituent influences thereon. Second, it was valuable to compare the calculated and measured geometries for the neutral molecules. Last, we wanted insight into the structure of the putative radical anion and to use calculated EPR hfs parameters to help in the interpretation of the complex EPR spectra detected through the SEEPR experiments.

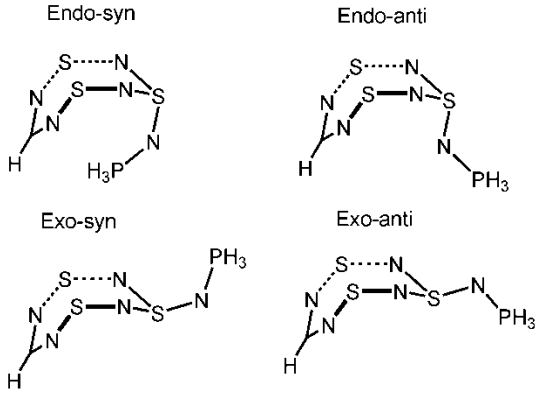

Chart S1. Conformations and their naming scheme for the models used in the computations

For **2'** we considered only the folded conformation of neutral trithiatetrazocine as both our own results and those of Knapp *et al.*[6] have shown this to be the ground state structure. However, four conformational isomers need to be considered (Chart S1). For substituted systems, *endo-anti* is the most common and the only one structurally characterized thus far for any iminophosphorane-substituted trithiatetrazocine, including **4** and **5** as discussed above. However, when E=As, structural isomerism has been demonstrated with both the *endo-anti* (thermodynamic isomer) and *exo-syn* (kinetic isomer) conformations characterized in the solid-state. Extensive NMR evidence has substantiated that all known E=P derivatives go through the same sequence with the kinetic isomer (presumed to be *exo-syn*) converting over time to the final *endo-anti* structure.

We have investigated these four conformational isomers for both the neutral and monoanions of **2'** and found that in all cases *exo-anti* is not a minimum on the energy surface with the starting geometries of this isomer minimizing to *exo-syn*. However, both *endo-anti* and *endo-syn* are stable minima (NB: within Cs symmetry restriction). Surprisingly, for this simple model it is *exo-syn* that is most stable, followed by *endo-syn* and *endo-anti* as the most energetic. However, the differences are small (less than 6 kJ/mol) and perhaps the most important conclusion is that these three isomers are so similar in energy. This fits with the experimental evidence

of the facile interconversion of *endo* to *exo* forms in solution. For the model systems, addition of one extra electron to the LUMO of the neutral molecule (which is S···S antibonding in nature) leaves the ring bent but with substantial opening of the ring to give d(S···S) = 3.082 Å *versus* 2.415(1) Å in the neutral compound.

When phenyl groups are added to the phosphine, however, the isomer preferences are reversed with the *endo-syn* conformation greatly disfavored due to steric clashes, and with the *endo-anti* now preferred by about 20 kJ/mol over *exo-syn*. The exact origin of the preference for *endo* over *syn* could not be determined. However, this energy difference is consistent with the experimental evidence for kinetic and thermodynamic products. The geometry of the neutral species especially in the CN_4S_3 cage, are quite comparable to the results from crystallography (both angles and distances deviate by less than 3%). Indeed, the only significant difference between the solid state experimental and gas phase computational geometries is in the transanular S···S which is 9% longer in the computational model.

Here too the optimized geometry for the radical anion of **4c** leads to further opening of the transannular S···S distance due to single-electron occupation of the SOMO which is antibonding across the rings (see Fig S20). Of greatest interest to us are the calculated hfs values from the *endo-anti* isomer of **4c** as calculated at the UB3LYP-6-311G+(d,p)/UB3LYP-6-31G(d,p) levels of theory. The values have been averaged to the expected effective C_s symmetry in solution to give: **P** -0.053; **N1** –0.042; **N2,3** 0.295; **N4,5** 0.336 milli-Tesla.

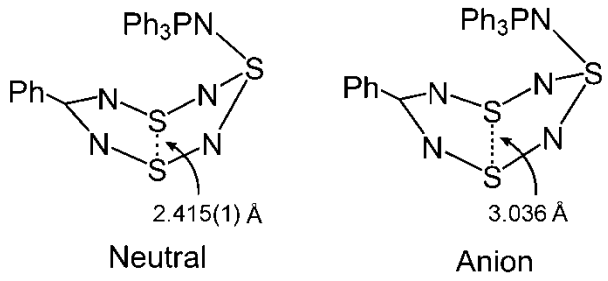

Figure S22. S···S distances for **4c** for both the neutral form (left) and the calculated radical anion form (right).

Table S9. Cartesian coordinates of computed geometries

DFT calculated $[S_4N_5]^+$ B3LYP/6-31G(d,p) Optimized and Freq Calc (0 imaginary)

No.	Symbol	X	Y	Z
1	S	-0.0010570	1.4051080	0.7357260
2	S	-2.0332560	-0.0017250	-0.7627760
3	S	0.0013230	-1.4038470	0.7373220
4	S	2.0329820	0.0007300	-0.7635250
5	N	-1.3267550	-1.3602120	-0.3706860
6	N	1.3293090	-1.3588980	-0.3696060
7	N	1.3269740	1.3596670	-0.3712750
8	N	-1.3297690	1.3583470	-0.3692340
9	N	0.0002620	0.0004880	1.6025220

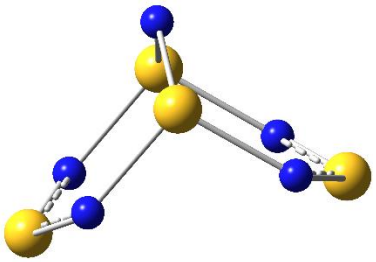

DFT calculated $[S_4N_5]^-$ B3LYP/6-31G(d,p) Optimized and Freq Calc (0 imaginary)

No.	Symbol	X	Y	Z
1	S	-0.2004410	1.3990800	0.8570810
2	S	-1.4605760	-0.2081100	-1.0717770
3	S	0.2004350	-1.3972320	0.8594810
4	S	1.4602560	0.2066630	-1.0722190
5	N	-1.1175020	-1.5653440	-0.2019480
6	N	1.5118990	-1.1915150	-0.1996790
7	N	1.1183430	1.5648290	-0.2022320
8	N	-1.5124590	1.1909610	-0.1991230
9	N	0.0004650	0.0001530	1.7799750

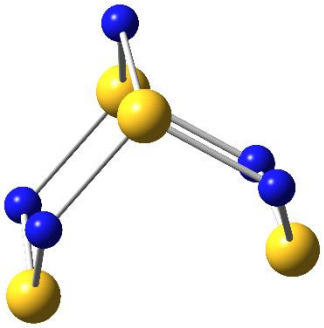

DFT calculated $[PhCN_5S_3]$ B3LYP/6-31+G(d,p) Optimized and Freq Calc (0 imaginary)

No.	Symbol	X	Y	Z
1	S	1.5817690	-1.3692040	-0.7714530
2	S	1.5814340	1.3699240	-0.7706820
3	S	2.9212840	-0.0004600	1.4351900
4	N	2.4304970	1.3635990	0.8185410
5	N	0.0016870	1.2165460	-0.3579190
6	N	2.4307400	-1.3642610	0.8177160
7	N	0.0019350	-1.2162430	-0.3577170
8	N	2.1110580	0.0004960	-1.5470560
9	C	-0.5612850	0.0000200	-0.2626640
10	C	-2.7361920	-1.2125110	0.0714150
11	H	-2.1921180	-2.1458930	-0.0136080
12	C	-4.1140320	1.2096780	0.2851790
13	H	-4.6471220	2.1522540	0.3679870
14	C	-2.0355500	-0.0000610	-0.0378330
15	C	-2.7362550	1.2123300	0.0717490
16	H	-2.1922270	2.1457620	-0.0129950
17	C	-4.8067810	-0.0001890	0.3922130
18	C	-4.1139710	-1.2099950	0.2848320
19	H	-4.6470140	-2.1526250	0.3673480
20	H	-5.8803200	-0.0002350	0.5580780

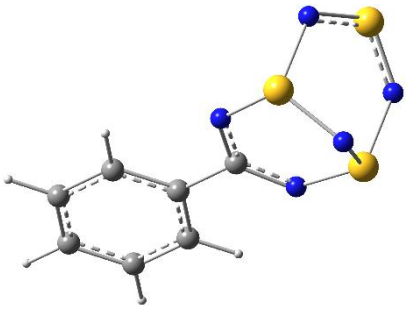

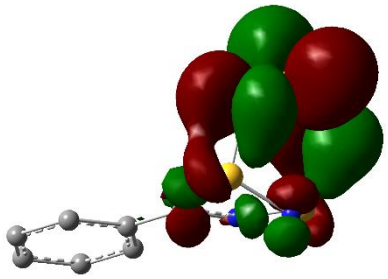

Depiction of LUMO of $PhCN_5S_3$

DFT calculated *doublet* **9**$^{-\bullet}$, $[PhCN_3S_2]^{-\bullet}$ UB3LYP/6-31G(d,p) Optimized and Freq Calc (1 imaginary)

No.	Symbol	X	Y	Z
1	S	2.4405360	1.4356030	0.0002980
2	S	2.4405340	-1.4356030	-0.0002840
3	N	0.7496640	-1.2256520	0.0001300
4	N	0.7496640	1.2256530	-0.0004390
5	N	3.3170270	-0.0000020	0.0002030
6	C	0.2172620	0.0000010	-0.0000420
7	C	-2.0039970	1.2055790	-0.0001970
8	H	-1.4379610	2.1304730	-0.0003450
9	C	-3.3983540	-1.2051240	0.0002330
10	H	-3.9370880	-2.1508990	0.0004160
11	C	-1.2839860	0.0000010	-0.0000290
12	C	-2.0039960	-1.2055790	0.0001830
13	H	-1.4379600	-2.1304720	0.0003130
14	C	-4.1064230	0.0000000	0.0000630
15	C	-3.3983550	1.2051240	-0.0001580
16	H	-3.9370900	2.1508980	-0.0002840
17	H	-5.1944150	-0.0000010	0.0000880

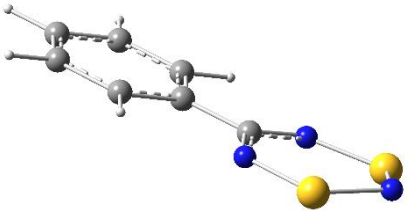

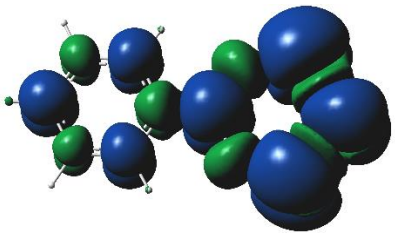

Depiction of total Spin Density of $PhCN_3S_2$

DFT calculated **7**, $[PhCN_5S_3–PPh_3]$ B3LYP/6-31+G(d,p) Optimized and Freq Calc (0 imaginary)

No.	Symbol	X	Y	Z
1	C	-3.4999840	0.4937440	-0.2812240
2	N	-2.6004380	-0.1997350	-1.0462720
3	N	-3.4206270	1.7466090	0.1312080
4	N	-1.2675830	2.0916940	-1.4702880
5	S	-1.3688900	0.5316110	-1.7435180
6	S	-1.9656190	2.5978730	0.1039840
7	N	-0.9795200	2.1209870	1.2827970
8	S	-0.6504460	0.4430460	1.5597020
9	N	0.1397930	-0.1538010	0.1796990
10	P	1.7606340	-0.2526270	0.0943940
11	C	-4.7503940	-0.2514470	0.0486760
12	C	-5.7250020	0.3400090	0.8688350
13	C	-4.9729050	-1.5413720	-0.4587540
14	C	-6.8991030	-0.3468790	1.1734730
15	H	-5.5450720	1.3348870	1.2598720
16	C	-6.1496120	-2.2257690	-0.1519240
17	H	-4.2190580	-1.9974200	-1.0898690
18	C	-7.1162430	-1.6316820	0.6641800
19	H	-7.6451830	0.1194360	1.8105330
20	H	-6.3113550	-3.2234550	-0.5501280
21	H	-8.0316660	-2.1657390	0.9032320
22	C	2.0805790	-1.1938120	-1.4352570
23	C	1.1621830	-2.1839960	-1.8233600
24	C	3.2216760	-0.9613840	-2.2173890
25	C	1.3904820	-2.9329860	-2.9791860
26	H	0.2714040	-2.3482790	-1.2260260
27	C	3.4453020	-1.7157240	-3.3715920
28	H	3.9299890	-0.1887840	-1.9364940
29	C	2.5316730	-2.7016630	-3.7529980
30	H	0.6740140	-3.6929520	-3.2765800

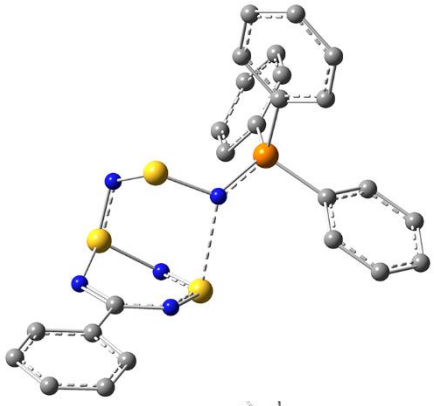

HOMO

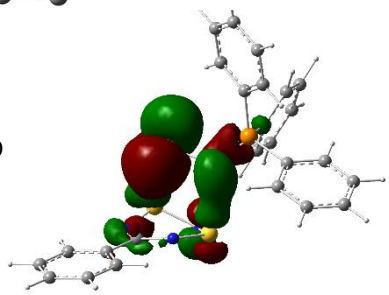

LUMO

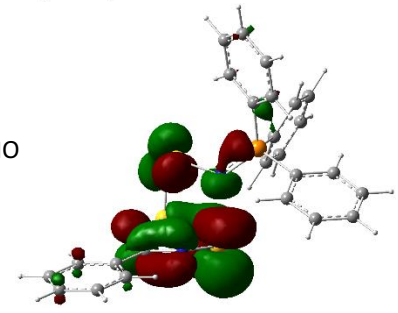

31	H	4.3284760	-1.5267720	-3.9745180
32	H	2.7050950	-3.2838210	-4.6534200
33	C	2.7098350	1.3102930	-0.0113180
34	C	4.0455790	1.3904940	0.4200730
35	C	2.0992830	2.4347590	-0.5889040
36	C	4.7608280	2.5801410	0.2708470
37	H	4.5271870	0.5319070	0.8773580
38	C	2.8213850	3.6213000	-0.7346750
39	H	1.0642780	2.3919120	-0.9117990
40	C	4.1489870	3.6965680	-0.3068730
41	H	5.7909090	2.6351490	0.6107750
42	H	2.3386200	4.4881990	-1.1755340
43	H	4.7045390	4.6234720	-0.4170630
44	C	2.5055710	-1.1838790	1.4861460
45	C	2.5602130	-0.5880270	2.7592770
46	C	2.9473010	-2.5065150	1.3272950
47	C	3.0500970	-1.3073300	3.8498110
48	H	2.2168200	0.4314250	2.9011010
49	C	3.4406120	-3.2206650	2.4222780
50	H	2.9119360	-2.9813840	0.3524530
51	C	3.4912160	-2.6237040	3.6837700
52	H	3.0843250	-0.8389940	4.8289080
53	H	3.7834470	-4.2421720	2.2866920
54	H	3.8723060	-3.1808040	4.5346740

DFT calculated **2c**-*exo*, [$PhCN_3S_2NSN{=}PPh_3$] B3LYP/6-31G(d,p) Optimized and Freq Calc (0 imaginary)

No.	Symbol	X	Y	Z
1	C	3.9834470	-0.0921100	0.1794460
2	N	3.4060430	-1.3024620	0.2371600
3	N	3.5441040	1.0772810	0.6727620
4	N	1.8325640	-0.3344910	2.2282850
5	S	2.0855310	-1.5535070	1.1927700
6	S	2.0510620	1.1734810	1.3974090
7	N	0.8472230	1.1181340	0.2791400
8	S	0.7183710	-0.1408040	-0.7984980
9	N	-0.8376400	-0.1895450	-1.2812280
10	P	-2.2021270	-0.0087240	-0.4175380
11	C	5.3001600	-0.0404820	-0.5291980
12	C	5.9803750	1.1788600	-0.6739820
13	C	5.8732970	-1.2094340	-1.0544450
14	C	7.2097710	1.2263550	-1.3319560
15	H	5.5332330	2.0786100	-0.2673600
16	C	7.1014400	-1.1584260	-1.7139560
17	H	5.3457660	-2.1494040	-0.9389010
18	C	7.7746400	0.0591100	-1.8548730
19	H	7.7269420	2.1759780	-1.4372630
20	H	7.5339370	-2.0698650	-2.1171300
21	H	8.7316370	0.0978230	-2.3679270
22	C	-3.4504160	-1.0042420	-1.2996320
23	C	-3.2738990	-1.2615000	-2.6677610
24	C	-4.5859810	-1.4987090	-0.6389730
25	C	-4.2312480	-1.9990350	-3.3668340

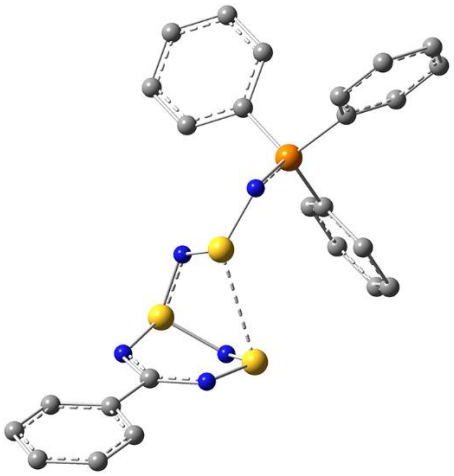

HOMO

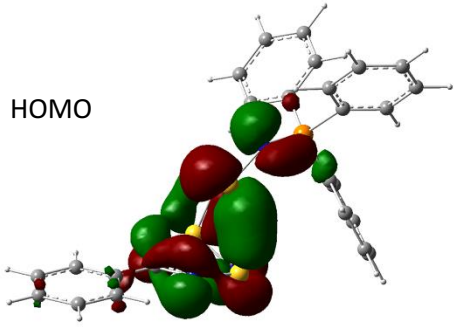

26	H	-2.3811520	-0.8990620	-3.1661630
27	C	-5.5396610	-2.2363160	-1.3442360
28	H	-4.7226260	-1.3239290	0.4241280
29	C	-5.3648720	-2.4842520	-2.7084520
30	H	-4.0875500	-2.1988260	-4.4244990
31	H	-6.4128440	-2.6212080	-0.8258910
32	H	-6.1060750	-3.0603900	-3.2546580
33	C	-2.1360490	-0.6310860	1.2971060
34	C	-2.4152090	0.1808650	2.4052720
35	C	-1.7502240	-1.9686260	1.4937930
36	C	-2.3149000	-0.3423910	3.6965150
37	H	-2.7027330	1.2173190	2.2642950
38	C	-1.6518490	-2.4849340	2.7849170
39	H	-1.5260370	-2.6026320	0.6405570
40	C	-1.9327290	-1.6716090	3.8872380
41	H	-2.5269250	0.2926570	4.5512910
42	H	-1.3487010	-3.5172880	2.9308440
43	H	-1.8463130	-2.0727620	4.8926310
44	C	-2.8175690	1.7158610	-0.3723360
45	C	-1.9157690	2.7601070	-0.1044990
46	C	-4.1711980	2.0098380	-0.6050490
47	C	-2.3730400	4.0786890	-0.0637770
48	H	-0.8669990	2.5337080	0.0680790
49	C	-4.6191320	3.3320460	-0.5620530
50	H	-4.8767870	1.2171190	-0.8287590
51	C	-3.7215690	4.3675950	-0.2907820
52	H	-1.6700790	4.8807310	0.1411000
53	H	-5.6667410	3.5502240	-0.7472840
54	H	-4.0704280	5.3958790	-0.2626930

LUMO

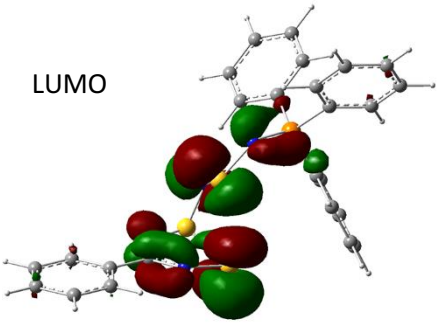

DFT calculated **2c**-*endo*, [$PhCN_3S_2NSN{=}PPh_3$] B3LYP/6-31G(d,p) Optimized and Freq Calc (0 imaginary)

No.	Symbol	X	Y	Z
1	C	2.7538090	-0.8070690	-0.2576370
2	N	2.4603240	-1.0810160	-1.5494060
3	N	2.5537040	-1.5402460	0.8366040
4	N	2.4241770	-3.6799020	-0.8233250
5	S	2.0346800	-2.6041350	-1.9565730
6	S	1.9360060	-3.1140010	0.7248220
7	N	0.2995900	-3.1505630	0.5796420
8	S	-0.4550390	-2.3795850	-0.6855550
9	N	-0.2865030	-0.7262180	-0.6460350
10	P	-1.4375910	0.2495290	-0.0651490
11	C	3.4124340	0.5160840	-0.0329800
12	C	3.7413960	0.9359560	1.2645930
13	C	3.7311550	1.3455760	-1.1186970
14	C	4.3672620	2.1628550	1.4708490
15	H	3.5054470	0.2847930	2.0980020
16	C	4.3601080	2.5710710	-0.9092630
17	H	3.4874720	1.0105890	-2.1202330
18	C	4.6787560	2.9849970	0.3855630

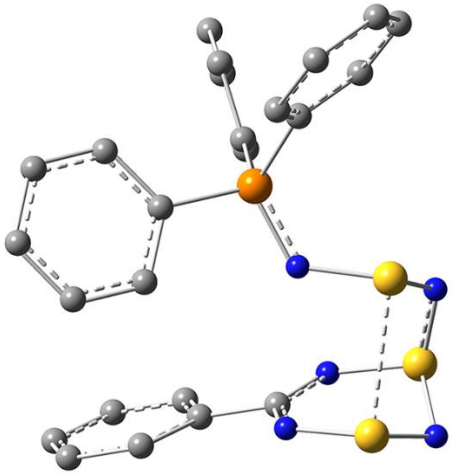

19	H	4.6165770	2.4770330	2.4803350
20	H	4.6064050	3.2022360	-1.7584490
21	H	5.1697250	3.9403710	0.5480480
22	C	-1.0482070	1.8947810	-0.7412960
23	C	-0.0140240	2.0177490	-1.6786000
24	C	-1.7636780	3.0312720	-0.3338660
25	C	0.2920350	3.2723140	-2.2083530
26	H	0.5444610	1.1333110	-1.9665750
27	C	-1.4548540	4.2787470	-0.8717320
28	H	-2.5556520	2.9488860	0.4042710
29	C	-0.4271030	4.3993680	-1.8105860
30	H	1.0987280	3.3665900	-2.9286500
31	H	-2.0110210	5.1557780	-0.5547240
32	H	-0.1847500	5.3734970	-2.2253370
33	C	-3.1515180	-0.1630060	-0.5555210
34	C	-3.8425640	-1.1787630	0.1269540
35	C	-3.7330290	0.4190200	-1.6923300
36	C	-5.0983020	-1.5924010	-0.3152860
37	H	-3.4025550	-1.6431170	1.0037250
38	C	-4.9915310	0.0046130	-2.1273720
39	H	-3.2052210	1.1967500	-2.2343190
40	C	-5.6749250	-0.9997890	-1.4401570
41	H	-5.6245930	-2.3778240	0.2184300
42	H	-5.4368940	0.4662050	-3.0034930
43	H	-6.6542410	-1.3218310	-1.7815690
44	C	-1.4558730	0.3823120	1.7587230
45	C	-0.2941450	0.0237810	2.4586930
46	C	-2.5687820	0.8709240	2.4629530
47	C	-0.2511600	0.1575750	3.8468700
48	H	0.5631210	-0.3721960	1.9235680
49	C	-2.5157160	1.0054430	3.8495140
50	H	-3.4819430	1.1288910	1.9353920
51	C	-1.3563520	0.6494100	4.5420400
52	H	0.6477600	-0.1300760	4.3834120
53	H	-3.3808200	1.3799990	4.3885870
54	H	-1.3186960	0.7494180	5.6228830

DFT calculated **4c**-*exo*, [$PhCN_2S_2N_2S$–N=PPh_3] B3LYP/6-31G(d,p) Optimized and Freq Calc (0 imaginary)

No.	Symbol	X	Y	Z
1	C	3.9834470	-0.0921100	0.1794460
2	N	3.4060430	-1.3024620	0.2371600
3	N	3.5441040	1.0772810	0.6727620
4	N	1.8325640	-0.3344910	2.2282850
5	S	2.0855310	-1.5535070	1.1927700
6	S	2.0510620	1.1734810	1.3974090
7	N	0.8472230	1.1181340	0.2791400
8	S	0.7183710	-0.1408040	-0.7984980
9	N	-0.8376400	-0.1895450	-1.2812280
10	P	-2.2021270	-0.0087240	-0.4175380
11	C	5.3001600	-0.0404820	-0.5291980

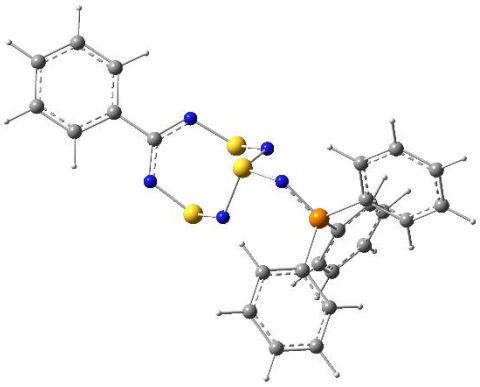

12	C	5.9803750	1.1788600	-0.6739820
13	C	5.8732970	-1.2094340	-1.0544450
14	C	7.2097710	1.2263550	-1.3319560
15	H	5.5332330	2.0786100	-0.2673600
16	C	7.1014400	-1.1584260	-1.7139560
17	H	5.3457660	-2.1494040	-0.9389010
18	C	7.7746400	0.0591100	-1.8548730
19	H	7.7269420	2.1759780	-1.4372630
20	H	7.5339370	-2.0698650	-2.1171300
21	H	8.7316370	0.0978230	-2.3679270
22	C	-3.4504160	-1.0042420	-1.2996320
23	C	-3.2738990	-1.2615000	-2.6677610
24	C	-4.5859810	-1.4987090	-0.6389730
25	C	-4.2312480	-1.9990350	-3.3668340
26	H	-2.3811520	-0.8990620	-3.1661630
27	C	-5.5396610	-2.2363160	-1.3442360
28	H	-4.7226260	-1.3239290	0.4241280
29	C	-5.3648720	-2.4842520	-2.7084520
30	H	-4.0875500	-2.1988260	-4.4244990
31	H	-6.4128440	-2.6212080	-0.8258910
32	H	-6.1060750	-3.0603900	-3.2546580
33	C	-2.1360490	-0.6310860	1.2971060
34	C	-2.4152090	0.1808650	2.4052720
35	C	-1.7502240	-1.9686260	1.4937930
36	C	-2.3149000	-0.3423910	3.6965150
37	H	-2.7027330	1.2173190	2.2642950
38	C	-1.6518490	-2.4849340	2.7849170
39	H	-1.5260370	-2.6026320	0.6405570
40	C	-1.9327290	-1.6716090	3.8872380
41	H	-2.5269250	0.2926570	4.5512910
42	H	-1.3487010	-3.5172880	2.9308440
43	H	-1.8463130	-2.0727620	4.8926310
44	C	-2.8175690	1.7158610	-0.3723360
45	C	-1.9157690	2.7601070	-0.1044990
46	C	-4.1711980	2.0098380	-0.6050490
47	C	-2.3730400	4.0786890	-0.0637770
48	H	-0.8669990	2.5337080	0.0680790
49	C	-4.6191320	3.3320460	-0.5620530
50	H	-4.8767870	1.2171190	-0.8287590
51	C	-3.7215690	4.3675950	-0.2907820
52	H	-1.6700790	4.8807310	0.1411000
53	H	-5.6667410	3.5502240	-0.7472840
54	H	-4.0704280	5.3958790	-0.2626930

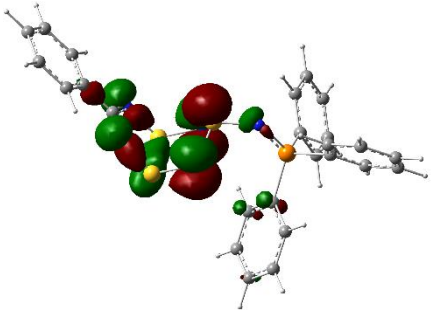

HOMO of 4c-exo

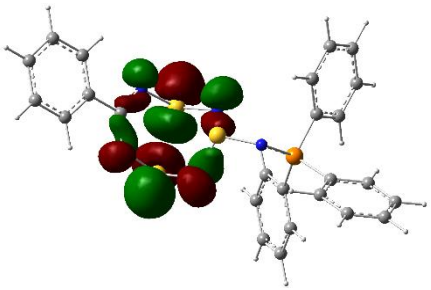

LUMO of 4c-exo

DFT calculated **4c**-*endo*, [$PhCN_2S_2N_2S$–N=PPh_3] B3LYP/6-31G(d,p) Optimized and Freq Calc (0 imaginary)

No.	Symbol	X	Y	Z
1	C	2.9287890	-1.0216080	-0.1381420
2	N	2.5355340	-1.5967940	1.0062520
3	N	2.8022160	-1.5195020	-1.3728990
4	N	0.4223240	-2.9365970	-1.7924110
5	N	0.1469570	-3.0493040	0.8171610
6	S	-0.5522780	-2.3781650	-0.5548780
7	N	-0.3137690	-0.7385440	-0.5267040
8	S	2.0421890	-2.9595690	-1.6259770
9	S	1.7691170	-3.0635440	0.9881270
10	P	-1.4356820	0.3145000	-0.0491470
11	C	-1.0345590	1.8692090	-0.9107240
12	C	-1.7207540	3.0588490	-0.6228500
13	C	-0.0147600	1.8649330	-1.8715070
14	C	-1.3976630	4.2310050	-1.3030710
15	H	-2.5011770	3.0768270	0.1316500
16	C	0.3057540	3.0443950	-2.5452880
17	H	0.5203470	0.9420040	-2.0682110
18	C	-0.3847030	4.2237510	-2.2654950
19	H	-1.9316100	5.1495300	-1.0791180
20	H	1.0997750	3.0393290	-3.2855590
21	H	-0.1317510	5.1396260	-2.7916000
22	C	-1.3923290	0.6408480	1.7481160
23	C	-0.2305710	0.2884540	2.4511260
24	C	-2.4545210	1.2623420	2.4250070
25	C	-0.1370290	0.5616240	3.8162820
26	H	0.5871660	-0.2062640	1.9357570
27	C	-2.3511160	1.5343340	3.7883020
28	H	-3.3698160	1.5142980	1.8979800
29	C	-1.1913380	1.1854470	4.4840440
30	H	0.7610650	0.2793160	4.3569720
31	H	-3.1774120	2.0104820	4.3076860
32	H	-1.1143230	1.3940170	5.5471460
33	C	-3.1648160	-0.1223820	-0.4513510
34	C	-3.8744980	-1.0064110	0.3788990
35	C	-3.7445610	0.3066920	-1.6552730
36	C	-5.1474600	-1.4416740	0.0130940
37	H	-3.4363500	-1.3510560	1.3104200
38	C	-5.0195910	-0.1290110	-2.0138040
39	H	-3.2016620	0.9813120	-2.3091260
40	C	-5.7215860	-1.0018300	-1.1809240
41	H	-5.6887090	-2.1252420	0.6599330
42	H	-5.4631460	0.2122480	-2.9441780
43	H	-6.7137480	-1.3412790	-1.4630870
44	C	3.6468700	0.2779320	-0.0193840
45	C	4.0847320	0.9501020	-1.1698930
46	C	3.8953040	0.8424250	1.2398990
47	C	4.7547210	2.1663920	-1.0612080
48	H	3.8948760	0.5009700	-2.1381590

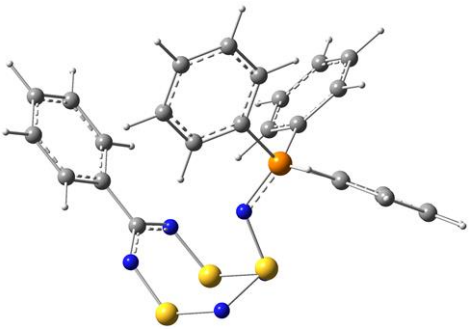

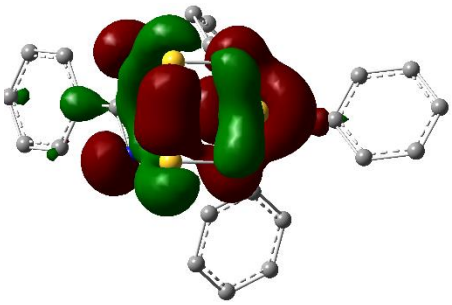

HOMO of 4c-endo

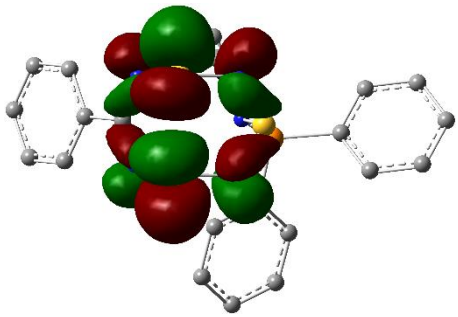

LUMO of 4c-endo

49	C	4.5653310	2.0591930	1.3451660
50	H	3.5625180	0.3116680	2.1245020
51	C	4.9964240	2.7251460	0.1958620
52	H	5.0917130	2.6782490	-1.9581030
53	H	4.7540100	2.4876290	2.3253160
54	H	5.5197640	3.6735090	0.2795380

DFT calculated *doublet exo*-**2c**$^{-\bullet}$, [$PhCN_3S_2NSN{=}PPh_3$]$^{-\bullet}$ UB3LYP/6-31G(d,p) Opt and Freq Calc (0 imaginary)

No.	Symbol	X	Y	Z
1	C	-4.1221870	-0.4802960	0.0305240
2	N	-3.8139360	-1.5192230	0.8094780
3	N	-3.4842490	0.0878180	-0.9996900
4	N	-1.8162410	-2.0816220	-1.0013080
5	S	-2.4116920	-2.3625930	0.5208560
6	S	-1.9829710	-0.4655710	-1.5632480
7	N	-0.8060240	0.5202200	-0.9834530
8	S	-0.6140150	0.7113610	0.7143410
9	N	0.8581440	-0.0819730	1.1322840
10	P	2.2240760	0.1249070	0.3388640
11	C	-5.4452360	0.1601250	0.3593610
12	C	-5.9008030	1.2702410	-0.3663010
13	C	-6.2485170	-0.3424910	1.3934210
14	C	-7.1280710	1.8603950	-0.0666800
15	H	-5.2688880	1.6516620	-1.1602870
16	C	-7.4752210	0.2483770	1.6925370
17	H	-5.8869430	-1.1997970	1.9500410
18	C	-7.9230470	1.3528460	0.9633860
19	H	-7.4651510	2.7216250	-0.6392220
20	H	-8.0848400	-0.1546180	2.4982540
21	H	-8.8801310	1.8136260	1.1969380
22	C	3.5355040	-0.4376510	1.4963920
23	C	3.2121890	-0.5225460	2.8580340
24	C	4.8300230	-0.7760340	1.0778300
25	C	4.1726090	-0.9272870	3.7847340
26	H	2.1962930	-0.2845280	3.1563630
27	C	5.7912610	-1.1743480	2.0087880
28	H	5.0874720	-0.7464750	0.0239260
29	C	5.4648790	-1.2493170	3.3635920
30	H	3.9102820	-0.9945900	4.8371320
31	H	6.7915630	-1.4347430	1.6730130
32	H	6.2123190	-1.5649090	4.0869550
33	C	2.4366880	-0.8977500	-1.1788330
34	C	3.4411730	-0.6460870	-2.1259090
35	C	1.5590980	-1.9711310	-1.3744210
36	C	3.5845260	-1.4768520	-3.2380350
37	H	4.0957490	0.2137210	-2.0105590
38	C	1.6967480	-2.7911040	-2.4947700
39	H	0.7404600	-2.1319760	-0.6817520
40	C	2.7133730	-2.5531240	-3.4210930
41	H	4.3638540	-1.2736990	-3.9682660

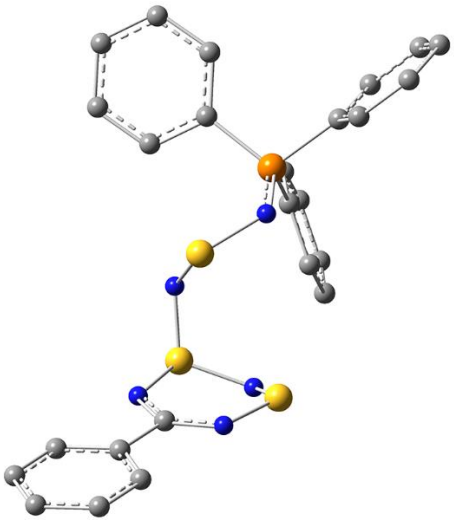

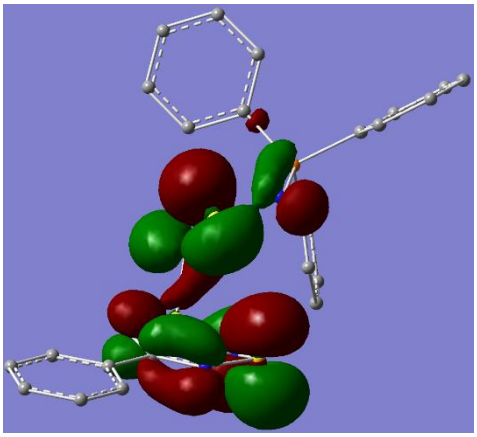

SOMO of exo-2cRadAnion

42	H	0.9894760	-3.6007820	-2.6471890
43	H	2.8170030	-3.1926420	-4.2941650
44	C	2.6782020	1.8223420	-0.2189740
45	C	1.8093740	2.4581480	-1.1267960
46	C	3.7599440	2.5387470	0.3149520
47	C	2.0453530	3.7819030	-1.5002660
48	H	0.9488610	1.9179510	-1.5215880
49	C	3.9928800	3.8592110	-0.0719380
50	H	4.4237280	2.0656930	1.0320120
51	C	3.1359160	4.4822790	-0.9813640
52	H	1.3675160	4.2680700	-2.1966290
53	H	4.8413450	4.4006620	0.3389270
54	H	3.3139510	5.5128720	-1.2782550

DFT calculated *doublet endo*-**2c**$^{-\bullet}$, $[PhCN_3S_2NSN{=}PPh_3]^{-\bullet}$ UB3LYP/6-31G(d,p) Opt and Freq Calc (0 imaginary)

No.	Symbol	X	Y	Z
1	C	3.5189080	-0.4948480	-0.2048760
2	N	3.9968190	-1.2045190	-1.2284290
3	N	2.6693670	-0.8108390	0.7818190
4	N	2.9249040	-3.4183350	0.0109560
5	S	3.6022880	-2.8115440	-1.3649880
6	S	1.9016400	-2.3215890	0.8779230
7	N	0.4087090	-2.3048500	0.2065880
8	S	0.1708000	-1.6378590	-1.3713080
9	N	-0.4911780	-0.0549120	-1.1609980
10	P	-1.7845490	0.2141350	-0.2666730
11	C	4.0720120	0.9032180	-0.1245170
12	C	3.8398620	1.7045750	1.0021940
13	C	4.8465000	1.4267510	-1.1704710
14	C	4.3649340	2.9939970	1.0810850
15	H	3.2473370	1.2896820	1.8094090
16	C	5.3670680	2.7173260	-1.0937910
17	H	5.0260380	0.7999720	-2.0365380
18	C	5.1303530	3.5088170	0.0329690
19	H	4.1752840	3.5994520	1.9644740
20	H	5.9598620	3.1081970	-1.9176880
21	H	5.5371510	4.5155690	0.0925840
22	C	-2.4651760	1.8123590	-0.8650260
23	C	-2.0579950	2.2613140	-2.1291000
24	C	-3.3657380	2.5865190	-0.1200650
25	C	-2.5547240	3.4591910	-2.6425100
26	H	-1.3370030	1.6611700	-2.6748140
27	C	-3.8667330	3.7815460	-0.6396530
28	H	-3.6657150	2.2681110	0.8732910
29	C	-3.4629550	4.2191330	-1.9020020
30	H	-2.2283920	3.8019740	-3.6207100
31	H	-4.5642350	4.3741630	-0.0535780
32	H	-3.8483890	5.1529130	-2.3033550
33	C	-3.1557960	-1.0156550	-0.2985940
34	C	-2.8579560	-2.3253410	0.1260550

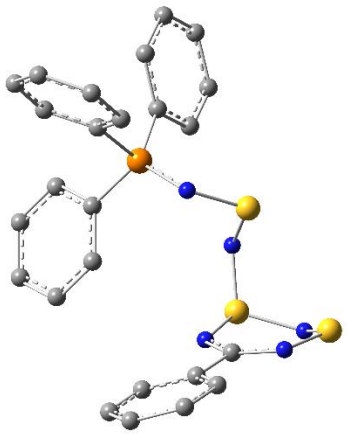

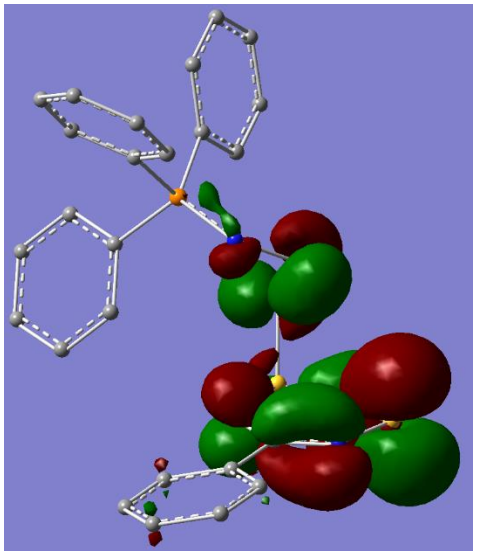

SOMO of endo-2cRadAnion

35	C	-4.4196080	-0.7390540	-0.8415190
36	C	-3.8275660	-3.3240320	0.0221670
37	H	-1.8698940	-2.5572090	0.5233580
38	C	-5.3854760	-1.7421970	-0.9317050
39	H	-4.6525800	0.2617900	-1.1916580
40	C	-5.0902790	-3.0366860	-0.4990170
41	H	-3.5891780	-4.3334200	0.3462980
42	H	-6.3659400	-1.5127320	-1.3415100
43	H	-5.8405810	-3.8198970	-0.5745700
44	C	-1.4746370	0.4652260	1.5325450
45	C	-0.1612400	0.7314030	1.9400110
46	C	-2.4997000	0.4183680	2.4895700
47	C	0.1149540	0.9661250	3.2876010
48	H	0.6425660	0.7064590	1.2108000
49	C	-2.2197600	0.6630360	3.8345910
50	H	-3.5136620	0.1673690	2.1896740
51	C	-0.9110130	0.9418420	4.2338910
52	H	1.1394260	1.1514860	3.5970450
53	H	-3.0191400	0.6219220	4.5702160
54	H	-0.6901810	1.1234580	5.2827820

DFT calculated *doublet exo*-**4c**$^{-\bullet}$, [$PhCN_3S_2NSN{=}PPh_3$]$^{-\bullet}$ UB3LYP/6-31+G(d,p) Opt and Freq Calc (0 imaginary)

No.	Symbol	X	Y	Z
1	S	-2.2134420	-2.1092080	-0.6055810
2	S	-2.0060910	0.7395100	-1.5803190
3	N	-0.8498000	-1.7635880	0.3084820
4	N	-0.6846010	0.8776290	-0.5360630
5	N	-3.5027020	0.8528060	-0.7747160
6	N	-3.6650290	-1.4823310	0.0216070
7	S	-0.7194350	-0.1621780	0.8109520
8	N	0.8556170	-0.0771150	1.3468020
9	P	2.1339690	0.0544130	0.3793050
10	C	-4.0541860	-0.2210600	-0.1969500
11	C	2.4263410	1.7269650	-0.3239330
12	C	3.3132620	1.9502100	-1.3856770
13	C	1.7589880	2.8129380	0.2581750
14	C	3.5470660	3.2478270	-1.8461080
15	H	3.8068730	1.1111000	-1.8671290
16	C	1.9935640	4.1060690	-0.2053310
17	H	1.0374640	2.6250530	1.0449020
18	C	2.8898970	4.3266830	-1.2536780
19	H	4.2320340	3.4119760	-2.6737050
20	H	1.4626430	4.9415780	0.2419160
21	H	3.0654630	5.3360580	-1.6165190
22	C	3.5322000	-0.2308940	1.5393370
23	C	4.8082130	0.3124390	1.3374250
24	C	3.2992580	-1.0360640	2.6638360
25	C	5.8393900	0.0456210	2.2397320
26	H	4.9968170	0.9551400	0.4834720
27	C	4.3323460	-1.3007850	3.5628760

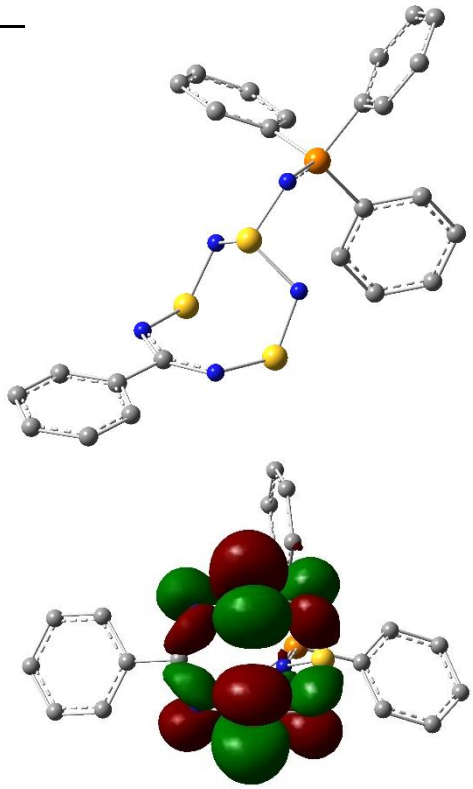

SOMO of exo-4cRadAnion 1

28	H	2.2988900	-1.4243410	2.8225220
29	C	5.6037390	-0.7633300	3.3523150
30	H	6.8237050	0.4758530	2.0757750
31	H	4.1415120	-1.9241430	4.4320850
32	H	6.4063350	-0.9684930	4.0559490
33	C	2.4177600	-1.1018660	-1.0281520
34	C	1.5033220	-1.1113670	-2.0948970
35	C	3.5080760	-1.9836650	-1.0484710
36	C	1.6919200	-1.9828430	-3.1652430
37	H	0.6427410	-0.4500720	-2.0555670
38	C	3.6885810	-2.8563250	-2.1239280
39	H	4.2178380	-1.9960360	-0.2285660
40	C	2.7823310	-2.8560490	-3.1834160
41	H	0.9742920	-1.9873710	-3.9804060
42	H	4.5357440	-3.5371800	-2.1276660
43	H	2.9200360	-3.5390850	-4.0177780
44	C	-5.4482710	0.0565160	0.3334130
45	C	-6.1861350	-0.9506440	0.9719470
46	C	-6.0284010	1.3257120	0.1943770
47	C	-7.4707930	-0.6976240	1.4523570
48	H	-5.7223270	-1.9248540	1.0776040
49	C	-7.3128740	1.5789710	0.6751410
50	H	-5.4435060	2.0953190	-0.2965210
51	C	-8.0421000	0.5686960	1.3066860
52	H	-8.0280760	-1.4918940	1.9445880
53	H	-7.7464850	2.5699100	0.5576900
54	H	-9.0433950	0.7666980	1.6831780

DFT calculated *doublet endo*-**4c**$^{-\bullet}$, $[PhCN_3S_2NSN{=}PPh_3]^{-\bullet}$ UB3LYP/6-31+G(d,p) Opt and Freq Calc (0 imaginary)

No.	Symbol	X	Y	Z
1	C	-2.9963710	-0.9650710	-0.0565020
2	N	-2.8840000	-1.4502870	-1.2967190
3	N	-2.6299870	-1.3988860	1.1504500
4	N	-0.2147490	-2.9312050	1.0871880
5	N	-0.5108450	-3.0312300	-1.6659570
6	S	0.4004420	-2.5575510	-0.3986910
7	N	0.3237490	-0.8215760	-0.5155940
8	S	-1.8891520	-2.9031880	1.3797650
9	S	-2.2073750	-2.9530690	-1.6387840
10	P	1.4384470	0.2065680	-0.0824300
11	C	1.0082210	1.8027480	-0.8769230
12	C	1.9577000	2.7955070	-1.1562250
13	C	-0.3365510	2.0151000	-1.2113600
14	C	1.5617770	3.9994970	-1.7419990
15	H	3.0078990	2.6241440	-0.9363990
16	C	-0.7275990	3.2217360	-1.7915360
17	H	-1.0555560	1.2224190	-1.0329650
18	C	0.2179840	4.2156990	-2.0532560
19	H	2.3034750	4.7633420	-1.9610500
20	H	-1.7744470	3.3765070	-2.0355480

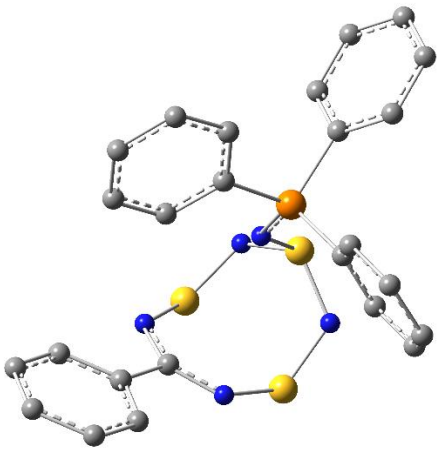

21	H	-0.0893330	5.1542580	-2.5075670
22	C	3.1572590	-0.1810310	-0.6528650
23	C	4.3183220	0.1031140	0.0786870
24	C	3.2730350	-0.8249570	-1.8957880
25	C	5.5746430	-0.2320000	-0.4316750
26	H	4.2424320	0.5761680	1.0525540
27	C	4.5279970	-1.1606470	-2.4013420
28	H	2.3725780	-1.0759260	-2.4488350
29	C	5.6811760	-0.8617410	-1.6721120
30	H	6.4682720	-0.0082860	0.1451610
31	H	4.6046780	-1.6641410	-3.3609650
32	H	6.6588500	-1.1278320	-2.0654220
33	C	1.6108060	0.5775260	1.7194810
34	C	1.2076170	-0.4137360	2.6277680
35	C	2.0962880	1.8026020	2.2053040
36	C	1.3184810	-0.1826150	4.0007390
37	H	0.7857230	-1.3511520	2.2597710
38	C	2.2041470	2.0247450	3.5782900
39	H	2.3740150	2.5932710	1.5149900
40	C	1.8184580	1.0290090	4.4784420
41	H	0.9973670	-0.9531480	4.6959090
42	H	2.5780690	2.9778220	3.9436560
43	H	1.8956570	1.2046100	5.5485600
44	C	-3.7209790	0.3643490	-0.0129600
45	C	-4.2124920	0.9524720	-1.1887240
46	C	-3.9097940	1.0392350	1.2021440
47	C	-4.8763850	2.1791850	-1.1494270
48	H	-4.0577780	0.4209130	-2.1210000
49	C	-4.5733190	2.2653550	1.2409990
50	H	-3.5200260	0.5761440	2.1015600
51	C	-5.0605520	2.8430100	0.0662700
52	H	-5.2549970	2.6165240	-2.0709410
53	H	-4.7080730	2.7744110	2.1928340
54	H	-5.5765270	3.8000850	0.0973180

DFT calculated *doublet* **11**$^{-\bullet}$, $[Ph_3P{=}NSNS]^{-\bullet}$ UB3LYP/6-31+G(d,p) Optimized and Freq Calc (0 imaginary)

No.	Symbol	X	Y	Z
1	S	3.4826170	0.4747350	0.6925230
2	N	3.1941730	-0.3504320	2.1414120
3	S	1.6682780	-0.9046850	2.5832390
4	N	0.3225300	-0.0797890	1.8901750
5	P	-0.1941990	-0.0310750	0.3857650
6	C	0.0900300	-1.4682460	-0.7416240
7	C	1.3842660	-1.6959320	-1.2433040
8	C	-0.9083580	-2.4315750	-0.9676830
9	C	1.6559020	-2.8486210	-1.9848760
10	H	2.1799190	-0.9858740	-1.0122220
11	C	-0.6321410	-3.5799450	-1.7137420
12	H	-1.9059240	-2.2867210	-0.5654070
13	C	0.6509950	-3.7880990	-2.2309160
14	H	2.6628740	-3.0137590	-2.3591940
15	H	-1.4180990	-4.3107320	-1.8883370
16	H	0.8674280	-4.6832820	-2.8092290
17	C	0.2677320	1.4712610	-0.5762950
18	C	0.1987700	1.5320840	-1.9743050
19	C	0.6284270	2.6191380	0.1450000
20	C	0.4885790	2.7262640	-2.6452430
21	H	-0.0519770	0.6435560	-2.5471640
22	C	0.9001150	3.8117880	-0.5233130
23	H	0.7198490	2.5494610	1.2239770
24	C	0.8338130	3.8689370	-1.9213990
25	H	0.4499640	2.7573000	-3.7315010
26	H	1.1916910	4.6913150	0.0445320
27	H	1.0613510	4.7962010	-2.4415250
28	C	-2.0356370	0.1188420	0.5180290
29	C	-2.6278380	-0.1115730	1.7678860
30	C	-2.8553060	0.4543080	-0.5715140
31	C	-4.0140350	-0.0253240	1.9225140
32	H	-1.9750190	-0.3467080	2.6034500
33	C	-4.2422380	0.5383010	-0.4175250
34	H	-2.4147560	0.6566950	-1.5428660
35	C	-4.8259550	0.2971260	0.8297390
36	H	-4.4593880	-0.2066990	2.8975700
37	H	-4.8645740	0.7975730	-1.2704760
38	H	-5.9043160	0.3661560	0.9500360

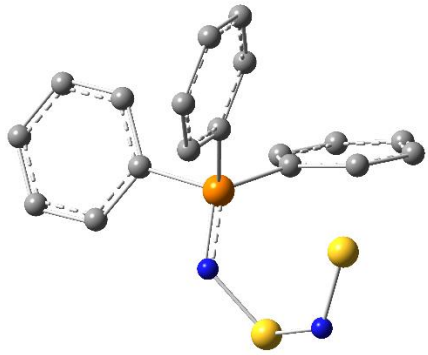

DFT calculated [Ph_3P] B3LYP/6-31+G(d,p) Optimized and Freq Calc (0 imaginary)

No.	Symbol	X	Y	Z
1	P	-0.0015600	-0.0015930	-1.2110850
2	C	-1.5834380	-0.5319040	-0.4031620
3	C	-2.1047060	0.0294020	0.7725980
4	C	-2.3137170	-1.5476050	-1.0429050
5	C	-3.3174610	-0.4210040	1.2979320
6	H	-1.5642120	0.8240390	1.2770870
7	C	-3.5192570	-2.0052750	-0.5121120
8	H	-1.9355860	-1.9782940	-1.9666750
9	C	-4.0252460	-1.4409350	0.6604370
10	H	-3.7083040	0.0259160	2.2078710
11	H	-4.0680790	-2.7938660	-1.0190350
12	H	-4.9687360	-1.7891950	1.0707760
13	C	0.3299170	1.6348840	-0.4053550
14	C	1.1099760	1.8112840	0.7472500
15	C	-0.0185310	4.0434100	-0.4913160
16	C	1.3239790	3.0874680	1.2721630
17	H	1.5540860	0.9493480	1.2346160
18	C	0.7582460	4.2053590	0.6576190
19	H	-0.4569670	4.9088860	-0.9799940
20	H	1.9326440	3.2066710	2.1642580
21	H	0.9262720	5.1971210	1.0674930
22	C	1.2530430	-1.1054580	-0.4075100
23	C	2.5150530	-1.1838380	-1.0206170
24	C	1.0153290	-1.8809070	0.7371620
25	C	3.5178030	-1.9964770	-0.4932340
26	H	2.7102690	-0.6068380	-1.9211380
27	C	2.0156100	-2.7044900	1.2581740
28	H	0.0448060	-1.8450250	1.2213000
29	C	3.2692000	-2.7616300	0.6480310
30	H	4.4883690	-2.0409190	-0.9791670
31	H	1.8137390	-3.3007340	2.1437380
32	H	4.0458350	-3.4027070	1.0550690
33	C	-0.2222210	2.7702570	-1.0221610
34	H	-0.8122090	2.6542480	-1.9278940

References for the Supporting Information

1. Burford, N.; Chivers, T.; Oakley, R. T.; Oswald, T. *Can. J. Chem.* **1984**, *62*, 712–715.
2. (a) Villena-Blanco, M.; Jolly, W. L. *Inorg. Synth*. **1967**, *9*, 98–102. (b) Maaninen, A.; Siivari, J.; Laitinen, R. S.; Chivers, T. *Inorg. Synth*. **2002**, *33*, 196–199.
3. Boeré, R. T.; Fait, J.; Larsen, K.; Yip, J. *Inorg. Chem*. **1992**, *31*, 1417–1423.
4. Boeré, R. T.; Cordes, A. W.; Oakley, R. T. *J. Am. Chem. Soc.* **1987**, *109*, 7781–7785.
5. (a) Boeré, R. T.; Oakley, R. T.; Cordes, A. W. *Acta Cryst.* **1985**, *C41*, 1686–1687. (b) Chivers, T.; Richardson, J. F.; Smith, N. R. M. *Inorg. Chem.* **1986**, *25*, 272–275. (c) Boeré, R. T.; Cordes, A. W.; Craig, S. L.; Graham, J. B.; Oakley, R. T.; Privett, J. A. J. *J. Chem. Soc., Chem. Comm.* **1986**, 807–808. (d) Boeré, R. T.; Ferguson, G.; Oakley, R. T. *Acta Cryst.* **1986**, *C42*, 900–902. (e) Boeré, R. T.; Cordes, A. W.; Oakley, R. T. *J. Am. Chem. Soc.* **1987**, *109*, 7781–7785.
6. Knapp, C.; Lork, E.; Maggiulli, R.; Watson, P. G.; Mews, R.; Borrmann, T.; Stohrer, W. D.; Behrens, U. *Z. Anorg. Allg. Chem.* **2004**, *630*, 1235–1244.
7. Knapp, C.; Lork, E.; Borrmann, T.; Stohrer, W.-D.; Mews, R. *Eur.J.Inorg.Chem.* **2003**,3211-.
8. Maggiulli, R.; Mews, R.; Stohrer, W.-D.; Noltemeyer, M.; Sheldrick, G.M. *Chem.Ber.* **1988**,*121*,1881-
9. Boeré, R. T.; Ferguson, G.; Oakley, R. T. *Acta Cryst.* **1986**, *C42*, 900–902.
10. C. Hansch and A. Leo, "Substituent Constants for Correlation Analysis in Chemistry and Biology," Wiley-Interscience, NY, **1979**.
11. Hermosilla, L.; Calle, P.; García de la Vega, J. M.; Sieiro, C. *J. Phys. Chem. A* **2005**, *109*, 1114–1124. (b) Hermosilla, L.; Calle, P.; García de la Vega, J. M.; Sieiro, C. *J. Phys. Chem. A* **2005**, *109*, 7626–7635.
12. (a) Boeré, R. T.; Tuononen, H. M.; Chivers, T.; Roemmele, T. L. *J. Organomet. Chem.* **2007**, *692*, 2683–2696. (b) Tuononen, H. M.; Chivers, T.; Armstrong, A.; Fedorchuk, C.; Boeré, R. T. *J. Organomet. Chem.* **2007**, *692*, 2705–2715.

END OF SUPPORTING INFORMATION